IS-T-446

ANOMALOUS ELASTIC BEHAVIOR OF POLYCRYSTALLINE Nb_2O_5

Ph. D. Thesis Submitted to Iowa State University, May 1971

William Roger Manning

Ames Laboratory, USAEC
Iowa State University
Ames, Iowa 50010

Date Transmitted: June 1971

PREPARED FOR THE U. S. ATOMIC ENERGY COMMISSION
DIVISION OF RESEARCH UNDER CONTRACT NO. W-7405-eng-82

DISCLAIMER

IS-T-446

ANOMALOUS ELASTIC BEHAVIOR OF POLYCRYSTALLINE Nb_2O_5

Ph. D. Thesis Submitted to Iowa State University, May 1971

William Roger Manning

Ames Laboratory, USAEC
Iowa State University
Ames, Iowa 50010

Date Transmitted: June 1971

PREPARED FOR THE U. S. ATOMIC ENERGY COMMISSION
DIVISION OF RESEARCH UNDER CONTRACT NO. W-7405-eng-82

IS-T-446

Available from: National Technical Information Service
Department A
Springfield, VA 22151

Price: Microfiche $0.95

Anomalous elastic behavior of polycrystalline Nb_2O_5

by

William Roger Manning

A Dissertation Submitted to the

Graduate Faculty in Partial Fulfillment of

The Requirements for the Degree of

DOCTOR OF PHILOSOPHY

Major Subject: Ceramic Engineering

Approved:

In Charge of Major Work

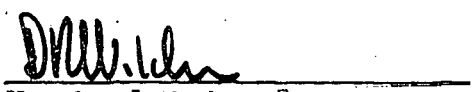

Head of Major Department

Dean of Graduate College

Iowa State University
Ames, Iowa

May 1971

TABLE OF CONTENTS

Anomalous elastic behavior of polycrystalline Nb_2O_5

William Roger Manning

ABSTRACT

The Young's modulus of polycrystalline niobium pentoxide was investigated as a function of temperature using the sonic resonance technique. For samples fabricated by sintering, the modulus increased three times in value over the range 600 to 1000°C, changed with time at constant temperatures in this interval, and showed a large hysteresis between heating and cooling data. For similar samples the room-temperature values for the Young's and shear moduli showed no correlation with sample density. For samples fabricated by hot-pressing, a small decrease in modulus with temperature, no variation in modulus with time, no hysteresis effects, and a linear relationship between room-temperature moduli and sample density were observed. Internal friction measurements revealed similar discrepancies between the two types of samples.

In addition, the bulk linear thermal expansion of both sintered and hot-pressed samples of niobium pentoxide was determined with a dilatometer from room temperature to 1000°C. The over-all linear expansion of the sintered samples was found to be unusually small and a hysteresis between heating and cooling data was observed. The over-all linear expansion of the hot-pressed sample was three times that of the sintered sample and no hysteresis was observed.

The observed phenomena are attributed to the occurrence and recombination of internal microcracks in the sintered samples arising from thermal stresses introduced when the solid is cooled from its fabrication temperature. The internal stresses are a result of the anisotropic lattice expansion of niobium pentoxide as revealed by high-temperature X-ray measurements. Microcracks are apparently absent from the hot-pressed material because of smaller grain size. Scanning electron micrographs of the sintered samples reveal that cracking occurs along the grain boundaries.

INTRODUCTION

The objective of this investigation was to explain why the Young's modulus of sintered niobium pentoxide (Nb_2O_5) increases by a factor of four over the temperature range 600 to 900°C (1). A review of the literature revealed that this anomalous behavior is most likely due to the healing of internal microcracks present in the polycrystalline solid. The microcracks result from thermal stresses introduced when the ceramic body is cooled from its fabrication temperature. In single phase materials these stresses can arise from anisotropy in the thermal expansion of the individual grains constituting the polycrystalline solid.

It is pointed out in the literature (2) that the presence of internal microcracks in a material has characteristic effects upon several properties of that material; e.g., (1) the strength, elastic moduli, and thermal expansion coefficient are abnormally low near room temperature; (2) the values for these three properties increase markedly with temperature; and (3) the property versus temperature curves for these same properties show a hysteresis between heating and cooling. In this investigation extensive elastic moduli, internal friction, and thermal expansion measurements were conducted to determine

if niobium pentoxide has properties similar to those expected of materials possessing microcracks. In addition, high-temperature x-ray thermal expansion measurements were used to indicate a possible cause of the hypothesized microcracks: anisotropic thermal expansion of the unit cell of niobium pentoxide. Finally, an attempt was made to reveal the possible existence of a microcrack system by microstructural examination.

Attempting to analyze the unconventional elastic behavior of niobium pentoxide is of more than academic interest. A common limitation of many refractory ceramic materials is their inability to withstand thermal shock, that is a rapid change in temperature. Recently it has been suggested (3,4) that a material possessing a high density of microcracks should have superior thermal shock damage resistance. Also, two properties that are used in the evaluation of the thermal shock resistance of materials are elastic modulus and thermal expansion coefficient. The data presented in this investigation could be useful in evaluating niobium pentoxide for high-temperature engineering applications.

LITERATURE REVIEW

Some Properties of Niobium Pentoxide

This section will contain a review of the previous investigations of the elastic properties, thermal expansion, and internal friction of niobium pentoxide. Since these properties can be influenced by crystal structure and polymorphism, a discussion of these two aspects of niobium pentoxide will be included.

Apparently the only previous study of the high-temperature elastic properties of polycrystalline niobium pentoxide was conducted by Durbin et al. (1). The authors used the sonic resonance method to measure the dynamic Young's modulus of samples fabricated by sintering the oxide powder. Their results show that this elastic modulus varied little with temperature from room temperature to about 600°C. However, at this temperature the modulus began to increase and rose sharply with increasing temperature to a value at 925°C (the maximum temperature of the study) which was a factor of four greater than the value at room temperature. No data were taken on cooling and no explanation was given for the anomalous behavior. Indeed the results were unusual; theoretically, the Young's modulus of a crystalline ceramic should decrease

slightly with increasing temperature (5). Wachtman (5) states "An order of magnitude rule is that at high temperatures, elastic moduli of crystalline ceramics decrease one percent with each increase of 100°C." This has been experimentally verified for many ceramic materials (5).

Only one other source of elasticity data for niobium pentoxide was found. Douglass (6) employed a static technique to measure the room-temperature Young's modulus of a hot-pressed sample. He reported a value of 1500 kilobars which disagrees substantially with the room-temperature value of 275 kilobars given by Durbin et al. (1). The discrepancy in results is greater than that expected from the difference in techniques.

Prior to their Young's modulus measurements, Durbin and Harman (7) investigated the linear thermal expansion of sintered niobium pentoxide by an interferometric technique. Data were obtained on heating only. They found that the average coefficient of thermal expansion was $0.48 \times 10^{-6}\ ^{o}C^{-1}$ for the temperature range 25 to 900°C. This value is low compared to values for more conventional ceramic materials. The authors observed that samples having different heat treatments displayed different expansion characteristics.

Douglass (6) used a dilatometer to measure the linear thermal expansion of stoichiometric and nonstoichiometric hot-pressed niobium pentoxide. The thermal expansion coefficients of the nonstoichiometric oxide, $Nb_2O_{4.978}$, are reported from 20 to 500°C, while the coefficients for the stoichiometric material are given for the interval 20 to 1000°C. The difference in values between the stoichiometric and nonstoichiometric oxides was small with slightly higher values observed for the latter. Cooling data were obtained from 500 to 20°C and the coefficients of the stoichiometric sample were generally lower on cooling than on heating. The average expansion coefficient from 20° to 900°C was calculated from the data tabulated by Douglass and found to equal 1.59×10^{-6} $^{\circ}C^{-1}$, a value roughly three times that reported by Durbin and Harman (7).

The dynamic internal friction of a sintered specimen of niobium pentoxide was measured by Makkay and Fine (8) from -150 to 125°C. A frequency of 100 kHz was used and the data was obtained in vacuum. A broad internal friction peak was observed at 50°C with the maximum value of internal friction equal to 45×10^{-4}. Vacuum annealing for 132 hrs at 125°C lowered the intensity of the peak and shifted it to 35°C.

The peak is attributed to stress-induced motion of point defects and the shift occurs because "the kinds of defects change during annealing".

The polymorphism of niobium pentoxide has been the subject of many papers. At least fifteen supposedly different crystallographic forms of the stoichiometric oxide have been reported in the literature (9). However, Schäfer et al. (10) pointed out that it is generally agreed that all varieties transform rapidly at temperatures in excess of 1100°C to H-Nb_2O_5, the high-temperature form. Several authors (10,11, 12,13,14) have independently verified that the transformation is irreversible and that the H-form is the true stable form. For a recent and complete discussion of polymorphism in niobium pentoxide the reader is referred to the detailed review article by Reisman and Holtzberg (9). It is important to note that all of the property measurements that were reviewed earlier in this section were conducted on samples fabricated at temperatures above 1100°C.

The crystal structure of the high-temperature form of niobium pentoxide has been worked out in detail by Gatehouse and Wadsley (15). According to these authors the H-form is monoclinic, space group P2, with fourteen formula units in the

cell. Twenty-seven of the Nb atoms are in octahedral coordination and one is in tetrahedral. The structure is characterized by the occurrence of rhenium oxide "blocks" of two different sizes. A block is composed of NbO_6 octahedra joined to neighboring octahedra by sharing of corners. Blocks are joined to one another in "shear planes" where the octahedra share edges. Within each block the corner linkage of the oxygen octahedra continues uninterrupted (∞) in the direction of the b axis (10); in both directions perpendicular to b, the extension of the blocks is limited to a typical number of octahedra. The two types of blocks occurring in the H-form can be formulated as ($3x4x\infty$) and ($3x5x\infty$), the number of octahedra in each edge of the block being given. The b-parameter of the unit cell corresponds to the length of the octahedral body diagonal while the a and c parameters are related to the distances between shear planes. Figure 1 is an idealized drawing of this complex structure looking down the b-axis. The upper dark shaded octahedra are 1/2 unit cell above the lower light shaded octahedra with which they share edges. The black circles are niobium atoms in tetrahedral positions and outline the unit cell in projection.

The high-temperature form of niobium pentoxide may

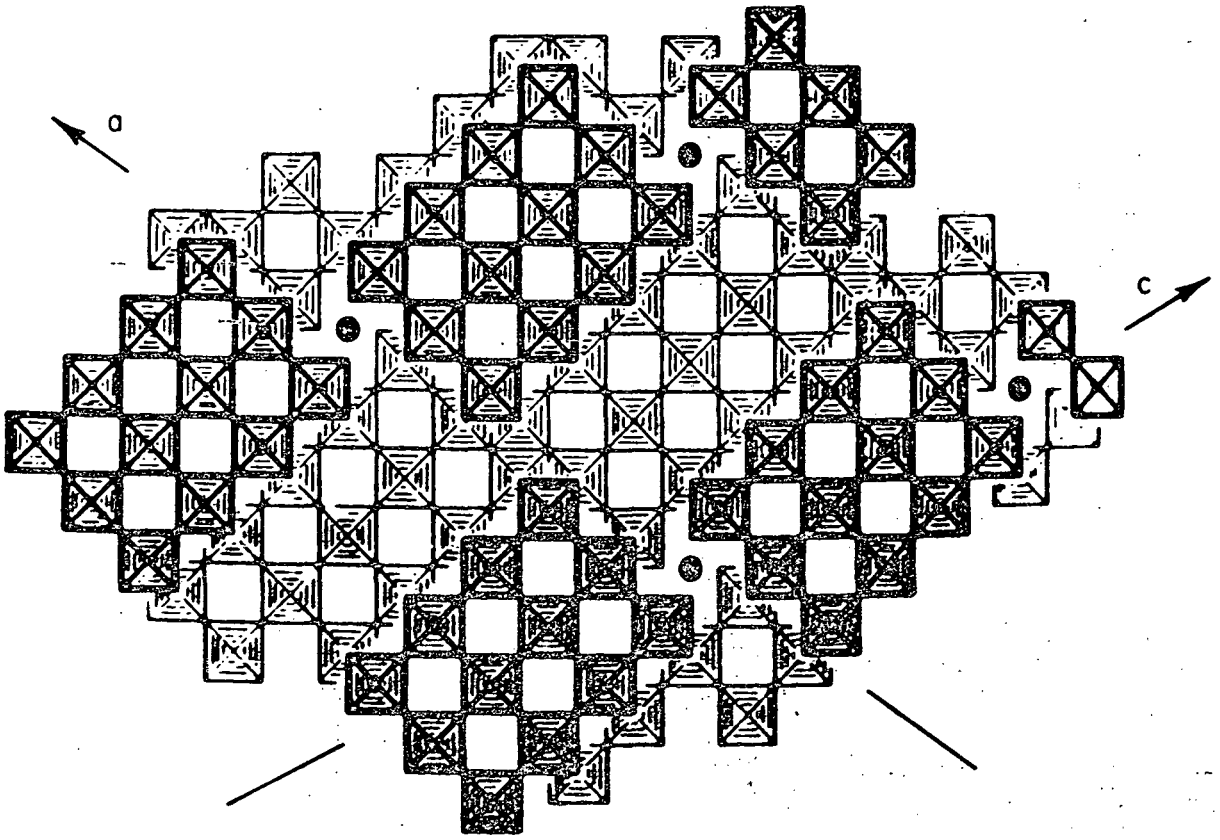

Figure 1. Idealized drawing of the structure of H-Nb_2O_5 (from Gatehouse and Wadsley (15))

exhibit deviations in stoichiometry. Kofstad (16) cites eight references that conclude nonstoichiometric niobium pentoxide is oxygen deficient and an n-type semiconductor. Although the existence of the nonstoichiometric form is well established, there is disagreement in the literature concerning its exact nature.

Brauer (17) reported a single phase region between $Nb_2O_{4.8}$ and Nb_2O_5 in the temperature interval 1350 to 1400°C. Lavrent'ev *et al.* (18) indicated that the composition $Nb_2O_{4.84}$ is a single phase and exhibits the structure of H-Nb_2O_5. They also found that if the oxygen deficiency increased to a point where the composition was $Nb_2O_{4.66}$, the system became two phase consisting of Nb_2O_4 and Nb_2O_{5-x} solid solution. Norin and Magneli (19) revealed discrete phases of $Nb_2O_{4.92}$ and $Nb_2O_{4.96}$ with structures similar to that of H-Nb_2O_5. Blumenthal *et al.* (20) concluded that there are no other stable oxides in the composition interval between Nb_2O_4 and Nb_2O_5. Realizing that their results disagreed with those of Norin and Magneli, these authors conducted additional experiments in an attempt to produce compositions claimed by the latter to be discrete phases. The compositions were generated and each was found to be a single phase solid solution

of Nb_2O_{5-x}. Finally, and most recently, Schäfer et al. (21) determined the 1300°C isotherm of the system Nb-O-H_2-H_2O within the composition range Nb_2O_4 to Nb_2O_5. They found the following equilibrium phases: Nb_2O_4-$Nb_2O_{4.048}$, $Nb_2O_{4.834}$, $Nb_2O_{4.906}$, $Nb_2O_{4.928}$-$Nb_2O_{4.934}$, $Nb_2O_{4.944}$-$Nb_2O_{4.956}$, $Nb_2O_{4.966}$, and $Nb_2O_{4.978}$-$Nb_2O_{5.000}$. They also found that the enthalpy of formation of Nb_2O_{5-x} from its two neighboring phases was only a few cal/mole of Nb_2O_{5-x}.

Materials Displaying Similar Elastic Behavior

The phenomenon of elastic constants increasing with increasing temperature has been observed for other materials. Metals and alloys have shown this behavior [for example, references (22), (23), and (24)] and the results are usually attributed to the presence of a phase transformation or to ordering. Generally the measurements are made on single crystals at low temperatures, and the magnitude of change is not as great as that found for niobium pentoxide. The remainder of this section will be a review of studies on polycrystalline ceramic materials exhibiting anomalous high-temperature elastic properties.

Graphite

The results of several independent investigations indicate that the elastic moduli of graphite increase with

temperature at high temperatures. Malmstrom et al. (25) observed a continuous 50% increase in the Young's modulus from room temperature to about 2000°C. Faris et al. (26) found similar behavior for Young's modulus and further observed that the shear modulus increased to a maximum at 1750°C and then decreased slightly up to 2000°C. The work of Davidson et al. (27) showed the existence of maxima in both the Young's and shear moduli. Further work (28,29) has confirmed that the elastic moduli of graphite increase with temperature to a maximum value at high temperatures. All of these studies used a dynamic method to measure the moduli and the graphites investigated were usually a commerical grade. None of the authors were able to explain their results.

Apparently Hove (30) was the first to offer a qualitative explanation for the unusual elastic behavior of polycrystalline graphite. He suggested that thermal expansion of the single crystallites in the c-direction "closes up some void space and locks the crystallites together more rightly to cause the elastic modulus to increase". Mrozowski (31) proposed that the void space is in the form of microcracks that are initiated during cooling from the graphitization temperature and are formed in order to relieve internal stresses

generated by the interaction between the restraining effect of strong, intercrystalline C-C bonds and anisotropic contraction of the crystal lattice.

Mason and Knibbs (32) used the microvoid hypothesis in the interpretation of their results. These authors employed the sonic resonance technique to measure Young's modulus from 20 to 1000°C. They observed the increase in modulus with temperature but also found that the modulus-temperature curve has a well-defined minimum in the region of 200°C. Other observations were the existence of a hysteresis between heating and cooling curves and a steady increase in Young's modulus with time when the temperature was held at some intermediate value. In a subsequent and more extensive investigation Mason and Knibbs (33) measured the dynamic modulus over the temperature range -196 to 1000°C on specimens of British nuclear-grade carbon heat treated at temperatures between 1200 and 3000°C and cut both parallel and perpendicular to the axis of extrusion. They found that for all samples the modulus fell in value from -196°C to a minimum in the range 200° to 300°C and then rose with temperature up to 1000°C. Again, a hysteresis was observed on cooling with the cooling curve lying above the heating curve. The authors concluded that below room tempera-

ture the negative temperature dependence, which is more negative than theoretically predicted, arises from "thermally dependent dislocation unpinning". Above room temperature the closing of microvoids becomes superimposed on the unpinning process and the observed modulus begins its rise with temperature. It is further pointed out that the effect of the microvoids which are generated on cooling down from the heat treatment temperature is large. For a sample treated at 3000°C, the modulus at room temperature was only 1/5 of what it would be if the microvoids were absent.

The process of microcrack formation and healing has also formed the basis for the explanation of the thermal expansion behavior of polycrystalline graphite. Sutton and Howard (34) found that the bulk thermal expansion coefficient was much smaller than that predicted by averaging over the single crystal coefficients. They characterized the thermal expansion of the polycrystalline body through the use of two parameters, one an accommodation coefficient which is a measure of the effective contribution of the lattice expansion to that of the bulk material, and the other a parameter which is a measure of the preferred orientation of the crystallites. Accommodation of thermal expansion was attributed to the presence of trans-

crystalline microcracks which were observed by electron microscopy of replicas. The cracks were found to exist in parallel arrays with individual crack lengths up to 10 microns, mean width of 250Å, and mean periodicity of 2 cracks per micron.

Slagle (35) used the microcrack hypothesis to interpret the hystereses that he observed during thermal expansion measurements on polycrystalline graphite samples. He employed an optical extensometer to measure sample length as a function of temperature while cycling from 1000° to 2400°C. Samples oriented perpendicular to the extrusion direction exhibited hysteresis for cycling to 2400° and 2200°C but little or no hysteresis for cycling to 2000° and 1800°C. A sample with parallel orientation showed no measurable hysteresis. For each hysteresis observed, the cooling data were lower in value than the heating data. The author proposed a one-dimensional model to theoretically describe crystallite cracking during cooling.

The healing of microcracks resulting from cooling stresses has also been proposed as an explanation for the observed increase in mechanical strength of graphite with temperature (31). Other mechanical properties of graphite such as stress-

strain curves, thermal cycling strain, and thermal creep have been related to the presence of thermally induced microvoids (36).

Multiphase ceramics

In 1927 Heindl and Pendergast (37) used a static technique to determine Young's modulus at elevated temperatures for sagger clays of various compositions. The authors found that for the majority of clays the modulus at 750°C was from 1 1/2 to 3 times that at room temperature. Subsequently (38) the same authors extended the investigation to higher temperatures and observed that the modulus decreased steadily from 750° to 1000°C. This increase was attributed to the onset of plastic flow. No explanation was given for the large increase in Young's modulus from room temperature to 750°C.

Several years later Heindl and Pendergast (39) determined the high-temperature Young's modulus for 10 brands of fire-clay brick (48 to 82 percent silica), 2 brands of silica brick (96 percent silica), and 1 brand of high alumina brick (16 percent silica). For 5 brands of fire-clay bricks the modulus increased gradually between 20 and 500°C and rather abruptly (50 to 80 percent) between 500 and 600°C; for 4 other brands of fire-clay bricks the increase was gradual between 20 and

600°C; for the 2 brands of silica bricks the modulus decreased from 20 to 175°C and increased from 175 to 600°C. The decrease of the modulus in the lower temperature range was noted also in highly siliceous fire-clay bricks. The modulus of the high alumina brick remained constant to 400°C, then increased gradually to 600°C. An approximately linear relationship was found between percentage increase in Young's modulus between room temperature and 600°C and the silica content. The observed elastic behavior was attributed to the phase inversions in crystalline silica.

Ault and Ueltz (40) used the sonic resonance technique to study the high-temperature elasticity of several ceramic materials. They present Young's modulus-temperature data for the following multiphase systems: 50% magnesia (MgO) + 50% magnesium aluminate spinel ($Al_2O_3 \cdot MgO$), a vitreous porcelain body, and clay-bonded silicon carbide. For each material a sharp increase (~100%) in Young's modulus with temperature and a hysteresis between heating and cooling data were observed. The authors concluded that the behavior displayed by the porcelain sample arises from the high-low phase inversion at 573°C of free quartz in the body. Similarly, the elastic modulus data for clay-bonded silicon carbide was explained on

the basis of phase inversion in cristobalite present in the sample. For magnesia + spinel, the increase in modulus and hysteresis were attributed to the closing of internal cracks and discontinuities resulting from stresses induced by the difference in thermal expansion between magnesia and spinel.

Lachman and Everhart (41) in attempting to determine safe cooling schedules for structural clay products measured the thermal expansion and Young's modulus of three commercial bodies in the range room temperature to 870°C. For each composition the Young's modulus was found to increase sharply with temperature by about 50% over the range 530 to 650°C Hystereses between heating and cooling curves were observed for both elastic modulus and thermal expansion data. The results are attributed to the presence of free quartz in the fired bodies. The authors express the following conclusions: "(1) differential contraction of the quartz with respect to the body causes some free quartz to separate from the matrix and leaves other quartz crystals in tension upon cooling; (2) reheating to a temperature within the softening point of the glassy phase results in rebonding; and (3) the sharp increase in the modulus of elasticity through the inversion is due to previously separated quartz crystals reoccupying their

former positions".

The effect of differential thermal expansion on elasticity-temperature relationships for multiphase ceramics was discussed in more detail by Roberts (42). To explain the results of his extensive studies of refractories containing silica minerals, the author wrote "The presence of phases having different expansion characteristics seems an essential condition for the development of the rigidity temperature increase...A likely explanation seems to be that, because of differential expansion, the contact area between the dissimilar phases is increased on heating and conversely, is more or less reversibly decreased on cooling. In short, differential expansion results in reduction of voidage to give an increased area or volume to resist the applied stress. On this hypothesis it follows that the increases in rigidity and strength that occur when a refractory is heated are simply the reversal of physical changes in texture that have taken place during the cooling stage of the initial firing process. When first fired, equilibrium between the relevant crystalline and liquid phases tends to be approached and the crystals to become more or less surrounded by the liquid. On cooling, crystals will tend to separate from the liquid once the later has solidified

provided that the respective contraction coefficients are sufficiently dissimilar. Thus, when cold the crystalline components are no longer completely surrounded by matrix but are partially or wholly isolated from it by minute voids. Loss of strength during cooling and regain of strength on subsequent reheating is thus consequential".

Single-phase ceramics

Unconventional high-temperature elastic behavior has been observed for single-phase ceramics other than graphite. In this section previous investigations on zirconia (ZrO_2), vitreous silica (SiO_2), magnesium dititanate ($MgO \cdot 2TiO_2$), and β-eucryptite ($Li_2O \cdot Al_2O_3 \cdot 2SiO_2$) will be reviewed.

Ault and Ueltz (40), in the investigation discussed previously, also determined the Young's modulus of unstabilized monoclinic zirconia as a function of temperature. The modulus decreased slightly to 600°C at which temperature the authors were unable to obtain more data because of poor "tone quality"; however, heating was continued to 1200°C and data were gathered on cooling from 700°C downward. For cooling the modulus values were well above those obtained on heating. The hysteresis was attributed to internal stresses resulting from the reversible monoclinic-to-tetragonal transformation that occurs

in zirconia at about 1150°C (40).

Smith and Crandall (43) present data on the temperature dependence of Young's and shear moduli for unstabilized zirconia. The authors made their dynamic measurements on samples fabricated by hot-pressing. The modulus-temperature curves shown in this study exhibit a curvilinear trend with the moduli falling more rapidly than expected with temperature. This behavior was thought to be due to the presence of a glassy phase present in the samples and resulting from impurities in the starting zirconia powder. In contrast to the study of Ault and Ueltz (40), who used sintered samples, no loss of signal was observed and no data were obtained on cooling.

More recently, Buckley and Braski (44) used a resonance technique to measure the Young's modulus at elevated temperatures of partly stabilized and highly stabilized zirconia. The authors found that the Young's modulus of zirconia partly stabilized with yttria (ZrO_2 + 3.5 mole% Y_2O_3) decreased slightly from room temperature to 700°C and then increased 100% from 700 to 950°C. For a sample partly stabilized with calcia (ZrO_2 + 4.3 mole% CaO) the Young's modulus behaved in a similar manner but showed a smaller increase (50%). Both partly stabilized materials exhibited large hystereses between

heating and cooling curves. Highly stabilized materials ($\geq$ 4.7% Y_2O_3 and $\geq$ 6.4% CaO) showed no increase in modulus and no hysteresis on cooling. The increasing modulus-hysteresis effects were attributed to the monoclinic-to-tetragonal transformation which the authors claim occurs at 650°C in the partly stabilized samples.

Spinner (45) found that the dynamic Young's and shear moduli for vitreous silica increased with increasing temperature from room temperature and followed a parabolic curve with a maximum between 1050 and 1200°C depending on the source of the specimen. The maximum values of the moduli were about 10% higher than the room-temperature values. This behavior has been explained on a theoretical basis (46) and was shown to be implied by the very low coefficient of thermal expansion for vitreous silica.

Bush and Hummel (47,48) used a static technique to measure the temperature dependence for the Young's moduli of sintered samples of magnesium dititanage and β-eucryptite. For magnesium dititanate the modulus remained nearly constant with temperature to 600°C and then increased in the range 600 to 1000°C to a value approximately six times that found at room temperature. A large hysteresis was observed on cooling with

the data lying well above the heating data. For β-eucryptite the Young's modulus began to increase at 400°C and more than doubled in value up to 800°C. Again a large hysteresis was obtained. In the same investigations the authors found (1) for both materials the modulus of rupture increased with temperature and exhibited hysteresis between heating and cooling curves; (2) both materials deformed with time under load at room temperature; and (3) the bulk thermal expansion of magnesium dititanate was unusually small up to 1000°C while the bulk thermal expansion of β-eucryptite, as previously determined by Gillery and Bush (49), was negative up to 800°C and exhibited, as did magnesium dititanate, hysteresis effects on cooling. All of the observed phenomena were attributed to the occurrence and recombination of internal fractures that result from stresses arising from the high anisotropy of thermal expansion associated with the lattices of magnesium dititanate and β-eucryptite. The authors present electron micrographs that reveal the presence of cracks both across and between the grains of the polycrystalline materials.

EXPERIMENTAL PROCEDURE

Sample Preparation

The samples used in this investigation were fabricated from a fine powder of niobium pentoxide (A. D. Mackay, Inc.) specified by the supplier to have a purity of 99.95% and an average particle size less than five microns. The results of a semiquantitative analysis of the powder performed by the Ames Laboratory Mass Spectrographic Group appear in Table 1. The as-received powder was examined by X-ray diffraction and found to have a pattern which corresponded closely with the data reported by Roth (50) for the stable high-temperature form of niobium pentoxide, H-Nb_2O_5. X-ray measurements were also conducted on powder heat-treated at 1150°C for 24 hrs; the results were identical to those found for the as-received powder.

Experimental samples were prepared by two techniques: sintering and hot-pressing. The procedure for the sintered specimens involved using a double-action steel die and a pressure of 3000 psi to compact the powdered oxide into prismatic bars with rectangular cross sections. The bars, having the approximate dimensions 1/4 in. x 1/2 in. x 4 in. were then inverted in the die and repressed at the same pressure to minimize warpage. The final step prior to sintering involved

Table 1. Spectrographic analysis of impurities

Element	Concentration (ppm)	Element	Concentration (ppm)
Cl	80	Te	≤2
K	2	I	≤0.2
Ca	20	Cs	<0.1
Sc	1	Ba	<2
Ti	<2	La	2
V	<0.2	Ce	≤10
Cr	2	Pr	2
Mn	<0.2	Nd	<2
Fe	10	Sm	<0.3
Co	<0.3	Eu	<0.08
Ni	0.8	Gd	<2
Cu	0.8	Tb	0.7
Zn	0.7	Dy	<1
Ga	0.1	Ho	2
Ge	0.09	Er	≤3
As	.03	Tm	≤0.2
Se	<1	Yb	10
Br	<2	Lu	2
Rb	≤0.1	Hf	<3
Sr	≤1	Ta	50
Y	0.5	W	<10
Zr	≤7	Re	-
Nb	10^6	Os	<0.9
Mo	≤10	Ir	<2
Ru	<0.4	Pt	<0.3
Rh	<0.1	Au	<0.3
Pd	<0.6	Hg	<0.3
Ag	<0.3	Tl	<0.2
Cd	<0.	Pb	<2
In	<0.3	Bi	<0.2
Sn	<3	Th	<0.5
Sb	<0.3	U	<5

placing the sample in a thin walled rubber container (Young's Drug Products, Corp.) and isostatically pressing it at 50,000 psi The samples were then set on platinum foil and fired at various temperatures under an air atmosphere in an electric resistance furnace with globar heating elements. After sintering the samples were machined on a surface grinder until the faces were flat and parallel within 0.001 cm. The bulk density of each specimen was determined from its mass and dimensions. The volume fraction porosity of the sintered bars was calculated through use of the relation

$$P = 1 - (\text{measured density}/\text{theoretical density}) \quad (1)$$

where P is the volume fraction of pores. The theoretical density of niobium pentoxide was considered to be 4.55 g/cm^3 which is the X-ray density reported by Gatehouse and Wadsley (15) and also the pycnometric density reported by Holtzberg et al. (11). Table 2 gives the firing treatment, dimensions, density, and calculated porosity of each sintered sample.

The hot-pressing procedure involved loading approximately 100 grams of niobium pentoxide powder into a double-acting graphite die with a 3.5 in. x 3/4 in. rectangular sample cavity. The powder was then compacted at room temperature with a pressure of 1000 psi. The plungers were removed and

Table 2. Firing treatment, dimensions, density, and volume fraction porosity of sintered samples

Sample No.	Sintering temperature (°C)	Time at sintering temperature (min.)	Length (cm.)	Width (cm.)	Thickness (cm.)	Density (g/cm^3)	Volume fraction porosity
D-1	1200	60	5.093	0.874	0.446	2.873	0.369
D-2	1250	60	5.088	.855	.488	2.897	.363
D-3	1365	60	5.075	.619	.323	3.139	.310
D-4	1380	60	5.081	.907	.293	3.256	.284
D-5	1410	60	5.070	.883	.377	3.556	.218
D-6	1410	60	5.072	.842	.340	3.637	.201
D-7	1430	60	5.083	.886	.382	3.816	.161
D-8	1450	60	5.072	.779	.402	3.982	.125
S-1	1450	120	5.839	1.461	.355	4.042	.112
S-2	1475	70	6.950	1.446	.366	4.055	.109
D-9	1470	120	5.088	.954	.264	4.099	.099
S-3	1475	90	7.200	1.391	.387	4.119	.095
S-4	1470	120	5.485	1.197	.262	4.119	.095
D-10	1475	90	5.088	.862	.387	4.123	.094
S-5	1480	60	7.308	1.932	.323	4.248	.066

coated with a boron nitride-acetone slurry used to minimize reaction between the die and sample material. The die was placed in a graphite-susceptor induction furnace and densification was carried out at various high temperatures for various times and at pressures in the range 1000 to 2000 psi. The pressure was released at high temperature and the samples were cooled to room temperature before being removed from the die. Despite the boron nitride coating some reaction between the sample surface and the die did occur and, to produce a crack-free specimen, it was necessary to use a band saw to cut the sample out of the die. Any apparent reaction product remaining on the sample surface was removed during subsequent surface grinding. The samples were black in color indicating the occurrence of partial reduction by contact with the graphite die. Each sample was sectioned on a cut-off wheel into three or four prismatic specimens which were machined to exact dimensions and used for experimental measurements.

The departure from stoichiometry for the reduced hot-pressed niobium pentoxide samples was determined by a weight change technique. Each reduced bar was fired in an air atmosphere at 1000°C for several hours, then cooled down and weighed. Subsequent firings and weighings continued until

the sample was white in color and no increase in weight was observed. Assuming that all weight changes which occurred were due to an increase in the oxygen content of the reduced sample, and assuming that Nb_2O_5 does not become hyperstoichiometric with respect to oxygen, the composition of the reduced hot-pressed specimens was determined by calculating x in the formula Nb_2O_{5-x}. The equation used was

$$x = \left(\frac{\text{wt gain}}{\text{mass after reoxidation}} \right) \left(\frac{\text{molecular wt } Nb_2O_5}{\text{atomic wt O}} \right) \qquad (2)$$

The samples were weighed on a Mettler balance with an accuracy of $\pm$ 0.0001 grams, and the weight changes observed were on the order of 0.0500 grams. Blumenthal *et al.* (20) employed a similar technique to determine the composition of their nonstoichiometric niobium pentoxide samples. Table 3 gives the hot-pressing treatment, dimensions, density, and departure from stoichiometry for each hot-pressed specimen.

Elasticity and Internal Friction Measurements

Elastic moduli and internal friction data for niobium pentoxide samples were experimentally obtained using the sonic resonance method originated by Forster (51) in 1927. The experimental technique has been discussed in detail by Spinner

Table 3. Hot-pressing treatment, dimensions, density, and departure from stoichiometry of hot-pressed samples

Sample No.	Observed hot-pressing temperature (°C)	Time at maximum temperature (min.)	Length (cm.)	Width (cm.)	Thickness (cm.)	Density (g/cm^3)	(5-x) in Nb_2O_{5-x}
1	1150	5	8.357	1.800	0.351	3.656	5.000
D-11	1150	5	5.083	.868	.336	3.840	5.000
2	1150	5	8.428	1.295	.336	3.855	4.995
3	1150	5	8.440	1.243	.258	3.877	4.993
4	1150	5	8.392	1.248	.380	3.895	4.997
5	1150	5	8.377	1.294	.359	3.926	4.999
6	1180	5	8.766	1.732	.407	4.155	4.934
7	1180	5	8.225	1.189	.462	4.176	4.938
8	1180	5	8.837	1.240	.357	4.194	4.942
9	1180	5	8.809	1.199	.458	4.240	4.942
10	1180	5	8.773	1.184	.436	4.252	4.930
11	1180	5	8.778	1.258	.349	4.272	4.933
12	1180	5	8.839	1.160	.418	4.274	4.930
13	1180	5	8.108	1.230	.343	4.297	4.928
14	1180	5	8.758	1.257	.375	4.305	4.917
15	1180	5	7.115	1.149	.273	4.322	4.926
16	1180	5	8.773	1.257	.359	4.337	4.911
17	1230	10	7.336	1.388	.524	4.413	4.946
18	1230	20	7.630	1.457	.310	4.433	4.941
19	1230	20	6.878	1.458	.308	4.449	4.935
20	1230	20	6.614	1.015	.384	4.454	4.957
21	1230	20	6.541	1.458	.269	4.466	4.938
22	1230	10	6.040	1.169	.273	4.498	4.945
23	1230	10	5.824	1.169	.226	4.512	4.945

and Tefft (52) and, more recently, by Marlowe (53).

Figure 2 is a block diagram of the equipment used in this investigation. A wide range (5 to 500,000 cps) variable frequency oscillator (Hewlett-Packard model 200CD) was employed to generate a sinusoidal electric signal which was amplified and controlled by an audio amplifier (Heathkit model EA-3, 14 watts). The amplified signal was converted to a mechanical vibration of the same frequency by the driver, a magnetic record cutting head (Astatic type M41-8). This mechanical motion was transmitted to the suspended specimen through cotton threads for room-temperature measurements or carbon yarn (Hitco) for elevated temperature determinations. At the other end of the specimen another thread conveyed the displacement of the bar to the pickup, a high-output piezoelectric phonograph cartridge (Astatic 62-1). The pickup transformed the mechanical vibration to an electrical signal which was then amplified by an audio preamplifier (designed and built by Ames Laboratory Instrumentation Group) and passed into a vacuum tube voltmeter (Hewlett-Packard model 400D) and onto the vertical plates of an oscilloscope (Hewlett-Packard model 120 BR). The signal from the oscillator was also supplied to the horizontal plates of the scope and to an electronic fre-

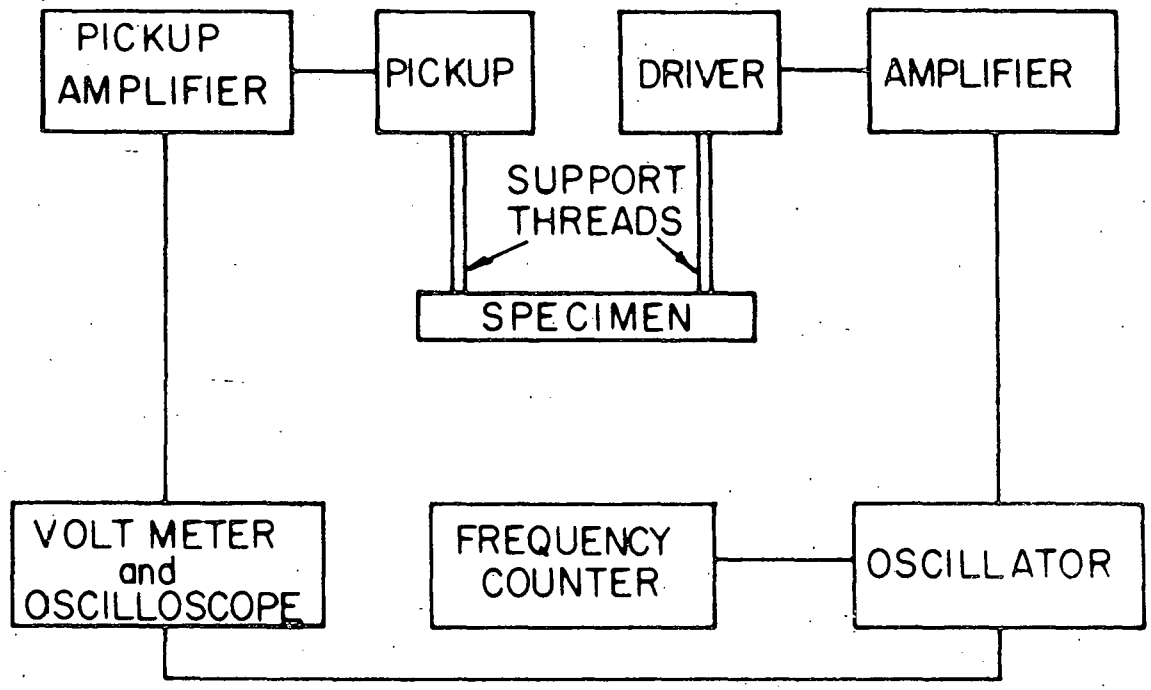

Figure 2. Block diagram of resonant frequency apparatus

quency counter (Hewlett-Packard model 5223 L).

High-temperature elasticity and internal friction data were obtained under vacuum at pressures less than 0.05 μm Hg. The sample was suspended in a carbon-rod resistance furnace and temperature was measured with a Pt-Pt 10% Rh thermocouple with its hot junction near the middle of the sample. The power input to the furnace was controlled manually and the furnace was allowed to approach thermal equilibrium before readings were made. For a more detailed description of the furnace and vacuum system, the reader is referred to the work of Marlowe (53).

Elasticity measurements were made by varying the signal from the oscillator until the suspended sample vibrated in resonance. Under this condition the amplitude of vibration reached a maximum which was detected on the oscilloscope. The exact value of the resonant frequency was determined by tuning the oscillator to give maximum deflection of the vacuum tube voltmeter and the resonant frequency was then read from the counter. The dynamic Young's and shear moduli were calculated from the resonant frequencies and the dimensions and mass of the specimen.

For a prismatic sample with a rectangular cross-section

a total of three fundamental resonant frequencies can be determined (54). The vibrations associated with these frequencies are illustrated in Figure 3 with the pickup and driver shown symbolically as rods. The relative amplitudes of vibration across the specimens are indicated by arrows. The three frequencies can be described as follows: (a) The first mode of flexural vibration, which takes place parallel to the shortest dimensions of the cross-section. This frequency is usually referred to as the "flatwise" flexural frequency; (b) The first mode of flexural vibration with the vibrations parallel to the longest side of the cross section. This is called the "edgewise" flexural frequency; and (c) The first mode of torsional vibration excited by tying the suspending threads on opposite sides of the specimen. In this case vibration takes place around an axis through the center and parallel to the length of the sample. This frequency is known as the torsional frequency. In addition to these three resonant frequencies, there is a longitudinal frequency which can be determined with a different experimental set-up.

The equations used to calculate elastic moduli from the resonant frequencies were given by Spinner and Tefft (52) and based on the relations proposed by Pickett (55) for prisms of

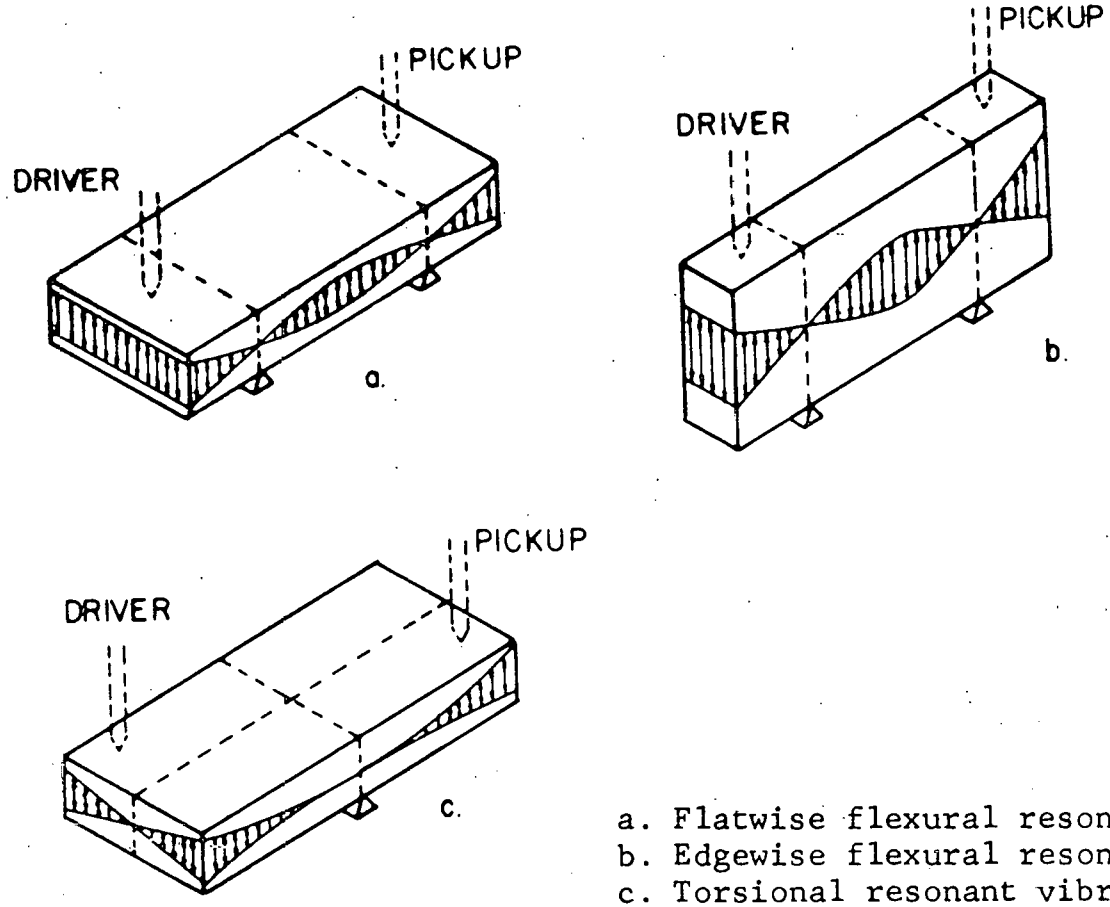

a. Flatwise flexural resonant vibration
b. Edgewise flexural resonant vibration
c. Torsional resonant vibration

Figure 3. First modes of resonant vibrations in prisms of rectangular cross-section (from Hasselman (54))

rectangular cross-section. Young's modulus was calculated from the equation

$$E = 0.94645 \frac{S_f m f^2}{b} \tag{3}$$

where E is the Young's modulus of the bar

m is the mass of the sample

f is the fundamental flatwise or edgewise resonant frequency

b is the dimension of the cross-section perpendicular to the direction of vibration

and S_f is a shape factor defined as

$$S_f = 1 + 6.585(1 + 0.0752\mu + 0.8109\mu^2)(t/L)^2 - 0.868(t/L)^4 - \frac{8.340(1 + 0.2023\mu + 2.173\mu^2)(t/L)^4}{1 + 6.338(1 + 0.14081\mu + 1.536\mu^2)(t/L)^2}$$

where t is the dimension of the cross-section parallel to the direction of vibration

L is the length of the specimen

and μ is Poisson's ratio for the bar.

The shear modulus, G, was computed from the equation

$$G = \frac{4LS_t m f_t^2}{A} \tag{4}$$

where L and m are as defined before

f_t is the fundamental torsional resonant frequency

A is the area of the cross section

and S_t is a shape factor given by

$$S_t = \frac{C/D + D/C}{4C/D - 2.52(C/D)^2 + 0.21(C/D)^6}$$

where C is the length of the shorter side, and

D is the length of the longer side of the cross-section.

Since Poisson's ratio was unknown, a value of 0.250 was assumed and used to calculate a tentative Young's modulus from Equation 3. From the shear modulus and the tentative value for Young's modulus, Poisson's ratio was calculated from the relation

$$\mu = \frac{E}{2G} - 1 \qquad (5)$$

which is valid for elastically isotropic solids such as polycrystalline bodies composed of randomly oriented particles. The computed value of μ was then compared to the assumed value, and if a discrepancy existed, Young's modulus was recalculated with the new value of μ. This process was repeated until three significant figures of Poisson's ratio remained constant. Usually no more than three recalculations were necessary.

The high-temperature Young's and shear moduli were calculated using the equation

$$M_T = M_{RT}\left(\frac{F_T}{F_{RT}}\right)^2 \qquad (6)$$

where M_T and F_T are, respectively, the elastic modulus (Young's or shear) and the resonant frequency at temperature T; and M_{RT} and F_{RT} are the values at room temperature. Since the thermal expansion of niobium pentoxide has been reported to be small (7), no correction was made for the change in specimen length at elevated temperatures. A sample calculation showed that neglecting this effect results in an error of less than 1 part per 1000 in the high-temperature modulus value.

The internal friction of samples was determined through use of the "peak width" technique. When the frequency of the driving oscillator is varied from the resonant frequency in either direction, the amplitude of vibration of the suspended sample simultaneously decreases. The frequencies, f_1 and f_2, at which the amplitude is 1/2 of the amplitude at resonance, correspond to the peak width of the resonance peak, $\Delta f_R = f_2 - f_1$. Thus, when the resonant frequency was found, the oscillator was varied on either side of the amplitude-versus-frequency peak to give a deflection of the vacuum tube

voltmeter equal to half of that observed at resonance. The frequencies at half-maximum amplitude were then read from the counter and used in the calculation of internal friction from the relation (56)

$$Q^{-1} = \frac{1}{3} \frac{\Delta f_R}{f_R} \qquad (7)$$

where Q^{-1} is the internal friction, Δf_R is the width of resonant peak at half the maximum amplitude, and f_R is the resonant frequency. It was found that the internal friction of the samples used in this investigation did not vary with the position of the support threads; consequently, the corrections suggested by Wachtman and Tefft (57) were not made.

In order to confirm the accuracy of the experimental apparatus, room-temperature elasticity measurements were made on a polycrystalline alumina elasticity standard (Prototype D) provided by the United States National Bureau of Standards. Table 4 shows the comparison between the values reported by NBS and the values measured on the resonance equipment used in this investigation.

Marlowe (53) has discussed the experimental error involved in the sonic resonance method for determining elastic moduli of polycrystalline ceramics. He states that

Table 4. Reported values and measured values for elasticity standard

	NBS values	Measured values
Flexural frequency (cps)	3807.66 ± 0.05	3807.7
Torsional frequency (cps)	18,883.6 ± 1	18,884
Shear modulus (kilobars)	1597 ± 6	1598
Young's modulus (kilobars)	3936 ± 24	3942
Poisson's ratio	0.232 ± 0.01	0.233

the over-all error in the room-temperature elastic modulus should be less than 1.3% with the largest portion of this due to dimensional inaccuracy. Astbury and Davis (58) point out that the error involved with the peak width methods of determining internal friction is about ± 10%.

Dilatometric Thermal Expansion Measurements

Bulk thermal expansion data for niobium pentoxide samples were experimentally obtained through use of a commercial dilatometer (Brinkmann model TD IX). The system uses alumina push rods and a linear variable differential transformer to measure length change; the sample is heated in an alumina (Al_2O_3) tube in an electric resistance furnace with an air atmosphere. Temperature was measured and controlled with a Pt-Pt 10% Rh thermocouple placed very close to and above the center of the

sample.

The dilatometer samples were among those used for elastic property determinations and are designated in Tables 2 and 3 by the letter D. The heating rate of the samples during the dilatometer measurements was approximately 100°C per hour, whereas the cooling rate was 80° per hour from maximum temperature to 500°C (the temperature at which the controller ceased to control), 30° per hour from 500° to 300°C, 10° per hour from 300° to 100°C, and 3° per hour from 100° to 25°C.

The change in length of the sample was determined at 50°C intervals from the relation

$$\Delta L_T = \Delta L_a + \Delta L_s \qquad (8)$$

where ΔL_T represents the actual change in length of the specimen from room temperature to temperature T, ΔL_a the apparent change, and ΔL_s the change in length of the measuring system. Values of ΔL_a were read from the recorded temperature-displacement traces generated by the dilatometer, and values of ΔL_s were determined from the calibration curve representing the expansion of the system. The percent expansion at a given temperature T was computed by dividing ΔL_T by L_{RT}, the length of the sample at room temperature.

The heating and cooling calibration curves for the

dilatometer system are shown in Figure 4. The curves were determined by measuring the change in length of a fused silica specimen. Equation 7 was then used to calculate ΔL_s at 50°C intervals from the measured ΔL_a values and from ΔL_T values reported in the literature (59) for fused silica. Each data point in Figure 4 represents the average of data obtained in 10 runs on fused silica. The scatter observed between the various fused silica runs was about 2% which suggests that the over-all error involved with the dilatometer measurements was also 2%.

Equations of the form $\Delta L = \Delta L_o(1 + aT + bT^2)$ were fit by a least squares technique to the heating and cooling data for the dilatometer system. The computed values for the constants of the heating curve equation are $\Delta L_o = -0.335469 \times 10^{-2}$ inches, $a = -0.448381 \times 10^{-1}$ C^{o-1}, and $b = -0.775456 \times 10^{-5}$ C^{o-2}. The values for the cooling curve equation are $\Delta L_o = -0.417407 \times 10^{-2}$ inches, $a = -0.316536 \times 10^{-1}$ C^{o-1}, and $b = -0.108420 \times 10^{-4}$ C^{o-2}. The standard error of estimate for the heating curve was calculated to be 0.702728×10^{-3} inches while that for the cooling curve was 0.694616×10^{-3} inches. The smooth curves shown in Figure 4 are the computed curves.

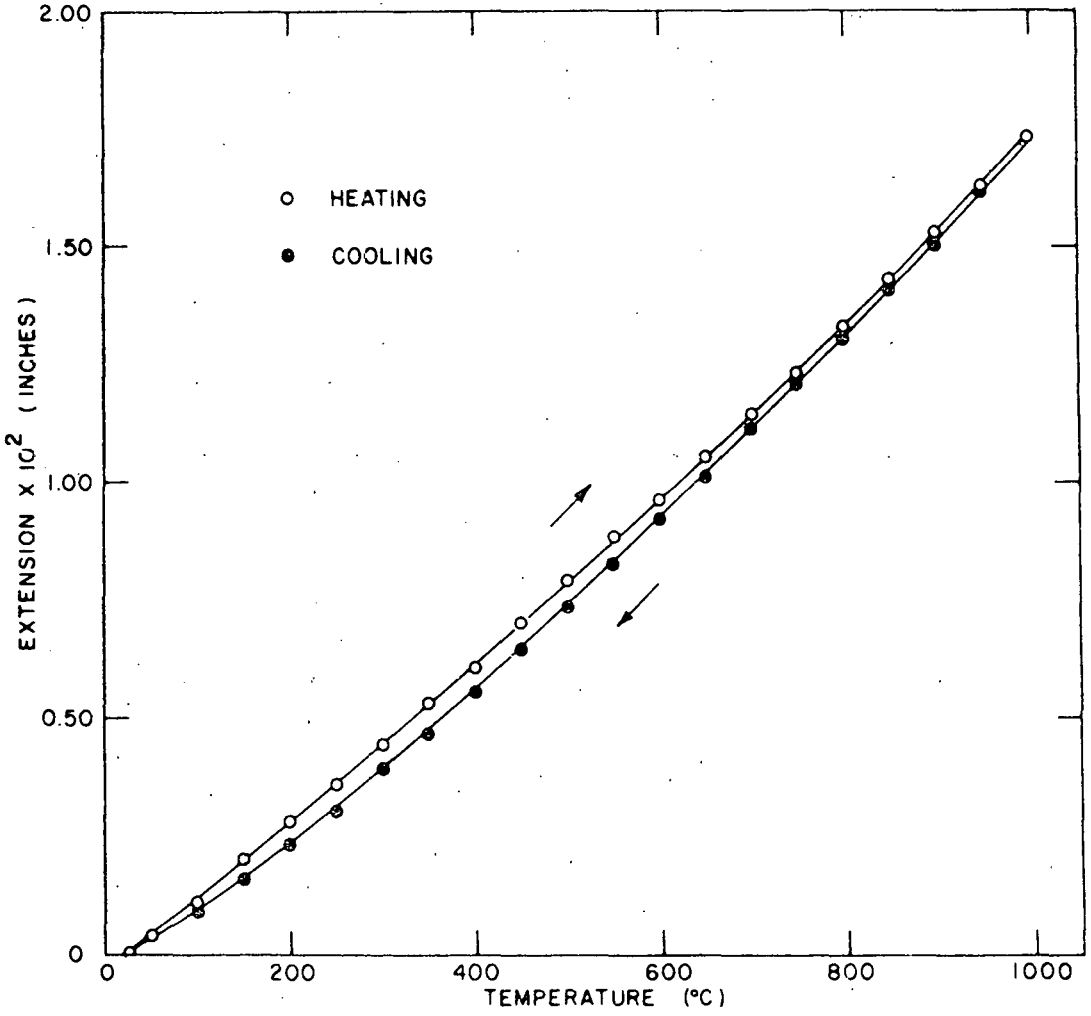

Figure 4. Calibration curves for the dilatometer

X-ray Thermal Expansion Measurements

The lattice thermal expansion of monoclinic niobium pentoxide (H-Nb_2O_5) was determined by high-temperature X-ray diffraction measurements on powdered samples. The elevated temperature powder patterns were produced with a recording diffractometer (Norelco Wide Range) using CuKα radiation with a scanning rate of 1^{o} 2θ per minute. A furnace attachment (Material Research Corporation model X-86-N3) was used to heat the sample in an air atmosphere. The powdered sample was mounted with Carbowax 4000 (Carbide and Carbon Chemical Co.) as a binder on a strip of Pt-Pt 40% Rh metal which served as both sample holder and heating element. The temperature was measured with a Pt-Pt 13% Rh thermocouple spot-welded to the sample holder. For a far more detailed description of the equipment the reader is referred to the works of Johnstone (60) and Stacy (61).

The combined heater/sample was mounted in the furnace and aligned relative to the X-ray beam. The alignment was checked with a special standard silicon sample fabricated for mounting in the furnace. It was found that once the furnace attachment was properly aligned, the alignment did not change from one run to the next, nor was it necessary to adjust the

alignment at elevated temperatures. The sample holder was heated to a temperature sufficient to burn off the binder, and, on cooling, alignment was again checked before high-temperature measurements were made.

The sample was brought to the desired temperature through manual control of the furnace power supply. Ten to 15 minutes were allowed for the temperature to stabilize. The sample was then continuously scanned from 15^{o} 2θ to 60^{o} 2θ. During the time of scanning the temperature remained constant within $10^{o}C$.

The room-temperature diffraction pattern of H-Nb_2O_5 was indexed according to the powder diffraction data given by Roth (50). The lattice parameters at each elevated temperature were calculated from the measured 2θ values and assigned hkl values associated with the Bragg reflections recorded on the diffractometer trace. A computer program originated by Vogel and Kempter (62) and modified[1] to include the monoclinic system was used for the computations. This program is based on the analytical method of Hess (63) and extrapolates

---

[1]Smith, J. and Bowman, A. Los Alamos Scientific Laboratory, Los Alamos, New Mexico. Unpublished modification to Vogel-Kempter lattice parameter program. Private communication to Mr. John Mason. 1964.

the calculated parameters against $\cos\theta \cot\theta$.

The accuracy of the equipment and technique involved in the high-temperature X-ray thermal expansion measurements has been discussed by Stacy (61). He measured the high-temperature lattice parameters of yttria (Y_2O_3), thoria (ThO_2), zirconia (ZrO_2), and hafnia (HfO_2) and found good agreement between his expansion curves and those reported in the literature. Figure 5 shows literature values (64-70) for the lattice parameter of thoria as a function of temperature compared to values obtained using the equipment and procedure mentioned here.

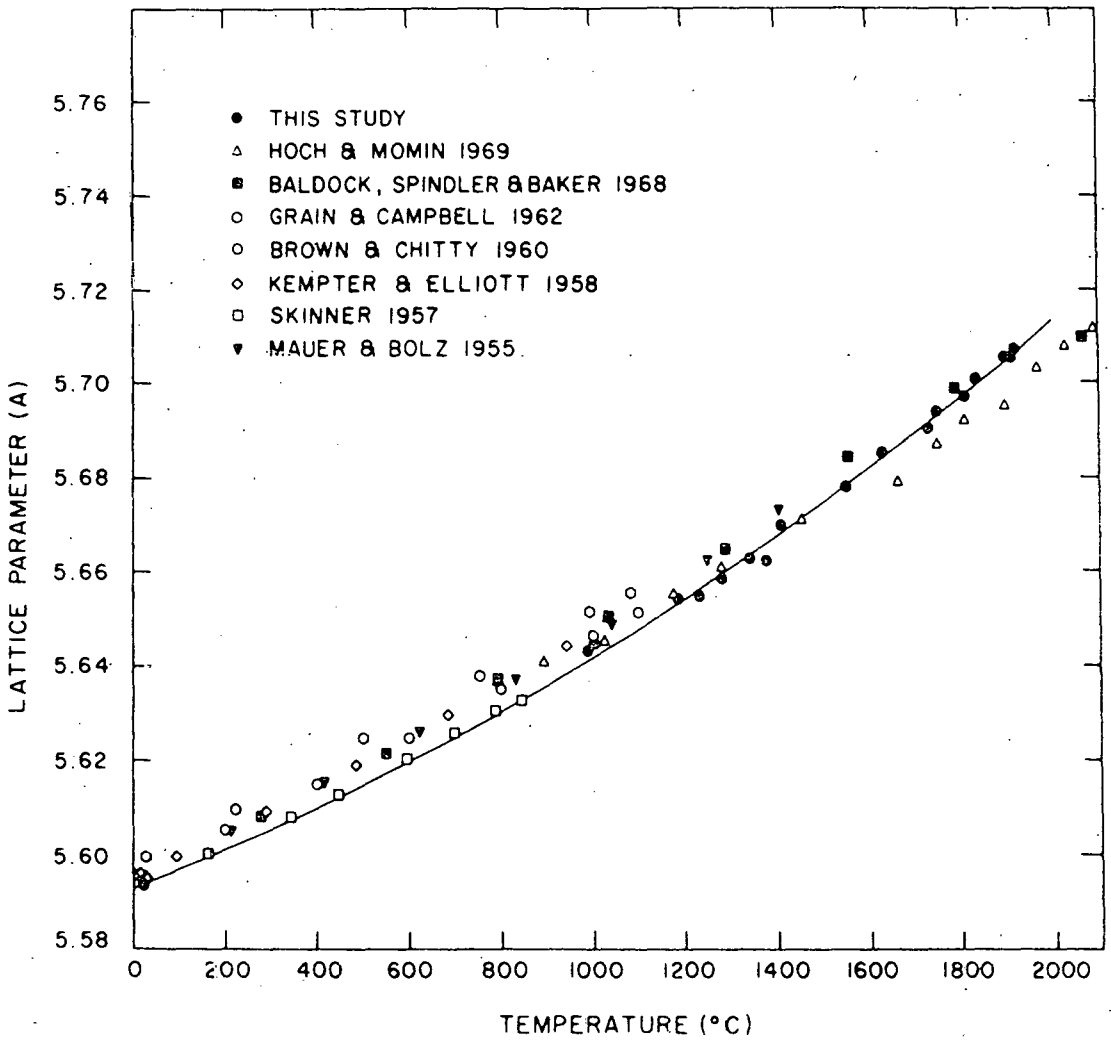

Figure 5. Comparison of X-ray thermal expansion results for ThO_2 with values reported in the literature (from Stacy (61))

RESULTS

Elastic Properties and Internal Friction of Niobium Pentoxide

The results of both high-temperature and room-temperature dynamic elasticity and internal friction measurements are presented in Figures 6 through 12. Figure 6 shows the Young's modulus of both sintered and hot-pressed niobium pentoxide as a function of temperature on heating and cooling from room temperature to about 1000°C. Also included in Figure 6 are the results of Durbin et al. (1). Figures 7 and 8 indicate how the Young's modulus varied with time when held at constant temperature for seven temperatures between 578 and 900°C. Figure 9 displays internal friction data for a sintered sample and a hot-pressed sample at elevated temperatures as high as 1000°C and 1100°C, respectively. Figures 10 and 11 show, respectively, the room temperature Young's modulus and shear modulus of both sintered and hot-pressed samples as a function of the bulk density of the samples. Figure 12 exhibits the room-temperature internal friction for sintered and hot-pressed niobium pentoxide. The data graphically represented here are tabulated in Appendix A.

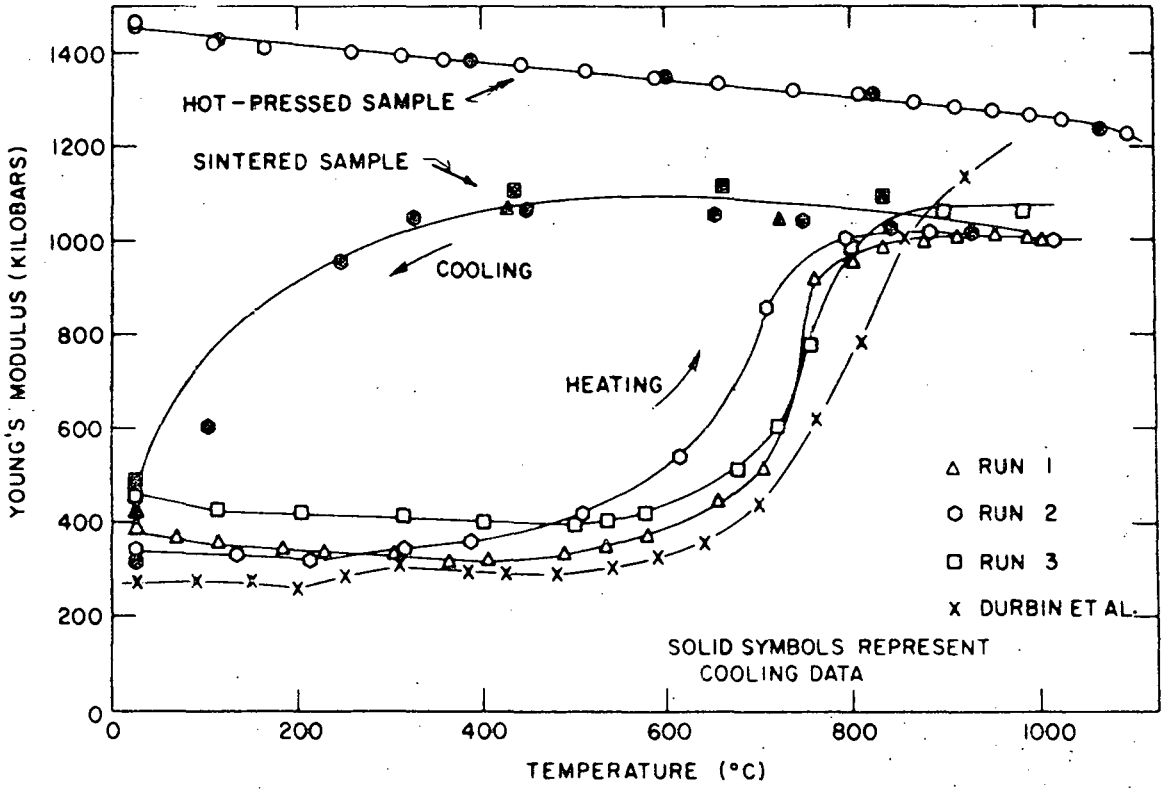

Figure 6. Elevated temperature Young's modulus for sintered and hot-pressed niobium pentoxide

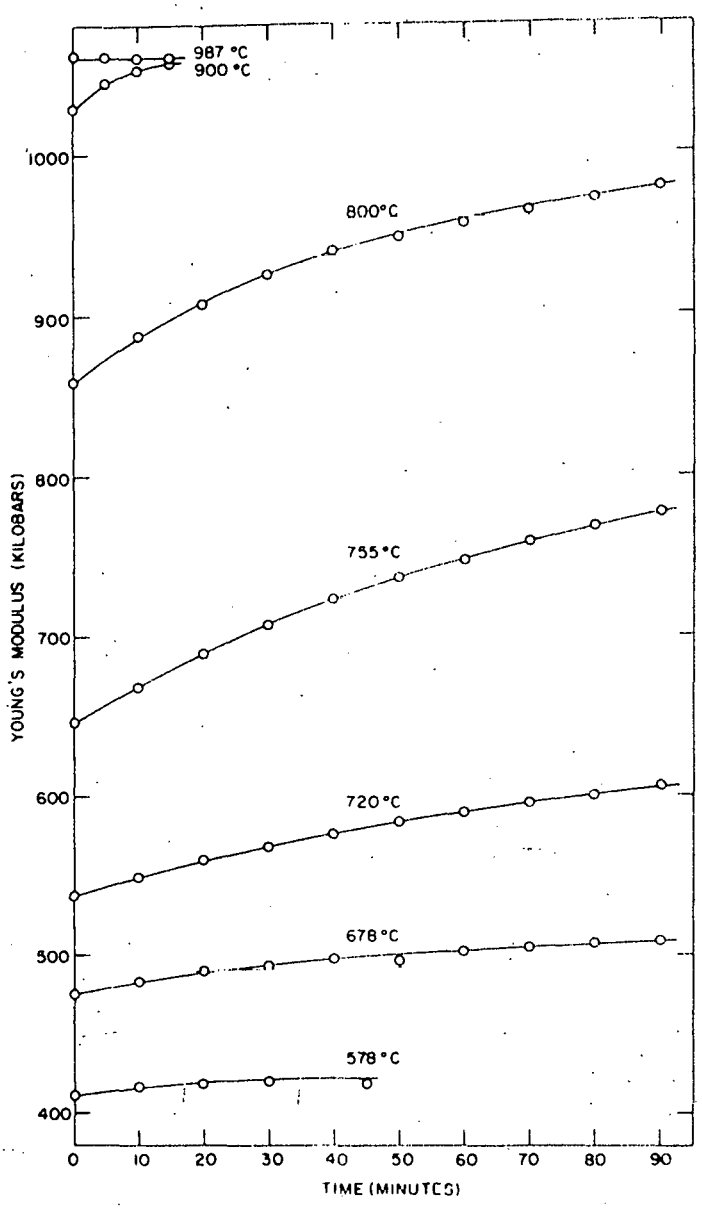

Figure 7. Young's modulus for sintered niobium pentoxide as a function of time at constant temperatures

Figure 8. Young's modulus for sintered niobium pentoxide as a function of time at 745°C

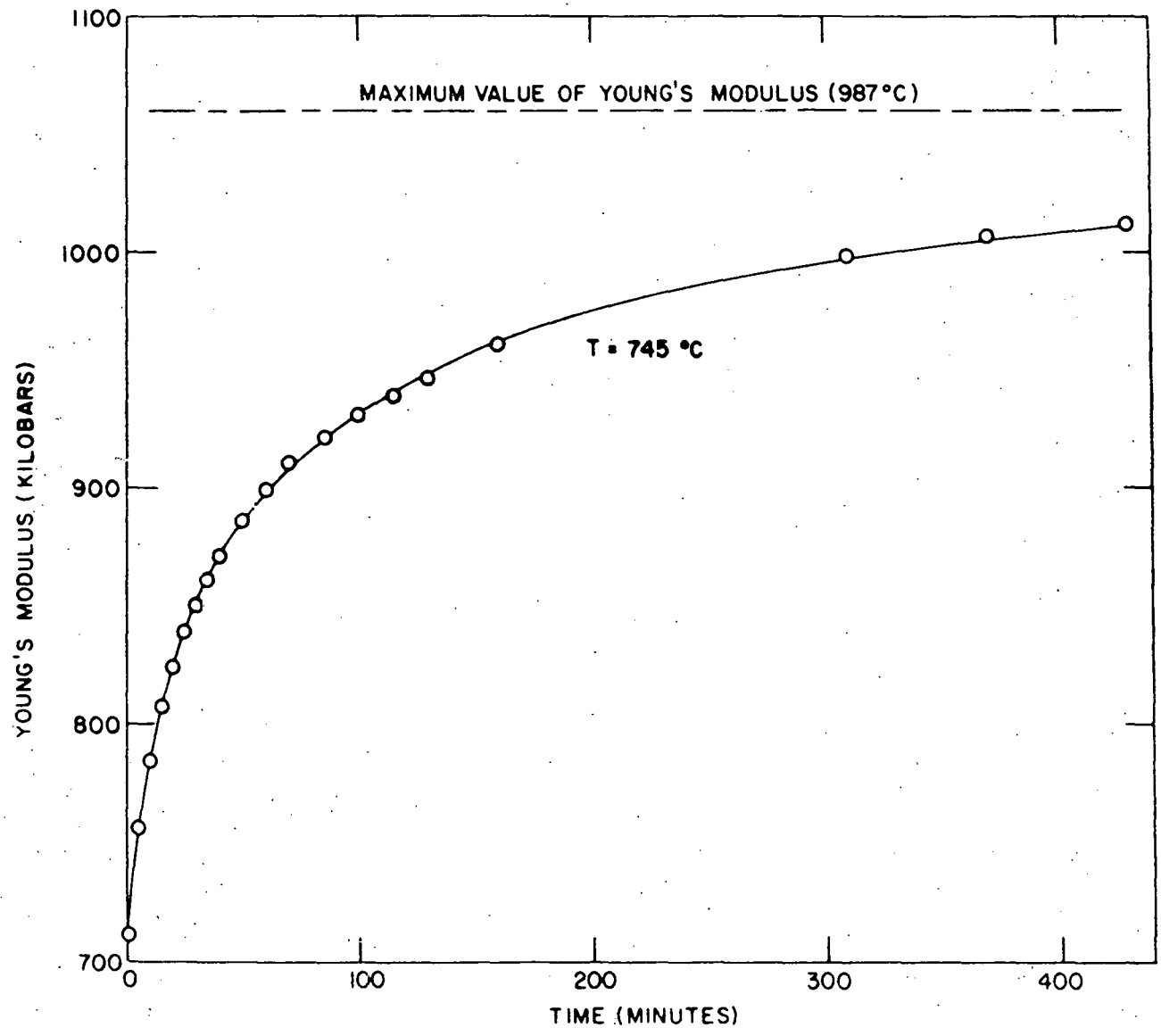
MAXIMUM VALUE OF YOUNG'S MODULUS (987°C)
T = 745 °C
YOUNG'S MODULUS (KILOBARS)
TIME (MINUTES)
1100
1000
900
800
700
0
100
200
300
400

Figure 9. Elevated temperature internal friction for sintered and hot-pressed niobium pentoxide

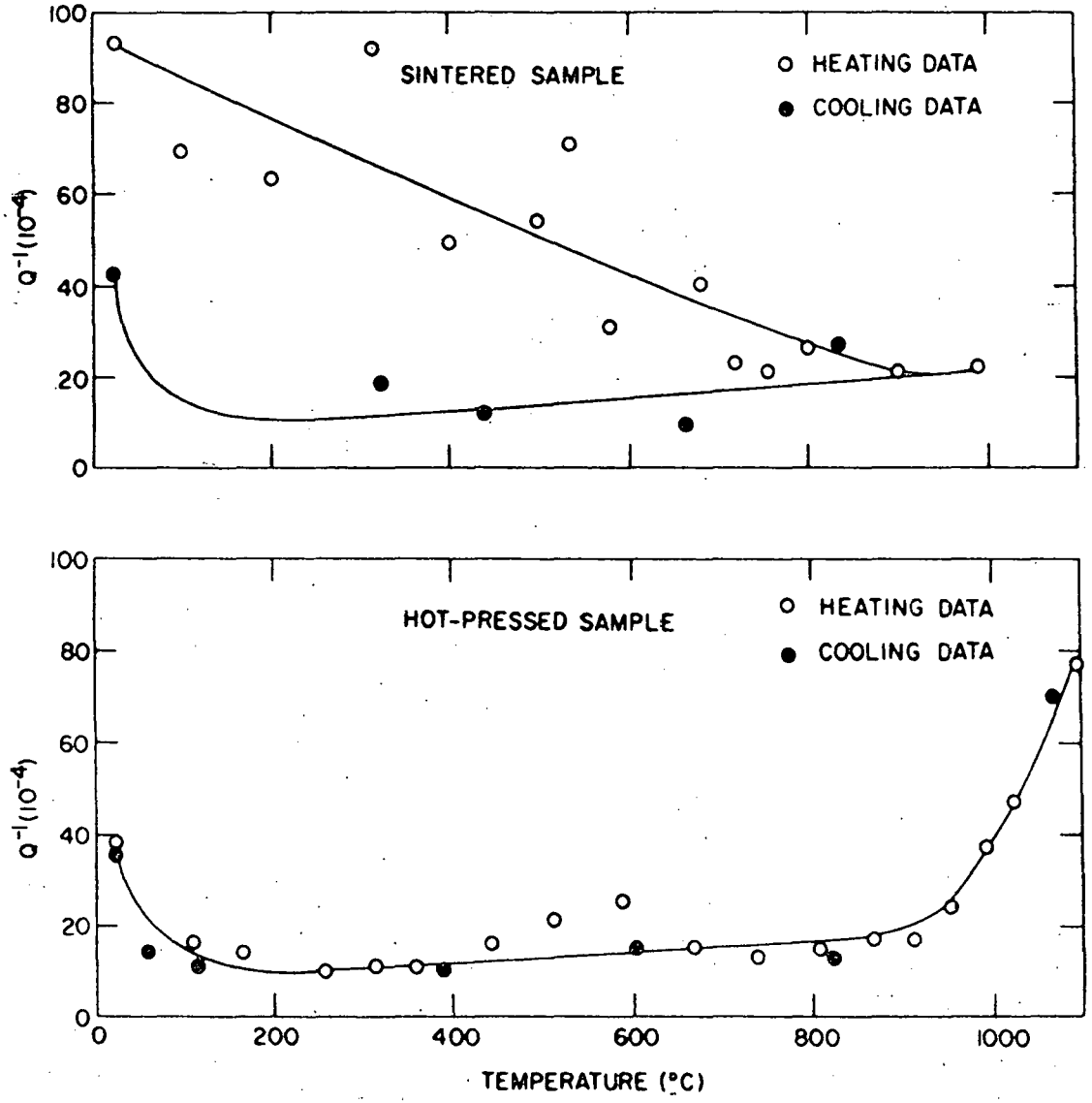
SINTERED SAMPLE
HEATING DATA
COOLING DATA
$Q^{-1}(10^{-4})$
100
80
60
40
20
0
HOT-PRESSED SAMPLE
HEATING DATA
COOLING DATA
$Q^{-1}(10^{-4})$
0
200
400
600
800
1000
TEMPERATURE (°C)

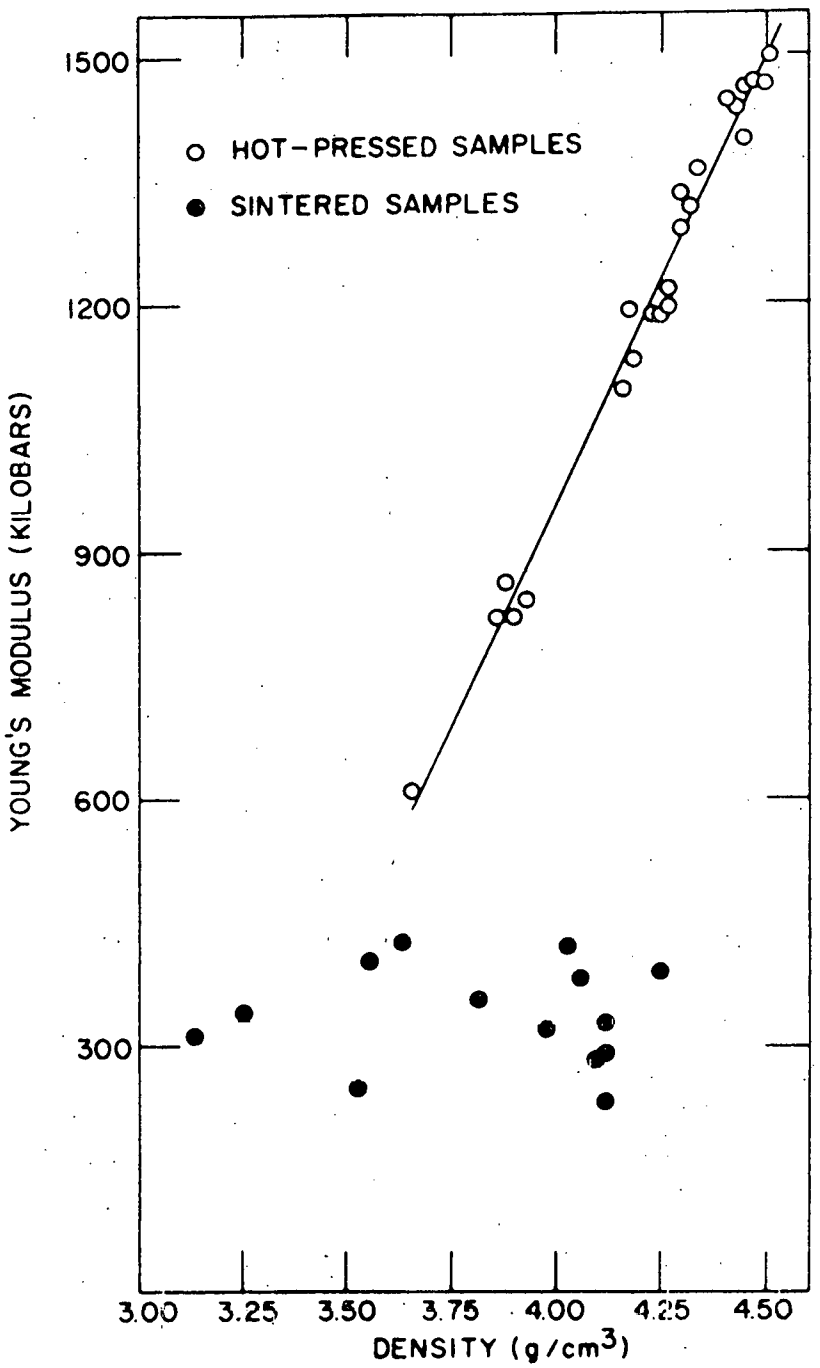

Figure 10. Room-temperature Young's modulus for sintered and hot-pressed niobium pentoxide as a function of density

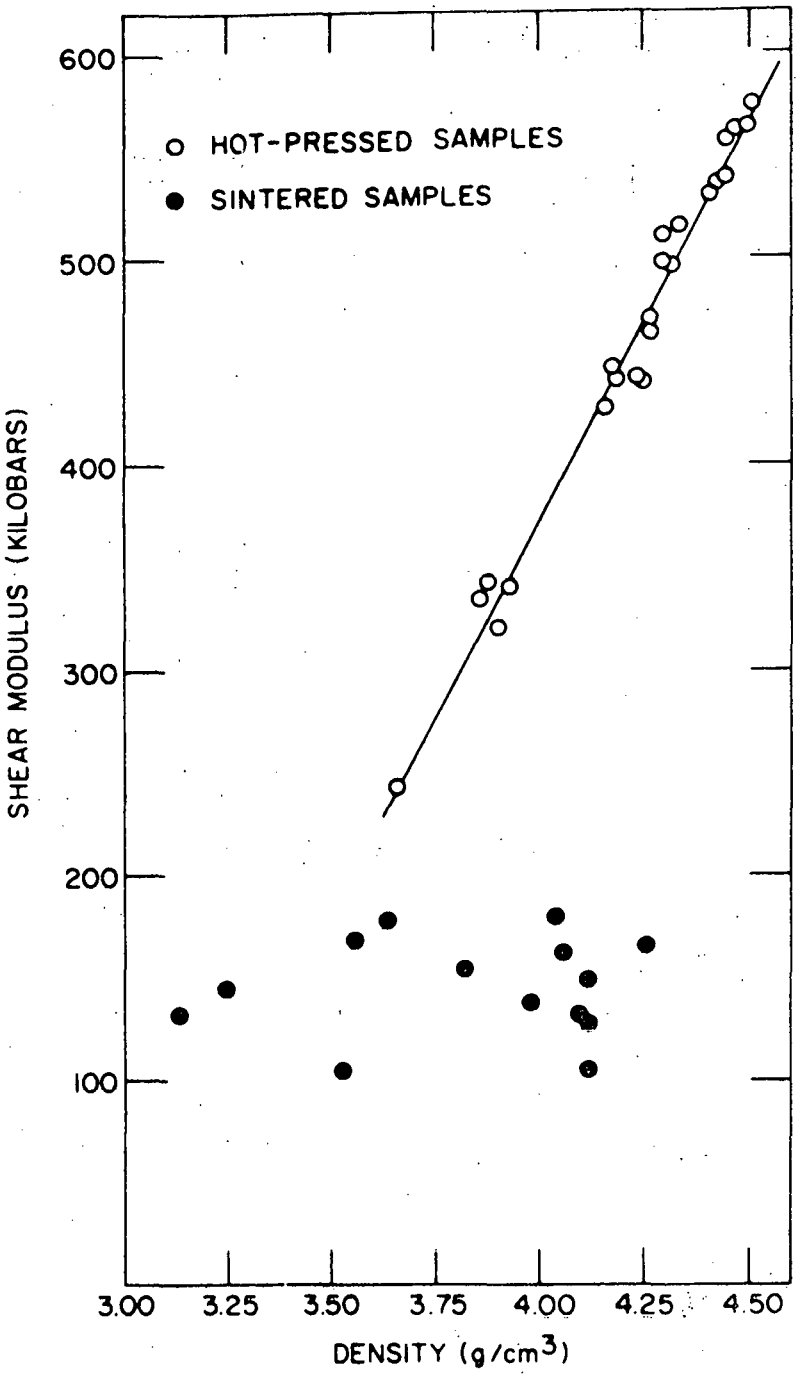

Figure 11. Room-temperature shear modulus for sintered and hot-pressed niobium pentoxide as a function of density

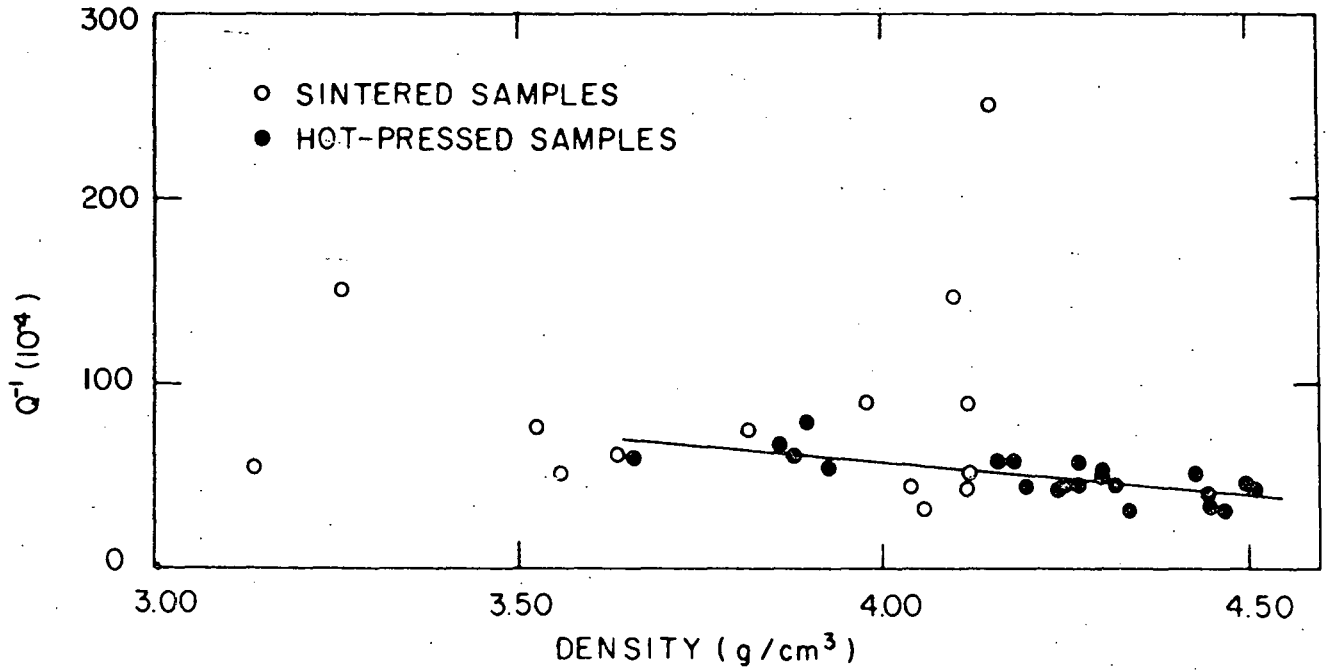

Figure 12. Room-temperature internal friction for sintered and hot-pressed niobium pentoxide as a function of density

Thermal Expansion of Niobium Pentoxide

Thermal expansion results obtained with the dilatometer are presented in Figures 13 through 22, while X-ray results are displayed in Figure 23. Figures 13 through 20 show expansion data for sintered samples varying in porosity from 37 to 10%. Figure 21 graphically represents measurements on a reoxidized hot-pressed sample, while Figure 22 shows the expansion behavior of the same bar after heat-treatment. The temperature range investigated was room temperature to 1000°C with several runs to 1200°C. Data were obtained on heating and cooling. Figure 23 gives the lattice parameters of monoclinic H-Nb_2O_5 as a function of temperature from room temperature to about 1350°C. The dilatometric data is tabulated in Appendix B and the X-ray data is in Appendix C.

Observation of Microstructure

Figures 24 through 28 are scanning electron micrographs (Cambridge model Mark II-A scanning electron microscope, Microanalysis Laboratory, Sperry Rand Corp.) of niobium pentoxide samples. Figure 24 shows the as-sintered surface of a sintered sample, while Figure 25 represents a diamond cut surface. Figures 26 and 27 display fracture surfaces of

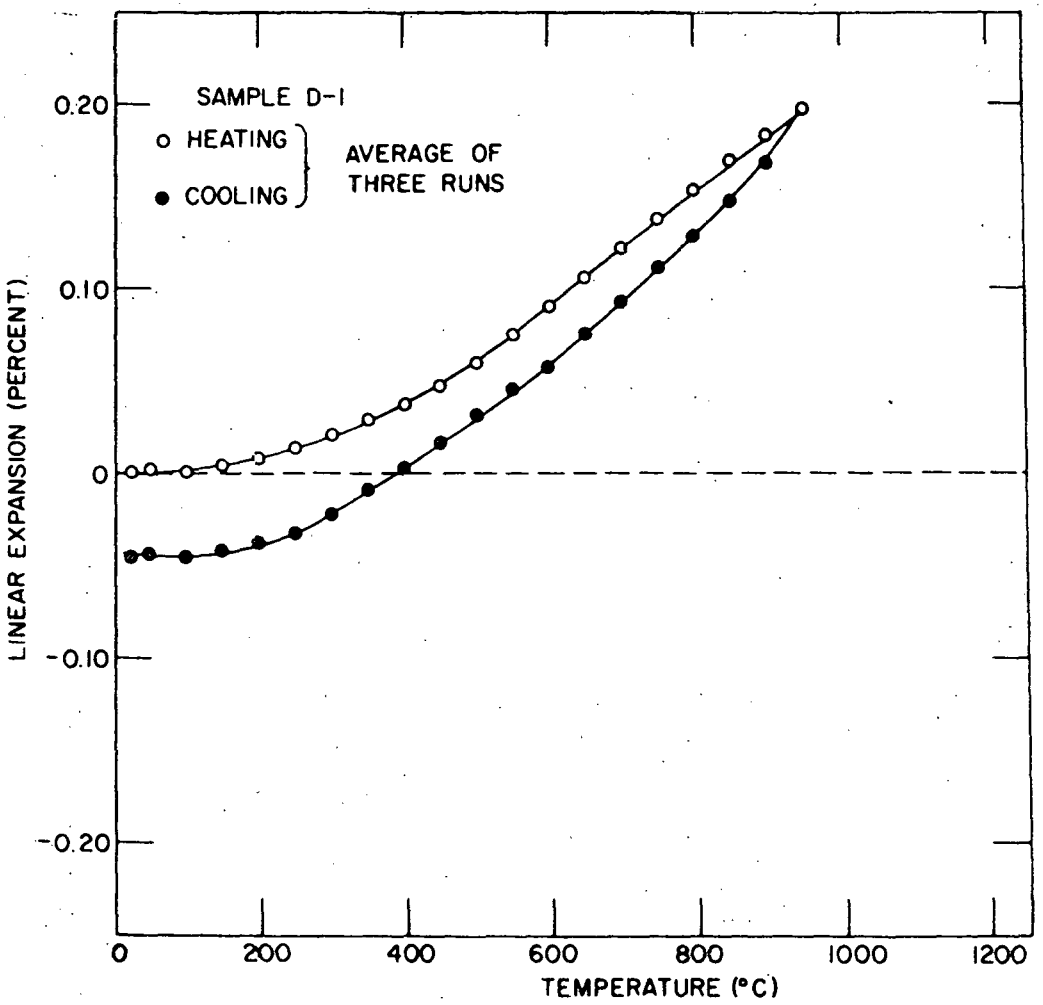

Figure 13. Linear thermal expansion of sintered niobium pentoxide, Sample D-1 (36.9% porosity)

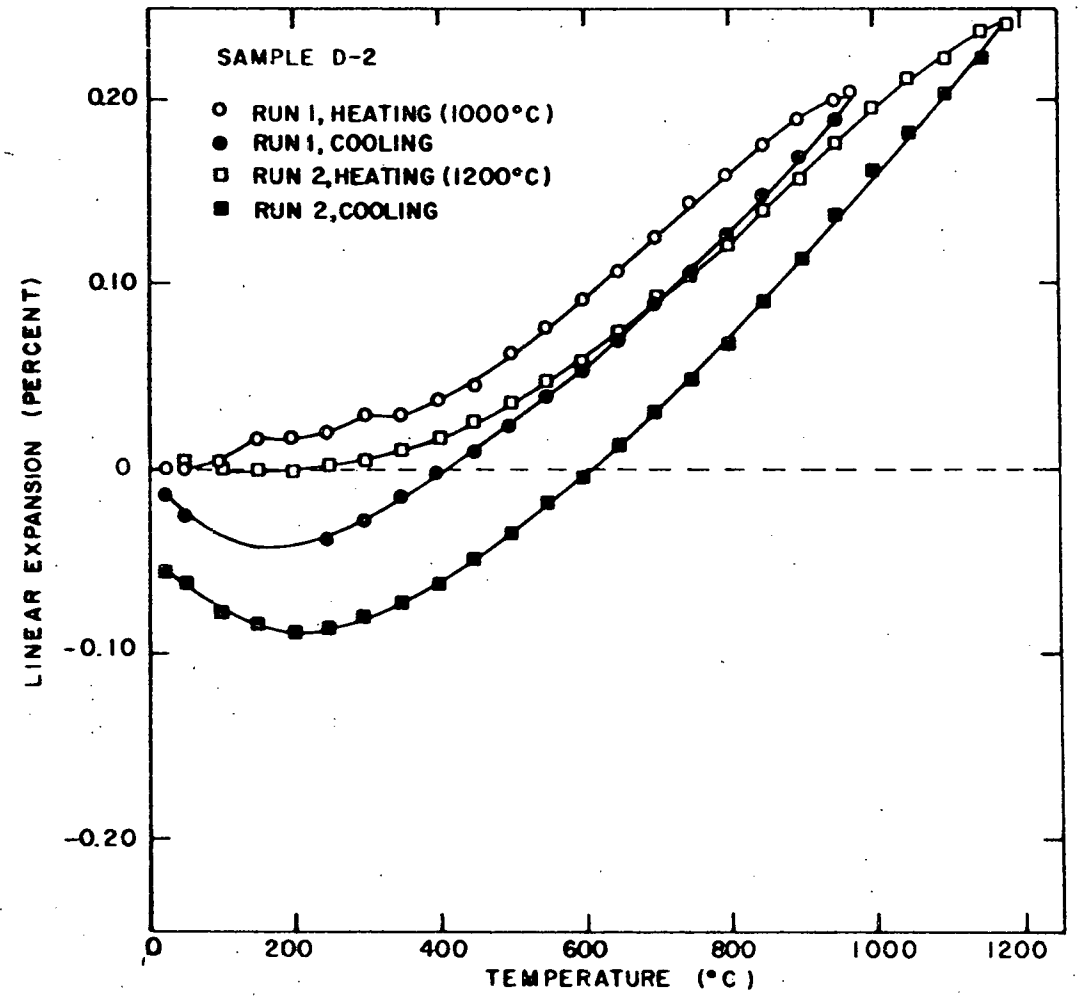

Figure 14. Linear thermal expansion of sintered niobium pentoxide, Sample D-2 (36.3% porosity)

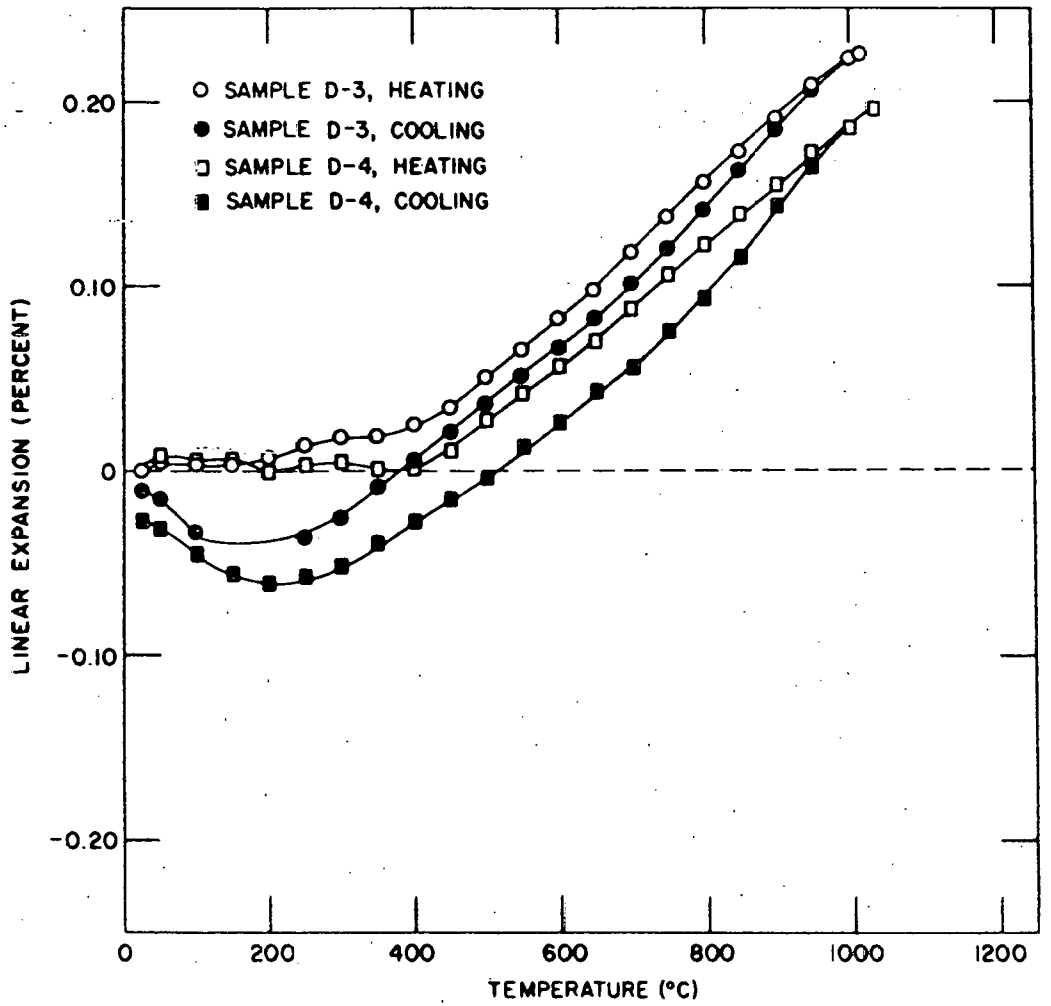

Figure 15. Linear thermal expansion of sintered niobium pentoxide, Samples D-3 (31.0% porosity) and D-4 (28.4% porosity)

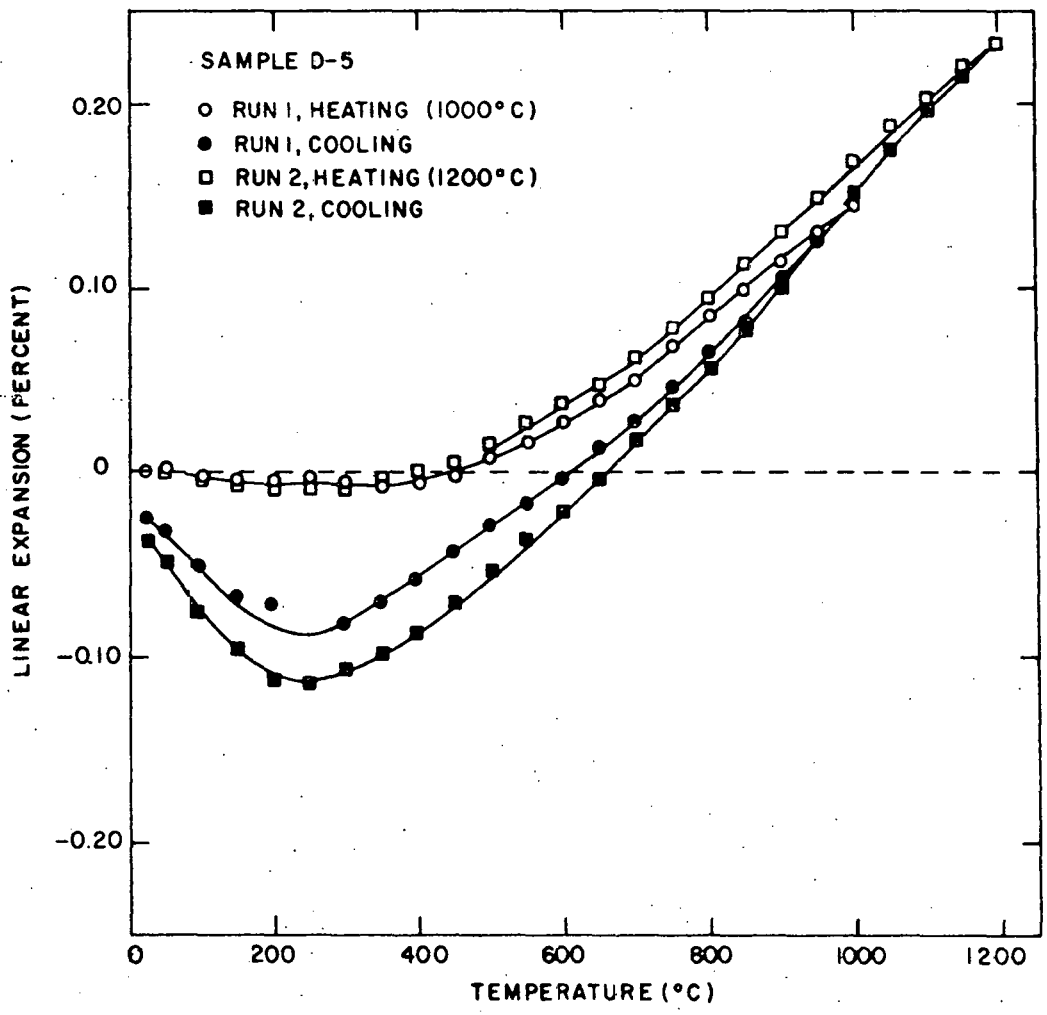

Figure 16. Linear thermal expansion of sintered niobium pentoxide, Sample D-5 (21.8% porosity)

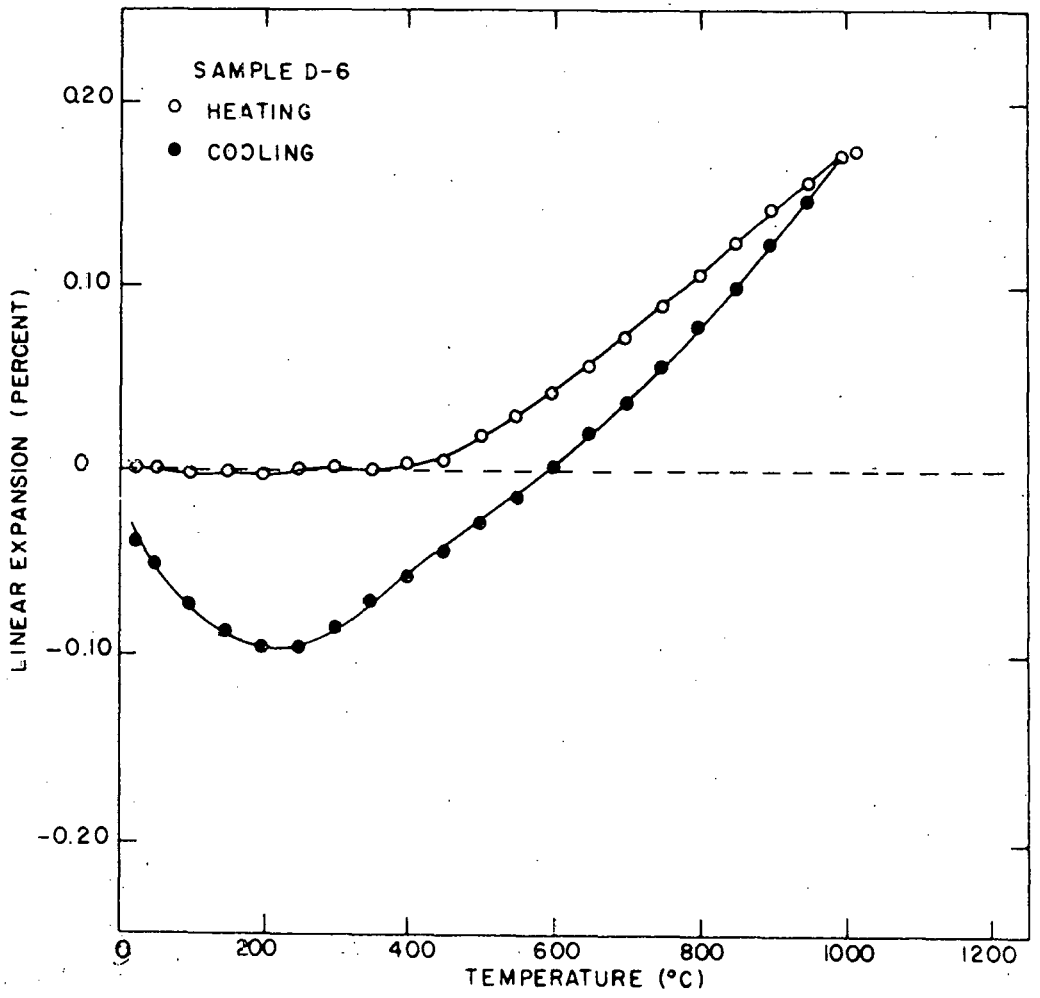

Figure 17. Linear thermal expansion of sintered niobium pentoxide, Sample D-6 (20.1% porosity)

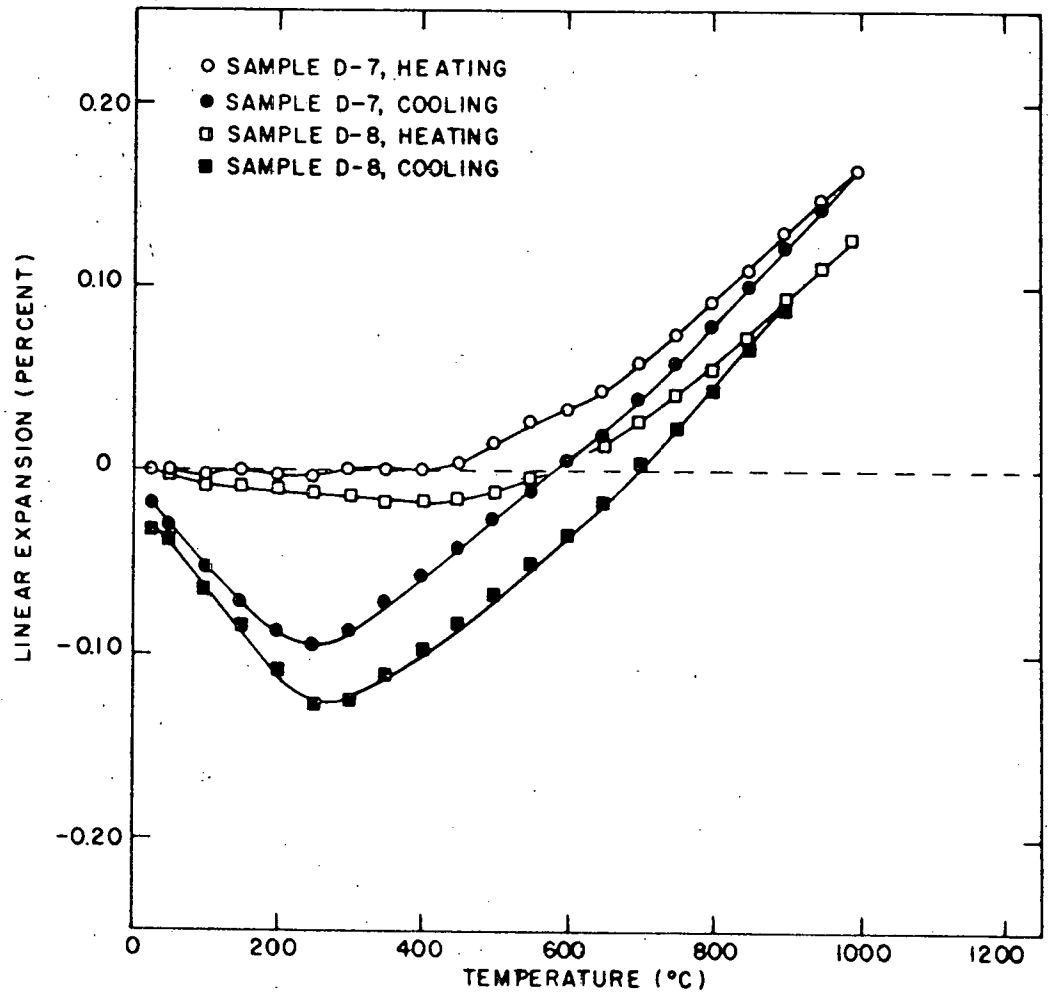

Figure 18. Linear thermal expansion of sintered niobium pentoxide, Samples D-7 (16.1% porosity) and D-8 (12.5% porosity)

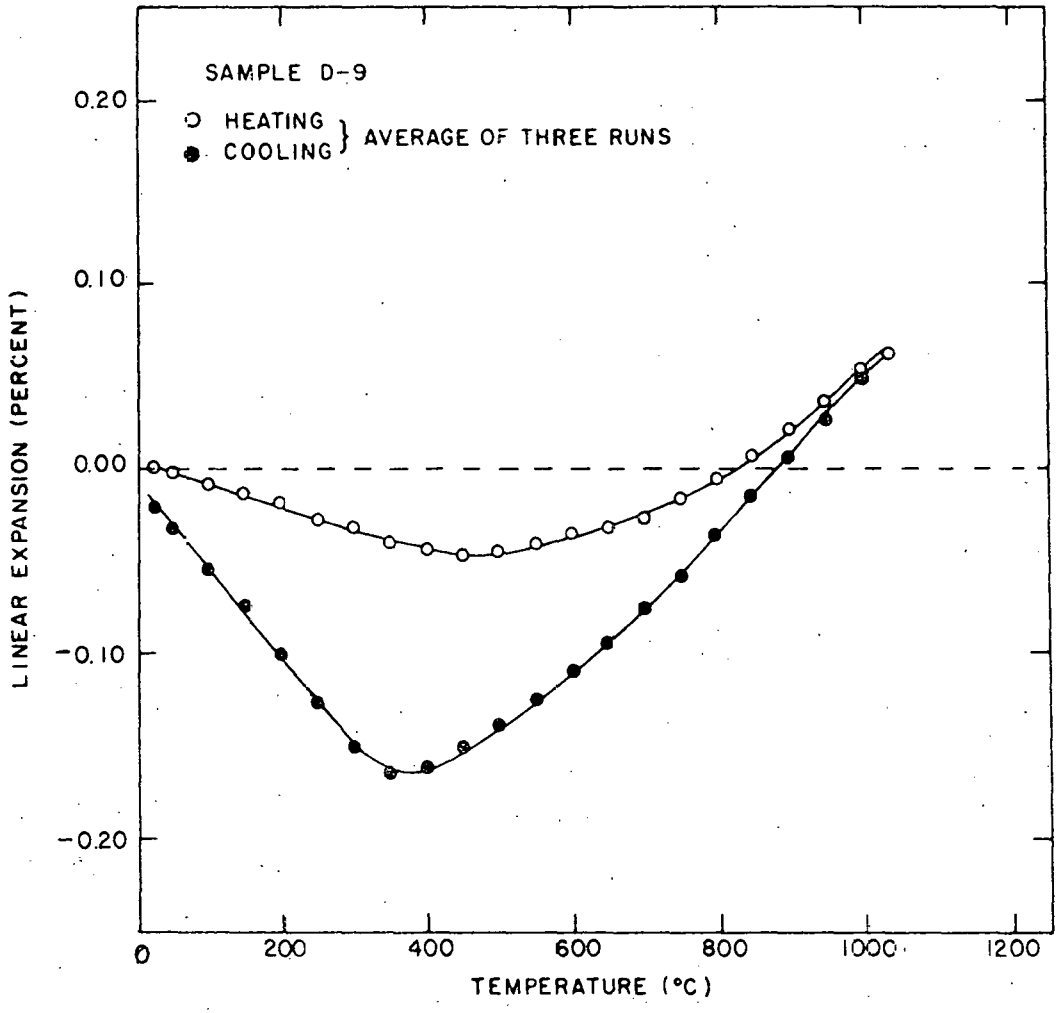

Figure 19. Linear thermal expansion of sintered niobium pentoxide, Sample D-9 (9.9% porosity)

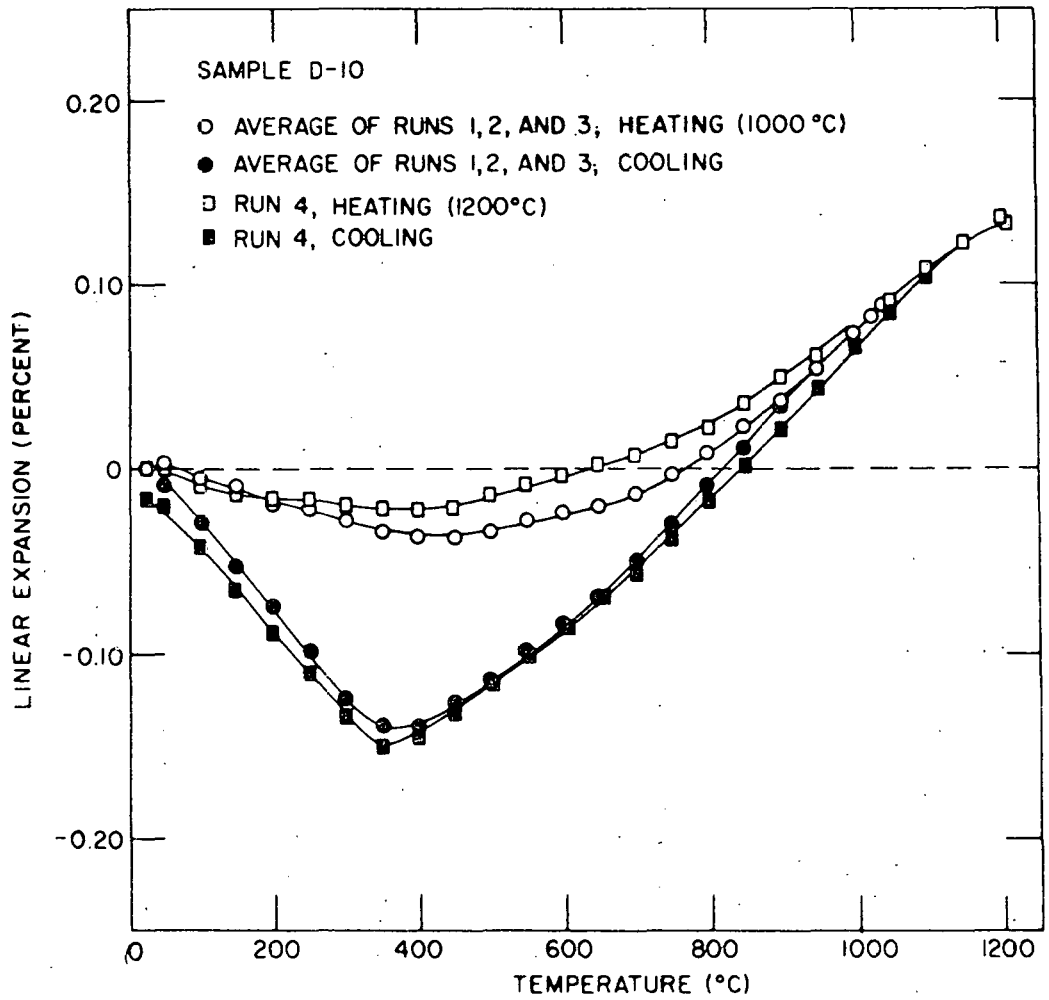

Figure 20. Linear thermal expansion of sintered niobium pentoxide, Sample D-10 (9.4% porosity)

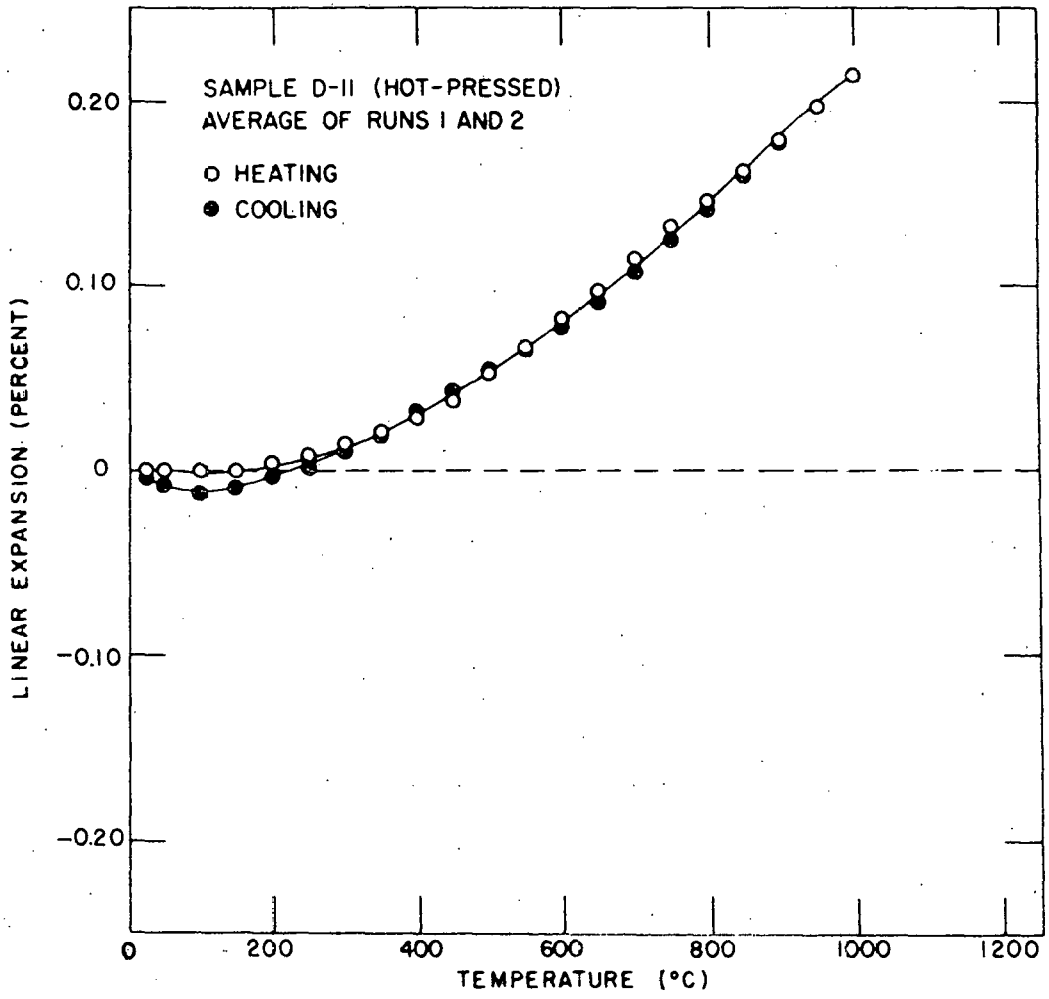

Figure 21. Linear thermal expansion of hot-pressed niobium pentoxide, Sample D-11 (16.5% porosity)

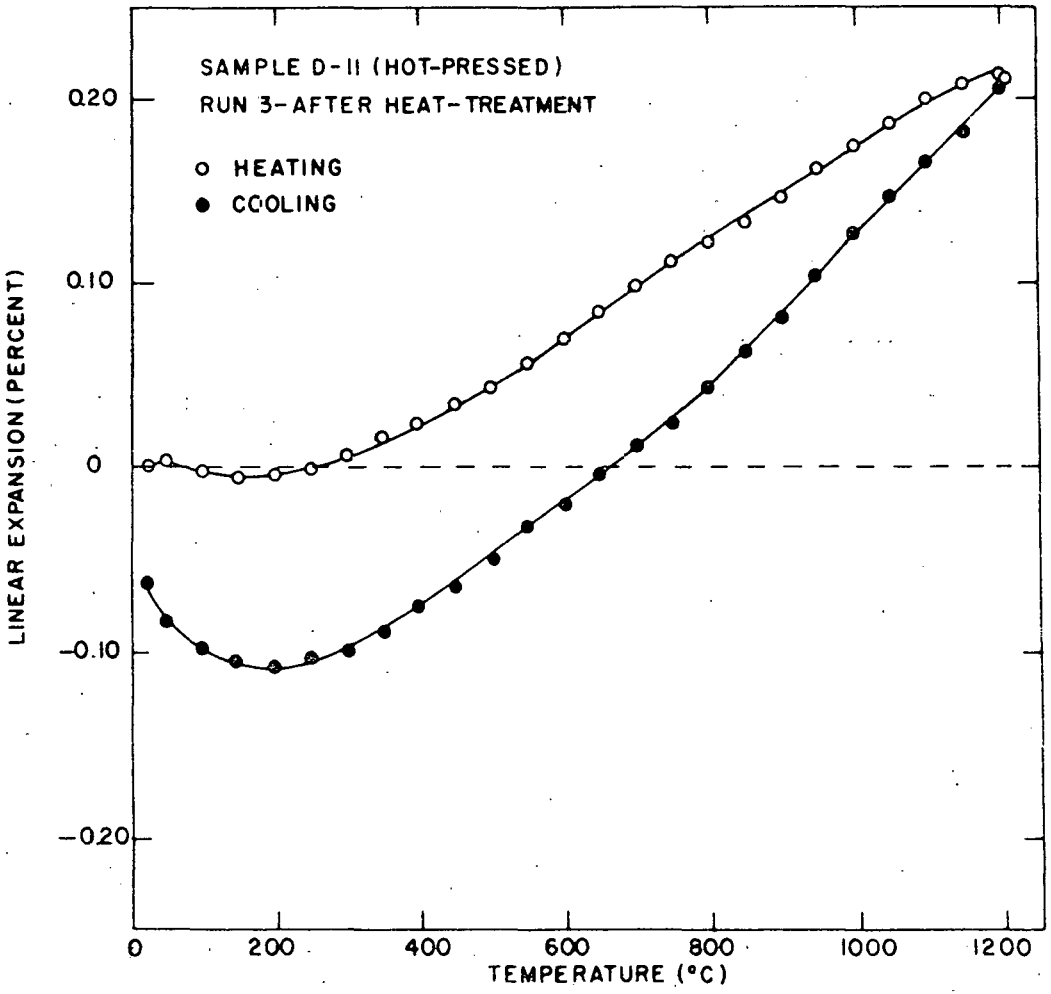

Figure 22. Linear thermal expansion of heat-treated, hot-pressed niobium pentoxide

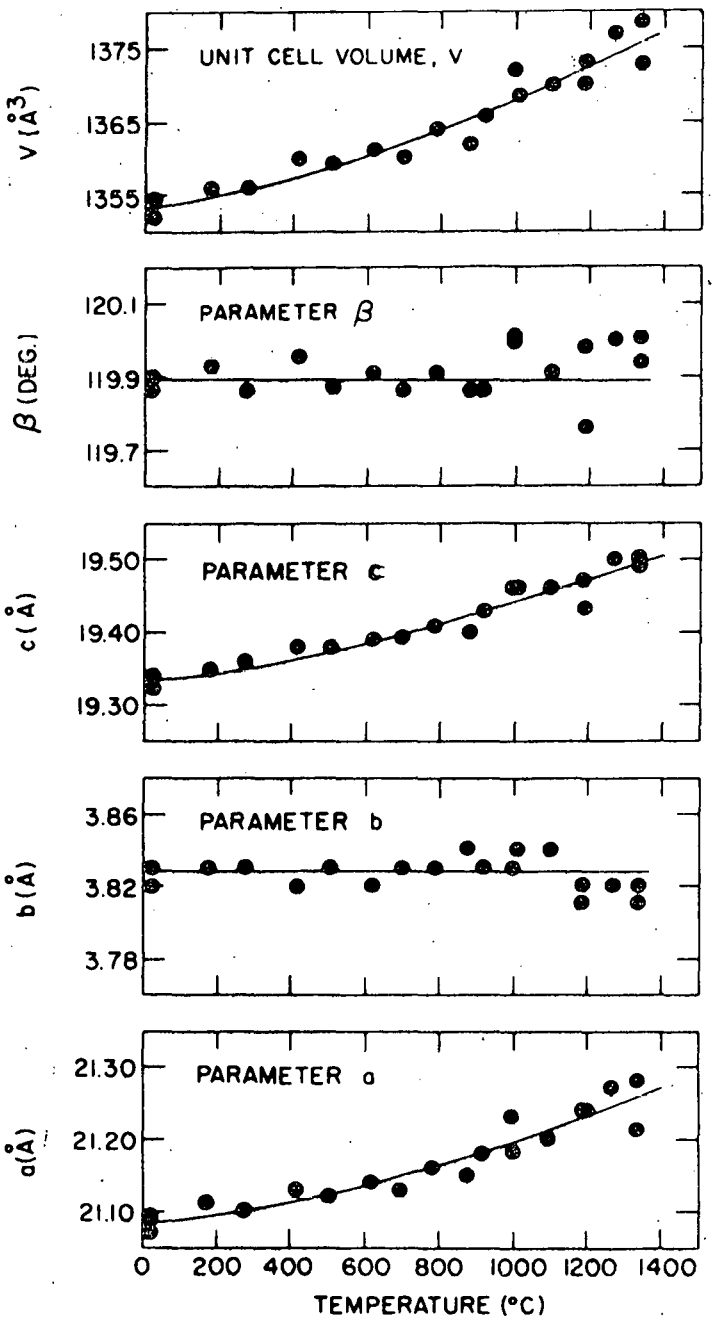

Figure 23. Elevated temperature lattice parameters for monoclinic niobium pentoxide

Figure 24a. Scanning electron micrograph of as-sintered surface of niobium pentoxide, Sample S-2; 690X

Figure 24b. Scanning electron micrograph of as-sintered surface of niobium pentoxide, Sample S-2; 2750X

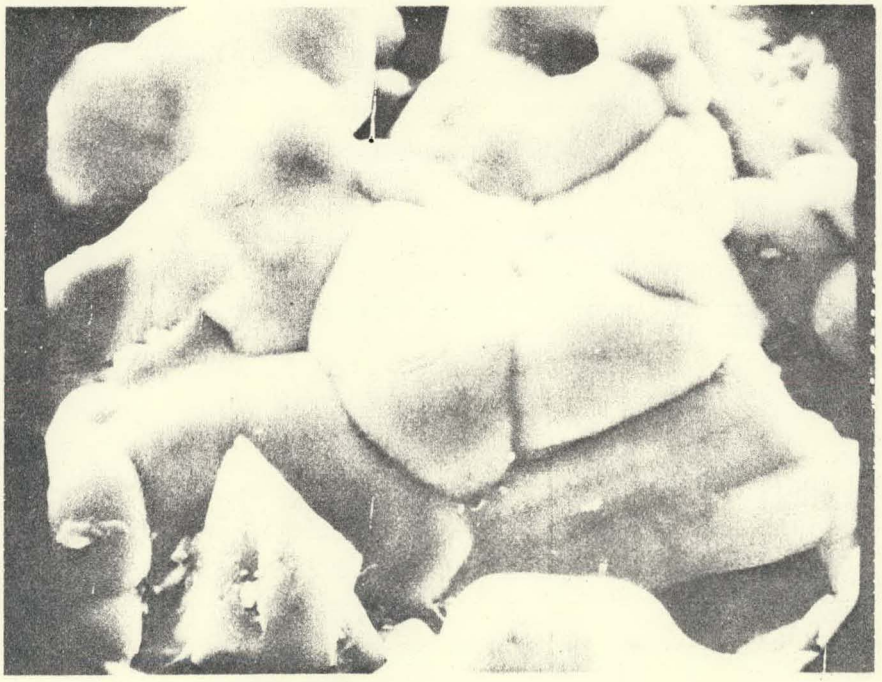

Figure 25a. Scanning electron micrograph of diamond-cut surface of sintered niobium pentoxide, Sample S-2; 650X

Figure 25b. Scanning electron micrograph of diamond-cut surface of sintered niobium pentoxide, Sample S-2; 2600X

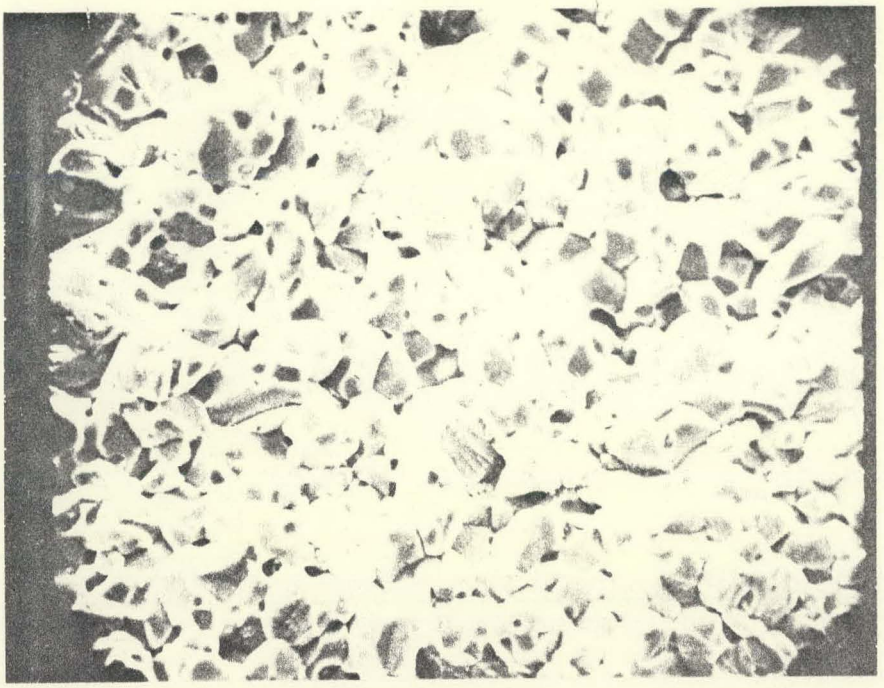

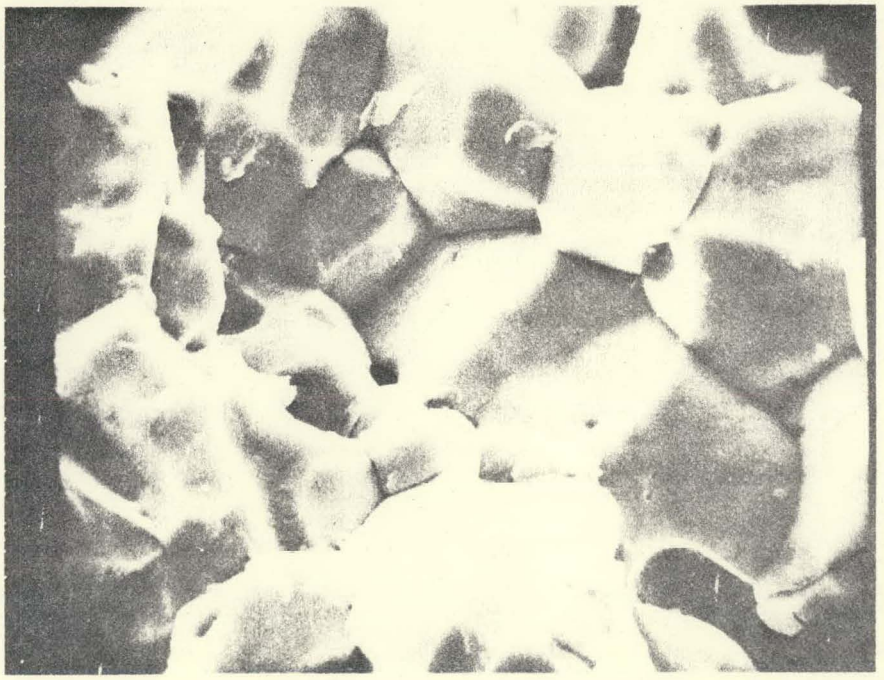

Figure 26a. Scanning electron micrograph of fracture surface of sintered niobium pentoxide, Sample S-2; 725X

Figure 26b. Scanning electron micrograph of fracture surface of sintered niobium pentoxide, Sample S-2; 2900X

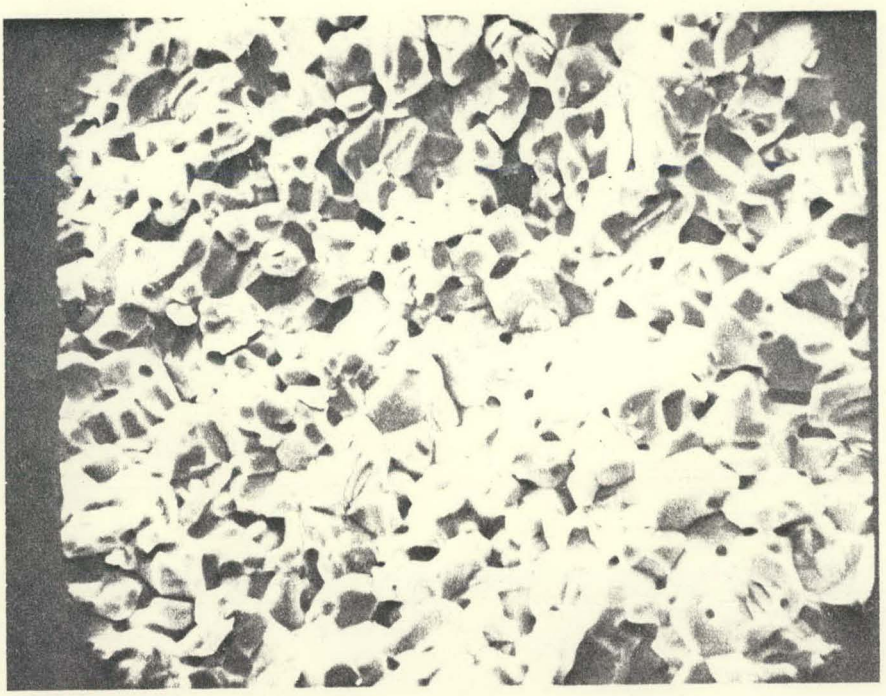

Figure 27a. Scanning electron micrograph of fracture surface of sintered niobium pentoxide, Sample S-2; 2700X

Figure 27b. Scanning electron micrograph of fracture surface of sintered niobium pentoxide, Sample S-3; 660X

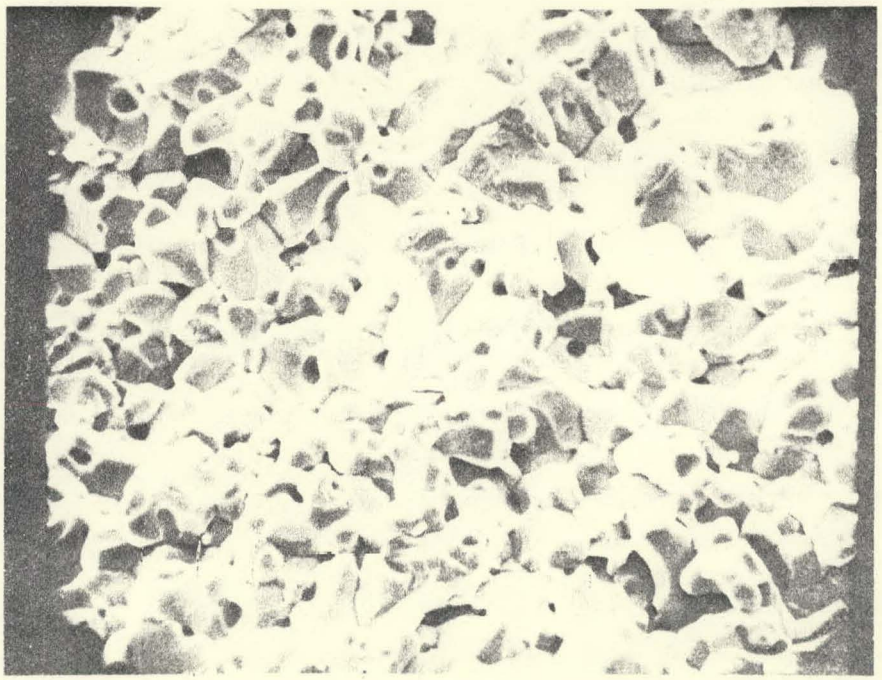

Figure 28a. Scanning electron micrograph of fracture surface of reoxidized hot-pressed niobium pentoxide, 610X

Figure 28b. Scanning electron micrograph of fracture surface of hot-pressed niobium pentoxide, 660X

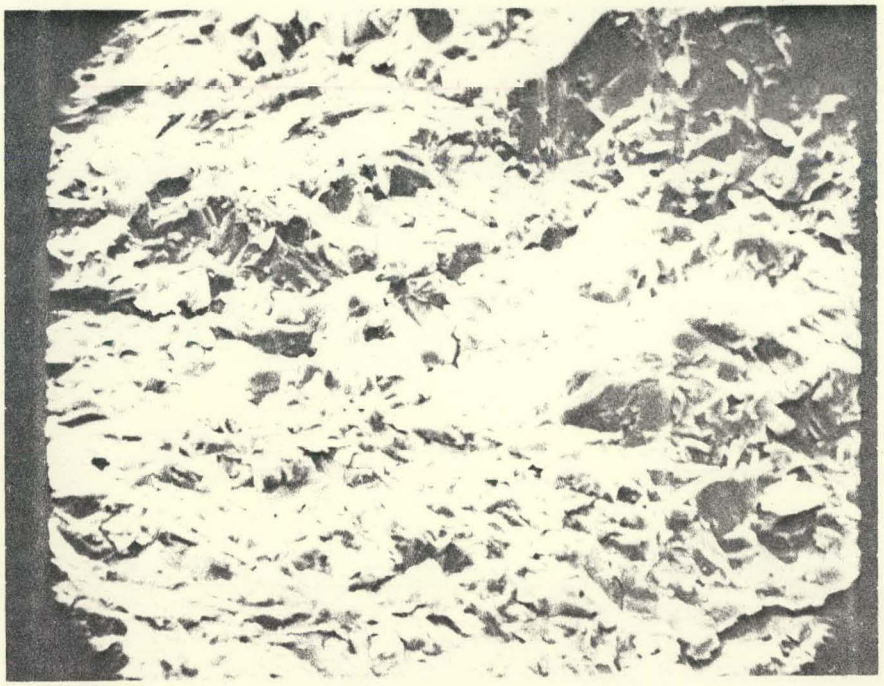

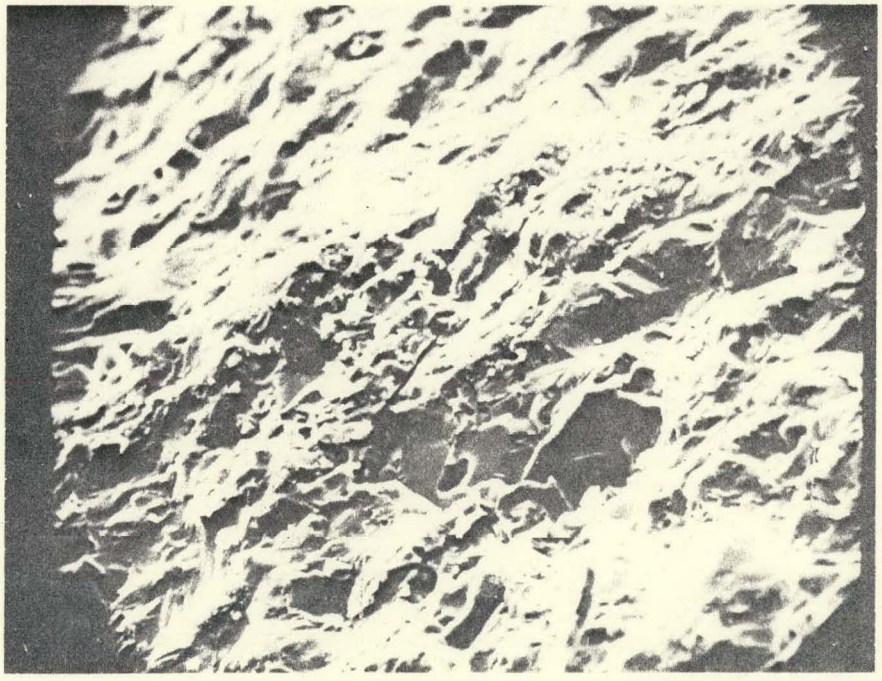

two different sintered samples, and Figure 28 reveals fracture surfaces for stoichiometric and nonstoichiometric hot-pressed samples.

Figure 29 shows two photomicrographs (Leitz Orthoplan microscope) of a polished section of a hot-pressed sample. The piece of sample was mounted, ground with 600 grit silicon carbide paper and polished lightly with fine alumina abrasives (Linde A, then Linde B). In order to reveal the grain structure, the sample was etched for 30 minutes in a 50% H_2SO_4-50% water solution at 200°C.

Figure 29a. Photomicrograph of grain structure of hot-pressed niobium pentoxide, 1000X

Figure 29b. Photomicrograph of grain structure of hot-pressed niobium pentoxide, 650X

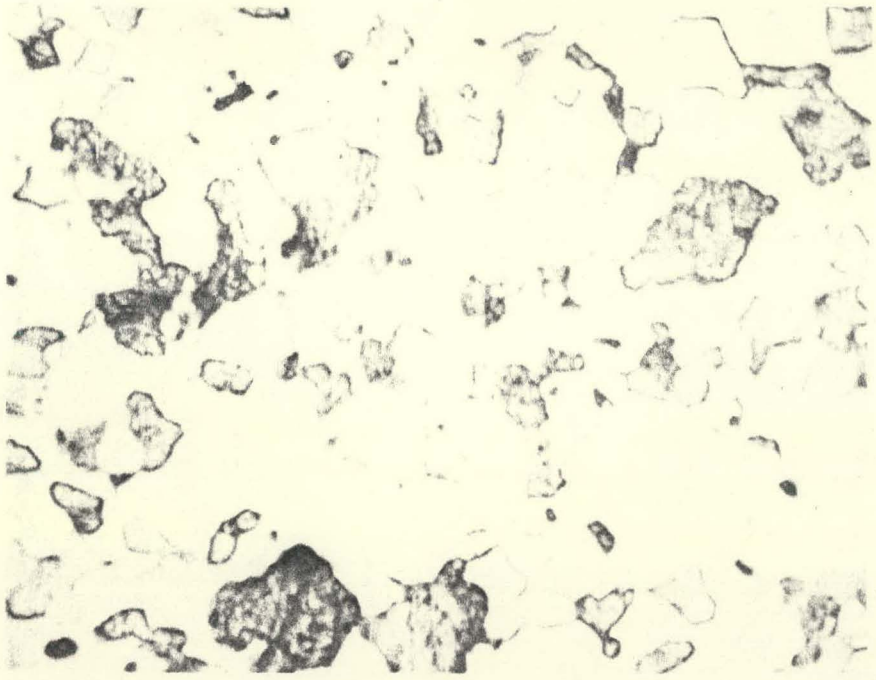

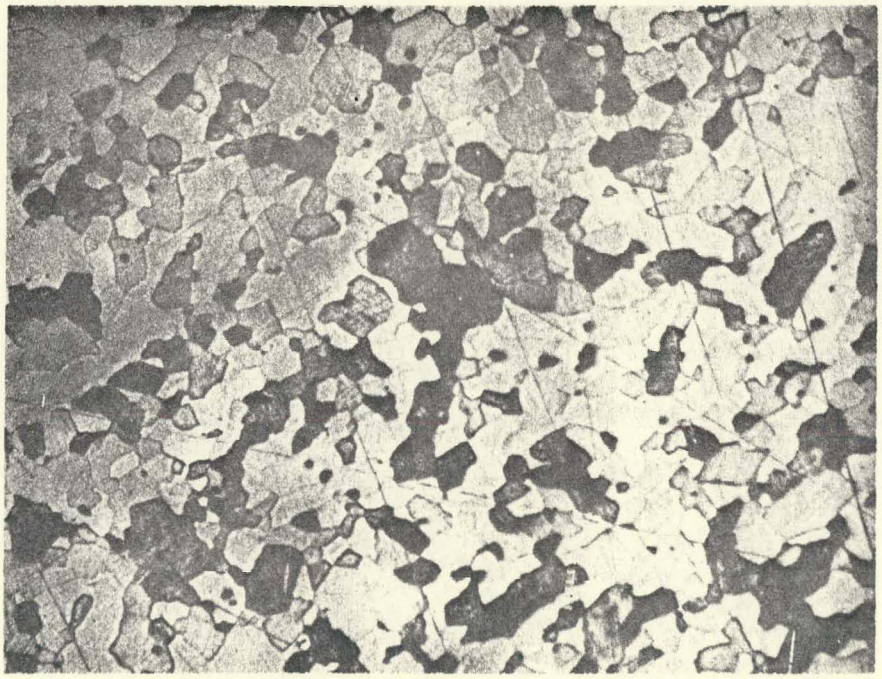

DISCUSSION

The purpose of this investigation, as pointed out in the Introduction, was to explain the anomalous increase in Young's modulus with temperature observed for polycrystalline niobium pentoxide. It is the author's opinion that the results presented in the previous section strongly support the hypothesis of this work; i.e., the unusual elastic behavior arises from the healing of internal microcracks present in the polycrystalline body. The remainder of the discussion will be devoted to explaining how the experimental data provides evidence for the existence of microcracks.

Figure 6 shows that the Young's modulus-versus-temperature data obtained in this study for sintered niobium pentoxide agrees well with that reported by Durbin et al. (1) and reproduces the anomalous behavior first observed by them. This investigation extends the previous work of Durbin et al. (1) by including cooling data which reveals the existence of a large hysteresis between the heating and cooling modulus-temperature curves. The high-temperature Young's modulus results presented here are analogous to those revealed in the literature for graphite (32,33) and nearly identical to elasticity results reported for magnesium dititanate and β-

eucryptite (48,49). As discussed in the Literature Review the elastic behavior of these other single-phase materials has been unequivocally attributed to the occurrence and recombination of internal microcracks.

Assuming that microcrack healing is the dominant mechanism involved, the high-temperature elastic behavior of sintered niobium pentoxide can be qualitatively described as follows: From room temperature to intermediate temperatures the thermal energy is insufficient for crack healing to occur and the modulus behaves as expected; i.e., it decreases slightly with increasing temperature. Between 500 and 600°C the healing of microcracks begins and the Young's modulus increases because the reduction in voidage gives the material increased volume to resist the applied dynamic stress. The modulus continues to increase with increasing temperature to a maximum value near 900°C. At this temperature the sample is crack-free and the Young's modulus, now two to three times its value at room temperature, decreases in a normal fashion from 900 to 1000°C. On cooling the modulus again behaves as it would for a crack-free material; that is, the modulus increases slightly with decreasing temperature. This continues down to about 400°C at which temperature the internal

stresses have reached sufficient magnitude to produce internal rupturing; the modulus then begins to decrease rapidly with decreasing temperature to a room-temperature value different than that observed at the beginning of the run. The difference in room-temperature values will be discussed later.

Figure 6 also reveals that the elastic behavior for a hot-pressed sample of niobium pentoxide is not anomalous: there is no increase in Young's modulus with temperature and no hysteresis effects are observed. It is possible to infer from these results that the hot-pressed sample is devoid of internal microcracks. In addition, Figure 6 shows that at high temperatures the Young's moduli of the hot-pressed and sintered samples approach the same value. Using an accepted linear relationship (5) to compensate for the effect of normal porosity on the elastic modulus of the more porous sintered bar, the Young's modulus for the sintered bar is equal to 1237 kilobars at 1000^{o}C while the value for the hot-pressed sample at the same temperature is 1267 kilobars.

The three Young's modulus-temperature runs shown in Figure 6 for the sintered sample were conducted on one specimen. A reason for the curves failing to coincide is that a different heating rate was used for each run. The heating

rate has an effect on the data since the Young's modulus changes with time at temperatures between 580 and 900°C. For runs 1 and 3 the average heating rate from room temperature to 1000°C was 70°C per hour while for run 2 the rate was 150°C per hour.

Figures 7 and 8 show how the Young's modulus varies with time at constant temperatures in the range 578 to 900°C. The results in Figure 8 were obtained in a separate run by heating the furnace as rapidly as possible (total time: one hour) to 745°C and then gathering data for seven hours. At the end of this time period the Young's modulus was still increasing but at a much slower rate. It is apparent that the Young's modulus changes more rapidly with time as the temperature is increased. This observation led to calculating an activation energy for the proposed crack-healing process by using the Arrehenius equation

$$\text{rate} = \text{constant} \times e^{-Q/RT} \qquad (9)$$

Since the exact mechanism of the crack-healing process is unknown, we cannot, a priori, write a rate expression for the change of Young's modulus with time, dE/dT. The best that we can do is to examine the data and present an empirical rate expression. The Young's modulus-versus-time curves appear to

be parabolic. A rate equation consistent with this observation is

$$dE/dt = k/E \tag{10}$$

where k is a rate constant. This equation has some physical significance since dE/dt should be proportional to the concentration of microcracks which in turn is inversely proportional to E. Using Equation 10, the initial rate, k_i, of the proposed crack-healing process was determined at each temperature by computing $E_i(dE/dt)_i$ where E_i is the Young's modulus at time equal zero and $(dE/dt)_i$ is the initial slope of the Young's modulus-versus-time curve. Figure 30 is an Arrehenius plot of k_i versus 1/T. A straight line was fit to the data by a least-squares technique and the slope of this straight line was used to compute an activation energy of 16.6 k-cal/mole with a standard error of estimate of 0.8 k-cal/mole.

The shear modulus for sintered niobium pentoxide was also found to increase with increasing temperature; however, because of experimental difficulties, only a limited amount of data was obtained. The results, in the form of the relative shear modulus, G_T/G_{RT} (where G_T is the shear modulus at temperature T and G_{RT} is the value at room temperature), are

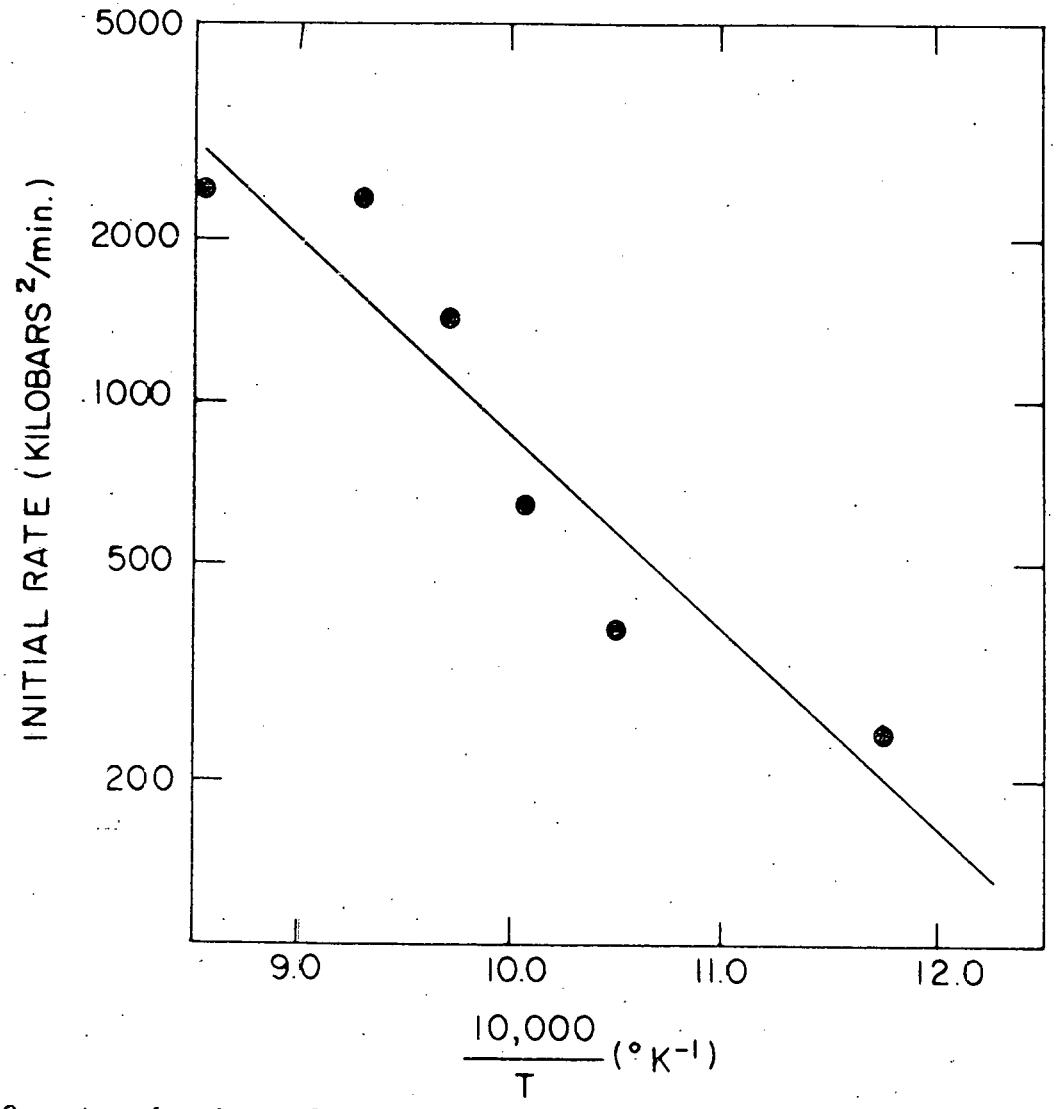

Figure 30. Arrehenius plot for the initial rate of the proposed crack-healing process in sintered niobium pentoxide

presented in Table 5 along with, for comparative purposes, the relative Young's modulus, E_T/E_{RT}. The overall increase in Young's modulus is greater than the increase in the shear modulus; thus, the computed Poisson's ratio, included in Table 5, also increases with temperature.

Table 5. Relative shear modulus, Young's modulus, and Poisson's ratio at elevated temperatures for sintered niobium pentoxide

Temp. (°C)	Relative shear modulus, G_T/G_{RT}	Relative Young's modulus, E_T/E_{RT}	Poisson's ratio
25	1.000	1.000	0.174
112	.967	.964	.170
203	.952	.953	.175
315	.942	.942	.174
402	.912	.905	.165
499	.907	.898	.162
537	.928	.920	.164
578	.970	.952	.152
678	1.16	1.16	.174
720	1.38	1.38	.174
755	1.72	1.77	.208
800	2.10	2.25	.258
900	2.21	2.41	.280

High-temperature internal friction results shown in Figure 9 are also consistent with the microcrack hypothesis. Others (58,71) have indicated that the presence of internal cracks has a large effect on the damping capacity (internal friction) of a material. The upper half of Figure 9 reveals

that the internal friction, Q^{-1}, for the sintered sample decreases somewhat erratically with increasing temperature but shows less scatter above 600°C and on cooling. A hysteresis effect and a decrease in internal friction with time at constant temperature were also observed. It seems reasonable to assume that the decrease in internal friction is due to crack healing. When the cracks disappear there are fewer "obstacles" within the solid body to dissipate vibration energy; consequently, the damping capacity decreases. The magnitude of internal friction on cooling is lower because the sample, on cooling, is crack-free down to about 400°C. Once again a large difference between the properties of the sintered and hot-pressed samples is apparent. The lower half of Figure 9 shows that the internal friction for the hot-pressed bar decreases from room temperature and then remains fairly constant up to 1000°C at which temperature a large increase in the internal friction occurs. This rapid rise is probably due to the onset of grain boundary relaxation. Analogous high-temperature internal friction behavior observed for other polycrystalline ceramic oxides (53,72,73) has been attributed to this phenomenon. No hysteresis effect was found for data obtained on cooling the hot-pressed sample.

The results shown in Figure 9 indicate some evidence for the presence of the near-room-temperature internal friction peak reported by Makkay and Fine (8).

Room-temperature Young's modulus, shear modulus, and internal friction results (shown in Figures 10 through 12) also reveal a large difference in the values for sintered and hot-pressed samples; e.g., at room temperature the Young's modulus for a sintered sample with a density of 4.20 g/cm^3 is 1/4 of the value for a hot-pressed sample of nearly the same density. The difference between the two types of samples is further reflected in calculated values for Poisson's ratio: the mean value of μ for all the sintered samples is 0.17 ± 0.02, while the mean value for the hot-pressed material is 0.30 ± 0.02. The results presented here are consistent with the discrepancy mentioned in the Literature Review between the Young's modulus reported by Durbin et al. (1) for sintered niobium pentoxide and that given by Douglass (6) for the hot-pressed oxide.

The room-temperature data for the sintered samples display a large amount of scatter. One factor responsible for this is the observation that for these samples the Young's modulus and internal friction vary with time at room tempera-

ture. The Young's modulus was found to decrease and the internal friction to increase until, after several days exposure to the laboratory atmosphere, it was impossible to find the resonant frequency for the sample. It was assumed that this phenomenon was related to the absorption of water vapor and all room-temperature measurements were subsequently conducted after drying the sample in a drying oven at 150°C for 24 hours and then allowing the sample to cool for 15 minutes before determining data. Following this procedure it was possible to reproduce within 5% the values for a given bar. This unusual room-temperature behavior was not observed for the hot-pressed samples.

Straight lines were fit by a least-squares technique to the room-temperature elastic moduli and internal friction data for the hot-pressed samples. The computed equation for the Young's modulus as a function of density is

$$E = -3339 + 1073\rho \pm 34 \text{ kilobars} \qquad (11)$$

where ρ is the bulk density in g/cm^3 and $\pm$ 34 is the standard error of estimate. The equation for the shear modulus-density line is

$$G = -1169 + 385\ \rho \pm 13 \text{ kilobars} \qquad (12)$$

and the equation describing the internal friction results is

$$Q^{-1}(\text{in units of } 10^{-4}) = 204 - 36\rho \pm 8 \qquad (13)$$

Several previous investigations (5,74,75,76,77) have shown that for polycrystalline oxides there is a linear variation of elastic moduli with sample density. A linear relation has also been suggested (58) for internal friction-density data.

As discussed previously, there is controversy in the literature concerning whether or not departure from the stoichiometric composition causes the appearance of different phases of niobium pentoxide. This raises the question as to whether or not the nonstoichiometric composition of the hot-pressed samples influences the elastic modulus and internal friction data. This author's opinion is that there may be a number of different phases in the reduced, hot-pressed samples but the phases are probably very similar and have little, if any, effect on the elastic properties of the polycrystalline solid. Some experimental evidence in support of this contention follows.

An attempt was made to determine Young's modulus as a function of deviation from stoichiometry by progressively reoxidizing a reduced hot-pressed sample and measuring the room-temperature modulus as the sample approached the stoi-

chiometric composition. Limited results were obtained because only one highly reduced sample withstood the reoxidation process without becoming saturated with large, readily discernible cracks. The data for this one sample appear in Table 6.

Table 6. The effect of deviation from stoichiometry on the Young's modulus for a hot-pressed sample of niobium pentoxide

Composition	Young's modulus (kilobars)
$Nb_2O_{4.966}$	1471
$Nb_2O_{4.985}$	1469
$Nb_2O_{5.000}$	1475

Lightly reduced samples, that is, those with (5-x) in Nb_2O_{5-x} equal to or greater than 4.993, showed no change in modulus or internal friction on reoxidation. Another indication that the elastic modulus for the hot-pressed material varies little with deviations from stoichiometry is that among the hot-pressed bars there are samples that have nearly the same density and the same elastic moduli, but quite different nonstoichiometric compositions; e.g., Sample No. 19 has a density of 4.449 g/cm^3, a Young's modulus equal to 1447 kilobars and a composition corresponding to $Nb_2O_{4.935}$,

whereas Sample No. 20 with a composition of $Nb_2O_{4.957}$ and density of 4.454 g/cm^3 has a Young's modulus equal to 1397 kilobars. Similar observations apply to the internal friction data.

The room-temperature X-ray diffraction pattern for highly reduced hot-pressed samples shows the same peaks as the pattern for the stoichiometric material; however, the 2θ values corresponding to the peaks are all shifted in either direction with the largest shift occurring in the $\bar{1}05$ peak which changes from d equal to 3.639Å in the stoichiometric material to d equal to 3.584Å degrees in the nonstoichiometric powder. The X-ray pattern for a reoxidized hot-pressed sample is identical to that for the as-received powder of niobium pentoxide.

Assuming that the theoretical density of the nonstoichiometric material is the same as that for the stoichiometric material and assuming that deviations from stoichiometry have little effect on the elastic properties, it is possible to estimate the isotropic elastic moduli for pore-free, theoretically dense niobium pentoxide. The computations were made by substituting the theoretical density of 4.55 g/cm^3 in Equations 11 and 12: the results for Young's modulus, shear

modulus, and Poisson's ratio are 1545 kilobars, 585 kilobars, and 0.32, respectively.

Coupled with the unusual elastic properties for niobium pentoxide are equally unconventional thermal expansion properties which can also be explained on the basis of microcrack occurrence and recombination. Figures 13 through 20 show linear thermal expansion results obtained on the dilatometer for sintered samples of niobium pentoxide while Figure 21 displays similar data for a reoxidized hot-pressed sample. For all of the sintered bars a hysteresis between heating and cooling data is quite evident; whereas, there are no hysteresis effects observed for the hot-pressed bar prior to heat-treatment. The presence of hystereses in the thermal expansion curves is probably proof in itself that the sintered bars have microcracks. Several authors (47,48,78,79) have attributed thermal expansion hystereses observed by them for single-phase polycrystalline ceramic oxides to the occurrence and healing of internal microcracks. A typical expansion curve for a sintered bar along with the curve for the hot-pressed sample is plotted in Figure 31 which includes results from the previous studies of Douglass (6) and Durbin and Harman (7). Also data from Wachtman et al. (80) for poly-

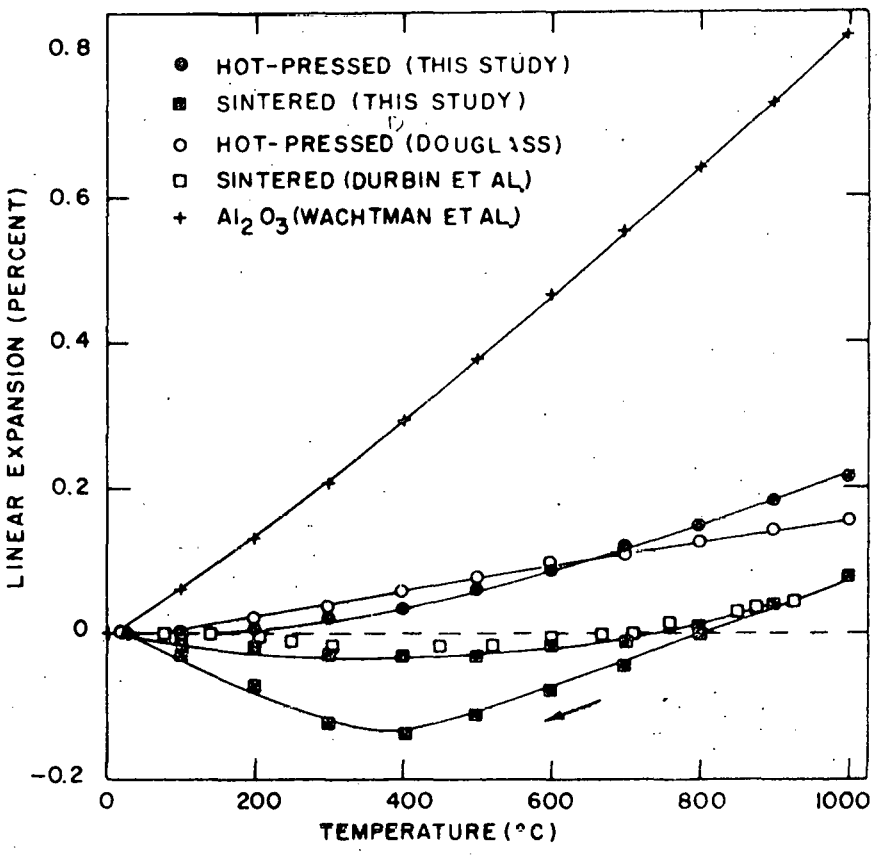

Figure 31. Linear thermal expansion of niobium pentoxide compared to literature values for the same oxide and for Al_2O_3 (80)

crystalline alumina is shown to indicate that the over-all thermal expansion of niobium pentoxide is small compared to that of a more conventional ceramic material. The thermal expansion results presented here agree well with those previously reported and indicate that the discrepancy between the results of Douglass (6) and those of Durbin and Harman (7) is due to the difference in techniques used to fabricate the samples.

A series of sintered samples was measured on the dilatometer because, early in this investigation, it was observed that the expansion characteristics seemed to vary with the density, or porosity, of the sample. This is unexpected behavior since it has been established (81) that porosity does not have a significant effect on the thermal expansion of polycrystalline ceramic oxides. Figure 32 shows over-all, or mean, coefficients of linear thermal expansion for sintered niobium pentoxide as a function of the volume percent porosity of the sample. The temperature interval considered was room temperature to 1000°C and the coefficients were calculated by dividing the over-all expansion at 1000°C by the magnitude of the temperature interval. Figures 13 through 20 also reveal that there is a tendency for the area of the hysteresis loop

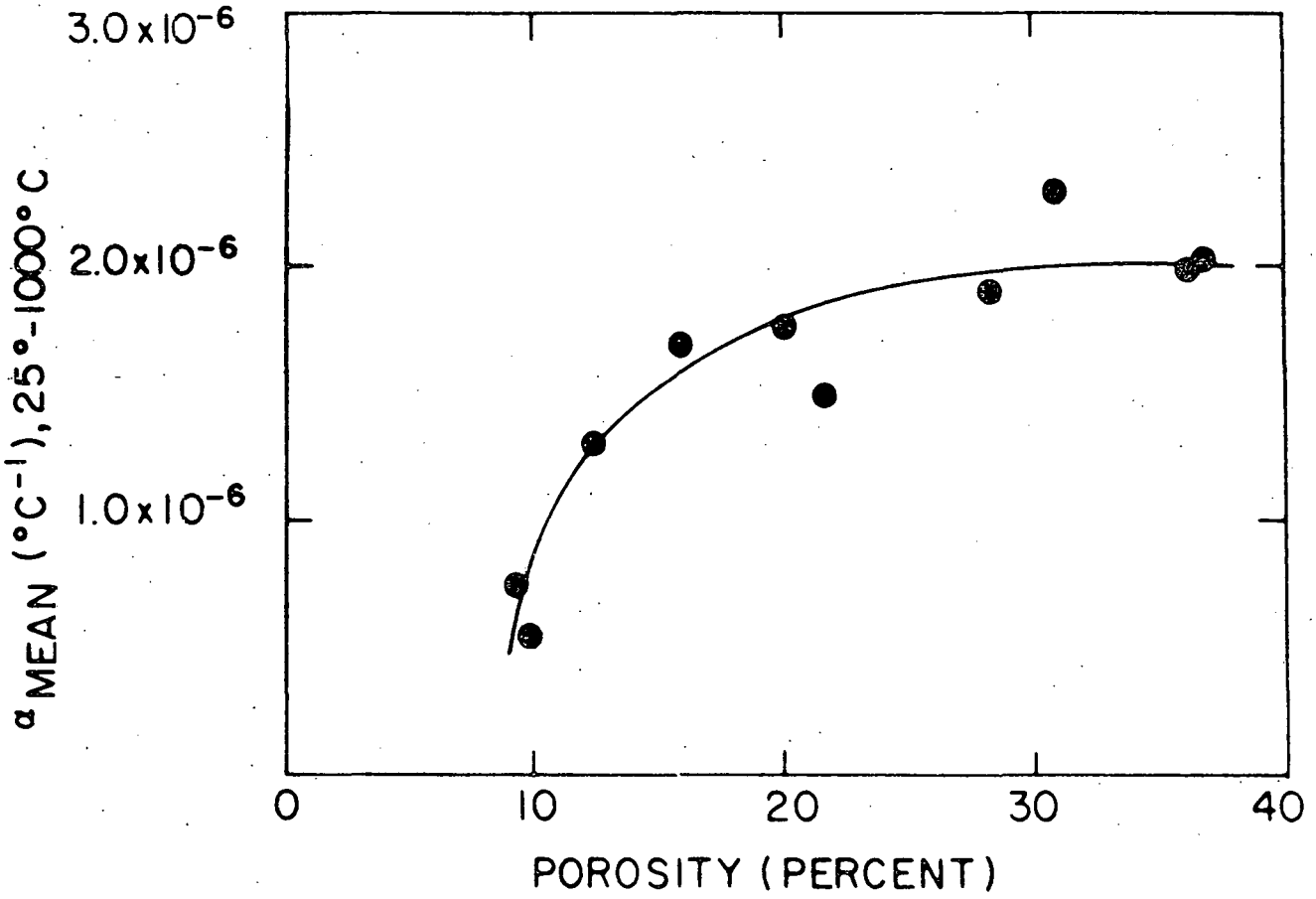

Figure 32. The over-all expansion coefficient (room temperature to 1000°C) for sintered niobium pentoxide as a function of porosity

to be greater for samples with lower porosity. These observations, along with the other dilatometric thermal expansion results, will be related to the microcrack hypothesis after the X-ray thermal expansion results are discussed.

Examination of the elevated temperature X-ray results shown in Figure 23 reveals that the lattice thermal expansion of monoclinic niobium pentoxide is anisotropic: the a and c parameters increase in value with increasing temperature whereas the b parameter and β do not. The anisotropy is probably a result of the complex structure of niobium pentoxide. Cartz (82) has suggested "One can anticipate anomalous thermal expansion behavior for crystal structures containing 'distorted' coordination polyhedra, that is where the bond lengths vary markedly about the cation." Gatehouse and Wadsley (15) have reported a large variation in the Nb-O distances for the NbO_6 octahedra of niobium pentoxide.

The unit-cell volume of niobium pentoxide was calculated from the lattice parameters at each elevated temperature. These results are included in Figure 23.

Equations of the form $L = Lo(1+AT+BT^2)$ were fit by a least-squares technique to the high-temperature parameter (a and c) and unit-cell volume data. Yagee and Foote (83) have

found that this quadratic expression adequately describes the thermal expansion behavior of many ceramic materials. The computed equation for the a parameter is, with T in ^{o}C,

$$a(\text{in } \mathring{A}) = 21.08(1 + 0.211645\times10^{-5}T + 0.305597\times10^{-8}T^{2}) \qquad (14)$$

with a standard error of estimate equal to $0.02\mathring{A}$. The equation for the c parameter has the form

$$c(\text{in } \mathring{A}) = 19.33(1 + 0.425420\times10^{-5}T + 0.157703\times10^{-8}T^{2}) \qquad (15)$$

with a standard error of estimate of $0.015\mathring{A}$; and, finally, the unit-cell volume equation is

$$V(\text{in } \mathring{A}^{3}) = 1353(1 + 0.633611\times10^{-5}T + 0.469546\times10^{-8}T^{2}) \qquad (16)$$

with a standard error of estimate of 2.0 $\mathring{A}^{3}$. Percent thermal expansion from room temperature to $1400^{o}C$ was calculated from Equations 14, 15 and 16, and is shown in Figure 33.

The parameter-temperature data, shown in Figure 23, exhibit a rather large amount of scatter. The average of the standard deviations of the high-temperature lattice parameters as computed by the program of Vogel and Kempter is $0.02\mathring{A}$. This large value is due, in part, to the complexity of the diffraction patterns and to the fact that most of the peaks used in the computations had 2θ-values less than 45^{o}. The

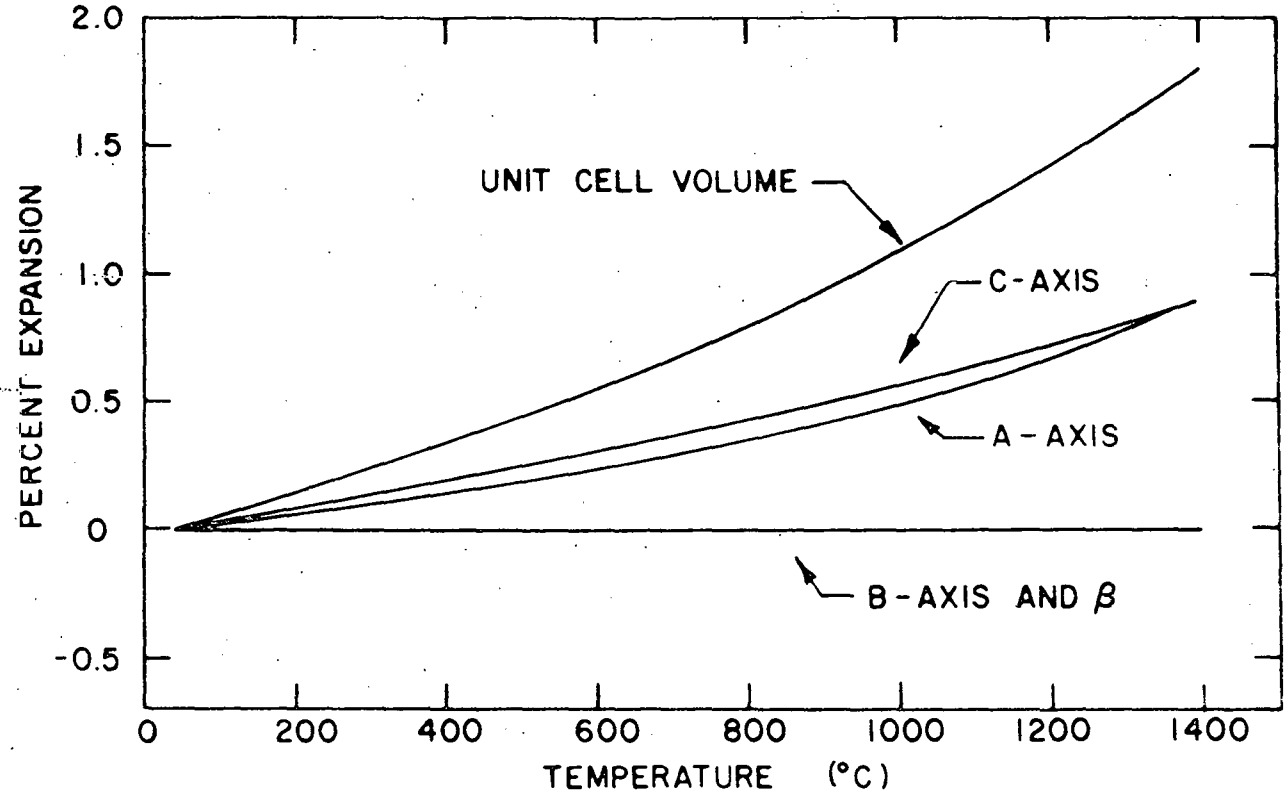

Figure 33. Axial and volume thermal expansion for monoclinic niobium pentoxide

results, however, are still significant since the over-all changes observed are greater than the scatter involved. Taking into consideration the error observed for the lattice parameter measurements, the over-all axial thermal expansion coefficients for the interval room temperature to 1000°C were calculated to be, for the a-axis, $5.25 \pm 1.00 \times 10^{-6}$; for the b-axis, $0 \pm 1.00 \times 10^{-6}\ ^{o}C^{-1}$; for the c-axis, $5.87 \pm 1.00 \times 10^{-6}\ ^{o}C^{-1}$; and for the unit-cell volume, $11.2 \pm 2.0 \times 10^{-6}\ ^{o}C^{-1}$.

The anisotropy of the lattice expansion for niobium pentoxide provides a cause for the existence of microcracks in the polycrystalline solid. The following discussion concerning the generation of internal cracks and the description of expansion behavior is essentially identical to that given by Buessem et al. (79) for aluminum titanate ($Al_2O_3 \cdot TiO_2$) and by Bush and Hummel (47) for magnesium dititanate.

After niobium pentoxide sinters at about 1400°C, no internal stresses exist in the sample. During cooling, however, the individual crystallites tend to contract unequally in the various crystallographic directions, and, consequently, a complex system of internal stresses arises within each crystallite of the polycrystalline body. In general, tensile

stresses arise in directions of high thermal expansion (actually contraction during cooling) while compressive stresses are associated with the directions of low thermal expansion. As cooling continues the magnitude of stresses increases until the strength of the crystallites or of the bonds between crystallites is exceeded and internal fracturing occurs. Because of the complexity of the problem, it is impossible to compute exact values for the thermal stresses involved; however, the magnitudes can be estimated by using equations given by Bush and Hummel (47) and taken from the work of Laszlo (84):

$$\sigma_a = \frac{E\Delta T[\mu(\alpha_b+\alpha_c-2\alpha) + (\alpha_a-\alpha)(1-\mu)]}{(1+\mu)\ (1-2\mu)}$$

$$\sigma_b = \frac{E\Delta T[\mu(\alpha_c+\alpha_a-2\alpha) + (\alpha_b-\alpha)(1-\mu)]}{(1+\mu)\ (1-2\mu)} \qquad (17)$$

$$\sigma_c = \frac{E\Delta T[\mu(\alpha_a+\alpha_b-2\alpha) + (\alpha_c-\alpha)(1-\mu)]}{(1+\mu)\ (1-2\mu)}$$

where σ_a, σ_b, and σ_c are the normal stresses in the indicated crystallographic directions; α_a, α_b, and α_c are the lattice thermal expansion coefficients; and α is the thermal expansion coefficient for the aggregate. The total stresses

developed in sintered niobium pentoxide during cooling from 1000 to 400°C (assumed to be the temperature at which microcracking begins to occur) were calculated from Equations 17. For these calculations, E and μ were assumed to be 22.4×10^6 psi (1545 kilobars) and 0.32, respectively; α_a, α_b, and α_c were computed from the X-ray data, and α was taken from the dilatometric thermal expansion results for a sintered sample. The results of the calculations show that the estimated values for the internal stresses σ_a, σ_b, and σ_c are 40,000 psi, -24,000 psi, and 41,000 psi, respectively.

Assuming that the internal stresses are sufficient to cause internal fracturing, the thermal expansion behavior for the less porous sintered samples of niobium pentoxide can be described as follows. When the sample is heated there is very little, or even negative, expansion up to about 500°C. This behavior is a direct result of the presence of microcracks: the individual crystallites are expanding in the a and c directions during this temperature interval, but, there is no over-all expansion of the body because the expansion occurring merely fills the cracks that are present. Above 500°C recombination of the fracture surfaces begins on a large scale and the body shows an over-all expansion up to the maxi-

mum temperature. On cooling to about 400°C the sample behaves as a crack-free body with an aggregate coefficient (3.7×10^{-6} $^{o}C^{-1}$) approximately equal to the average of the lattice coefficients ($4.2 \times 10^{-6} {}^{o}C^{-1}$). At 400°C the cracks begin to open and the body ceases to contract and begins to expand down to room temperature. The hysteresis does not close because the new crack system is different than that present in the bar at the beginning of the run.

As mentioned previously, the expansion characteristics of the sintered samples vary with the porosity of the samples. Examination of the thermal expansion curves reveals that, in general, as the sintered samples become more porous (1) the over-all expansion at any given temperature increases; (2) the minimum in the cooling curve shifts toward lower temperatures; and (3) the size of the hysteresis loop decreases. This behavior suggests that the more porous samples possess a lower density of microcracks. With fewer cracks present the over-all expansion of the body is greater because a smaller amount of the crystallite expansion is "taken up", or accommodated, by cracks. The shift in the minimum for the cooling curve and the decrease in area of the hysteresis loop occur because fewer cracks have opened up on cooling. There might

be several reasons for the porous samples to have fewer cracks: (1) the pores, themselves, could act as crack arrestors; (2) the porous samples were fired at lower temperatures and the cooling stresses are thus smaller since the magnitude of stress is proportional to the temperature change; or (3) the crack density could depend on grain size and the porous samples most likely have smaller grains than the dense samples. The contention that fewer cracks are present in the porous bars is also supported by the room-temperature elasticity results which show that porous sintered bars have modulus values lying close to the extrapolation of the curve describing the modulus-density relationship for the hot-pressed samples.

The occurrence and recombination of microcracks also explains the difference between the dilatometer results for the sintered samples and those for the hot-pressed body. The absence of hysteresis effects and the larger value for the over-all expansion coefficient ($2.19 \times 10^{-6}{}^{o}C^{-1}$, from room temperature to $1000^{o}C$, compared with $0.73 \times 10^{-6}{}^{o}C^{-1}$ for a sintered bar) provide additional evidence that the hot-pressed bars do not have internal microcracks.

Since the hot-pressed samples are also fabricated at

high temperatures, the question arises as to why this type of sample is not subject to internal cracking. The author believes that the answer is related to grain size. Recently Kirchner and Gruver (85) attributed microcracks in polycrystalline titania (TiO_2) to thermal expansion anisotropy and found "... the probability that a particular grain will be cracked is approximately 10 times as great in bodies in which the grain size is 100 to 200 microns as it is in bodies having a grain size of 30 to 60 microns." The authors conclude "As the grain size of TiO_2 bodies increases, the tendency for localized cracks to form during cooling after sintering also increases." Because of insufficient information, no grain size analysis was made in this work. It is generally true, however, that hot-pressed ceramics have smaller grains than sintered ceramics. It is thus suggested that hot-pressed niobium pentoxide has a grain size smaller than some "critical" size defined as the smallest grain size at which microcrack formation can occur. In order to substantiate this contention an attempt was made to induce grain growth in a hot-pressed sample for the purpose of exceeding the critical grain size and thus generating microcracks. The results are given in Table 7 which shows the Young's modulus of a hot-

Table 7. The effect of heat-treatment on the Young's modulus of a hot-pressed sample of niobium pentoxide

Heat-treatment temp. (°C)	Time at temp. (hrs)	Young's modulus (kilobars)
Before heat-treatment		861
1100	1	861
1100	9	785
1150	2	818
1150	8	735
1150	10	689
1150	10	667
1200	1	645
1200	15	563
1250	10	435
1300	18	276

pressed bar after each step of the progressive heat-treatment. The Young's modulus is appreciably lowered by the heat-treatment. It thus appears that microcracking has been induced in the hot-pressed sample. Additional evidence for the generation of cracks in a once crack-free body is provided by Figure 22 which shows the dilatometric thermal expansion of a hot-pressed sample after it was heat treated at 1200°C for 6 hrs. The presence of a hysteresis is evident; no such effect was observed for the sample prior to heat-treatment (Figure 21). Also, the Young's modulus for this sample changed on heat-treatment from 882 to 451 kilobars.

An attempt was made to reveal the proposed existence of microcracks by microstructural examination. Since it proved impossible to prepare polished sections for the sintered samples, scanning electron micrographs were obtained and are shown in Figures 24 through 27. No cracks across grains are evident; however, there is indication that cracks exist along grain boundaries and are manifested as grain boundary separation. It is plausible that the internal stresses generated on cooling are of such magnitude to cause cracking only at the grain boundaries. The fracture surfaces shown in Figures 26 and 27 suggest that intergranular fracture has occurred. Kingery (86) attributes the intergranular fracture of aluminum oxide and beryllium oxide (BeO) to boundary stresses arising from anisotropic thermal expansion. The fracture surface for hot-pressed samples, as revealed in the scanning electron micrographs of Figure 25, is quite different and shows no evidence for intergranular fracture which might suggest that the grain boundaries in the hot-pressed material are free of microcracks. The rather large cracks that do appear probably occurred when the samples were prepared for microstructural examination. No cracks are revealed in the photomicrographs (Figure 29) of a polished section of the hot-pressed bar.

As mentioned previously, the amount of microstructural information obtained is insufficient to analyze the grain size of the samples. It must be remembered that the micrographs represent very small areas of very small sections of only a few of the samples. The most that can be said is that a "typical" grain revealed in the micrographs for the sintered samples has a maximum dimension of 20 microns whereas a typical grain for the hot-pressed material has a maximum dimension of 10 microns. The author suggests that a worthwhile subject for a future investigation would be a study of the effect of grain size on the mechanical properties of niobium pentoxide.

Several quantitative relations have been proposed (87, 88) to show that cracks in solids appreciably reduce the elastic moduli. All of the equations, however, require a knowledge of crack shape, size, and density. Since this information has not been determined, no attempt was made to compare the theoretical relations with the experimental results.

As discussed in the Literature Review, others have attributed increases in Young's modulus with temperature to the presence of phase transformations. The high-temperature

X-ray measurements conducted here indicated that no phase transformation occurs in the material used to fabricate the samples. In addition it was confirmed by X-ray diffraction that the sintered bars were composed of the stable form of niobium pentoxide. Finally, thermogravimetric analysis revealed that the stoichiometry of sintered niobium pentoxide remains constant as the material is heated in air to 1000°C, thus ruling out phases changes related to deviations from stoichiometry.

CONCLUSIONS

The experimental evidence presented strongly supports the hypothesis that the anomalous elastic behavior observed for polycrystalline niobium pentoxide is due to the occurrence and recombination of internal microcracks resulting from anisotropic thermal expansion of the individual crystallites constituting the polycrystalline body.

LITERATURE CITED

1. Durbin, E. A., Wagner, H. E., and Harmon, C. G. Properties of some columbium oxide-basis ceramics. Battelle Memorial Institute Report No. BMI-792. 1952.

2. Buessem, W. R. Internal ruptures and recombinations in anisotropic ceramic materials. In Kriegel, W. W. and Palmour, H., eds. Mechanical properties of engineering ceramics. Pp. 127-148. New York, N.Y., Interscience Publishers, Incorporated. 1961.

3. Hasselman, D. P. H. Analysis of the strain at fracture of brittle solids with high densities of microcracks. American Ceramic Society Journal 52: 458. 1969.

4. Rossi, R. C. Thermal-shock-resistant ceramic composites. American Ceramic Society Bulletin 48: 736-737. 1969.

5. Wachtman, J. B., Jr. Elastic deformation of ceramics and other refractory materials. In Wachtman, J. B., Jr., ed. Mechanical and thermal properties of ceramics. National Bureau of Standards Special Publication 303: 139-168. 1969.

6. Douglass, D. L. The thermal expansion of niobium pentoxide and its effect on the spalling of niobium oxidation films. Journal of the Less-Common Metals 5: 151-157. 1963.

7. Durbin, E. A. and Harman, C. G. An appraisal of the sintering behavior and thermal expansion of some columbates. Battelle Memorial Institute Report No. BMI-791. 1952.

8. Makkay, R. W. and Fine, M. E. Vacuum reduction of α-Nb_2O_5 at low temperatures. Journal of Applied Physics 33: 745. 1962.

9. Reisman, A. and Holtzberg, F. Nb_2O_5 and Ta_2O_5 structure and physical properties. In Alper, A. M., ed. High-temperature oxides. Part II. Oxides of rare earths, titanium, zirconium, hafnium, niobium, and tantalum. PP. 217-257. New York, N.Y., Academic Press, Inc. 1970.

10. Schäfer, H., Gruehn, R., and Schulte, F. The modifications of niobium pentoxide. Angewandte Chemie, International Edition in English 5: 40-52. 1966.

11. Holtzberg, F., Reisman, A., Berry, M. and Berkenbilt, M. Chemistry of the group VB pentoxides. VI. The polymorphism of Nb_2O_5. American Chemical Society Journal 79: 2039-2043. 1957.

12. Zvinchuk, R. A. An X-ray investigation of polymorphism in in Nb_2O_5. Kristallografiya 3: 750-753. 1958.

13. Goldschmidt, H. J. A high-temperature X-ray investigation on niobium pentoxide and some problems concerning the oxidation of niobium. Institute of Metals Journal 87: 235-239. 1958.

14. Guha, J. P. Studies on niobium oxides and polymorphism of niobium pentoxide. Indian Ceramic Society Transactions 28: 97-101. 1969.

15. Gatehouse, B. M. and Wadsley, A. D. The crystal structure of the high-temperature form of niobium pentoxide. Acta Crystallographica 17: 1545-1554. 1964.

16. Kofstad, P. Comment on the defect structure of α-Nb_2O_5. Journal of the Less-Common Metals 14: 153-155. 1968.

17. Brauer, G. Oxides of columbium. Zeitschrift fur Anorganische and Allegemine Chemie 248: 1-31. 1941.

18. Lavrent'ev, V. I., Gerasimav, Ya. I., Rezukhina, T. N. Thermodynamic characteristics of niobium oxides (equilibrium with hydrogen and electrochemical measurements). Doklady Akademia Nauk SSSR 136: 1372-1375. 1961.

19. Norin, R. and Magneli, A. New niobium oxide phases. Naturwissenschaften 47: 354-355. 1960.

20. Blumenthal, R. N., Moser, J. B., and Whitmore, D. H. Thermodynamic study of nonstoichiometric niobium pentoxide. American Ceramic Society Journal 48: 617-622. 1965.

21. Schäfer, H., Bergner, D., Gruehn, R. Chemistry of the elements niobium and tantalum. LXXXI. The thermodynamic stability of the seven phases existing between 2.00 and 2.50 O/Nb. Zeitschrift fur Anorganische and Allegemine Chemie 365: 31-50. 1969.

22. Westbrook, J. H. Mechanical properties of intermetallic compounds - A review of the literature. In Westbrook, J. H., ed. Mechanical properties of intermetallic compounds. Pp. 1-70. New York, N.Y., John Wiley and Sons, Inc. 1960.

23. Rosen, M. Elastic moduli and ultrasonic attenuation of praeseodymium, neodymium, and samarium from 4.2 to 300°K. Physical Review 180 (2): 540-544. 1969.

24. Clinard, F. W., Jr. Anomalous decrease in Young's modulus of γ-cerium alloys at low temperatures. Journal of Applied Physics 40: 3067-3069. 1969.

25. Malmstrom, C., Keen, R., and Green, G., Jr. Some mechanical properties of graphite at elevated temperatures. Journal of Applied Physics 22: 533-600. 1951.

26. Faris, F. E., Green, L., Jr., and Smith, C. A. The thermal dependence of the elastic moduli of polycrystalline graphite. Journal of Applied Physics 23: 89-95. 1952.

27. Davidson, H. W., Lusty, H. H. W., and Ross, A. M. The mechanical properties of graphite at elevated temperatures. In Industrial carbon and graphite. Pp. 551-559. London, Society of Chemical Industry. 1958.

28. Lund, H. H. and Bortz, S. A. High-temperature physical properties of molded graphites. In Proceedings of the fourth conference on carbon. Pp. 537-546. New York, N.Y., Pergamon Press. 1960.

29. Armstrong, P. E. and Brown, H. L. Dynamic Young's modulus measurements above 1000°C on some pure polycrystalline metals and commercial graphites. The Metallurgical Society of AIME Transactions 230: 962-966. 1964.

30. Hove, J. E. Some physical properties of graphite as affected by high temperature and irradiation. In Industrial carbon and graphite. Pp. 501-510. London, Society of Chemical Industry. 1958.

31. Mrozowski, S. Mechanical strength, thermal expansion, and structure of cokes and carbons. In Proceedings of first and second conferences on carbon. Pp. 31-45. Buffalo, New York, University of Buffalo. 1956.

32. Mason, I. B. and Knibbs, R. H. Variation with temperature of Young's modulus of polycrystalline graphite. Nature 188: 33-35. 1960.

33. Mason, I. B. and Knibbs, R. H. The Young's modulus of carbon and graphite artefacts. Carbon 5: 493-506. 1967.

34. Sutton, A. L. and Howard, V. C. The role of porosity in the accommodation of thermal expansion in graphite. Journal of Nuclear Materials 7: 58-71. 1962.

35. Slagle, O. D. Thermal expansion hysteresis in polycrystalline graphite. Carbon 7: 337-344. 1969.

36. Jenkins, G. M. The effect of microporosity on the elastic modulus and yield curve of polycrystalline graphite. Journal of Nuclear Materials 29: 322-328. 1969.

37. Heindl, R. A. and Pendergast, W. L. Third progress report on investigations of sagger clays: their elasticity and transverse strength at several temperatures. American Ceramic Society Journal 10: 524-534. 1927.

38. Heindl, R. A. and Pendergast, W. L. Fourth progress report on investigation of sagger clays: their elasticity, transverse strength, and plastic flow at 1000°C. American Ceramic Society Journal 10: 995-1004. 1927.

39. Heindl, R. A. and Pendergast, W. L. Young's modulus of elasticity at several temperatures for some refractories of varying silica content. U.S. National Bureau of Standards Journal of Research 13: 851-862. 1934.

40. Ault, N. N., Ueltz, H. F. G. Sonic analysis for solid bodies. American Ceramic Society Journal 36: 199-203. 1953.

41. Lachman, I. M. and Everhart, J. O. Development of safe cooling schedules for structural clay products. American Ceramic Society Journal 39: 30-38. 1956.

42. Roberts, A. L. Elasticity-temperature relationships in refractories. British Ceramic Society Transactions 53: 724-730. 1954.

43. Smith, C. F. and Crandall, W. B. Calculated high-temperature elastic constants for zero porosity monoclinic zirconia. American Ceramic Society Journal 47: 624-627. 1964.

44. Buckley, J. D. and Braski, D. N. Elastic modulus of stabilized zirconia. American Ceramic Society Journal 50: 220-221. 1967.

45. Spinner, S. Temperature dependence of elastic constants of vitreous silica. American Ceramic Society Journal 45: 394-397. 1962.

46. Dienes, G. J. The temperature-dependence of the elastic moduli of vitreous silica. Journal of Physics and Chemistry of Solids 7: 290-294. 1958.

47. Bush, E. A. and Hummel, F. A. High-temperature mechanical properties of ceramic materials: I, magnesium dititanate. American Ceramic Society Journal 41: 189-195. 1959.

48. Bush, E. A. and Hummel, F. A. High-temperature mechanical properties of ceramic materials: II, beta-eucryptite. American Ceramic Society Journal 42: 388-391. 1959.

49. Gillery, F. H. and Bush, E. A. Thermal contraction of β-eucryptite ($Li_2O \cdot Al_2O_3 \cdot 2SiO_2$) by X-ray and dilatometer methods. American Ceramic Society Journal 42: 175-177. 1959.

50. Roth, R. S. Phase equilibrium relations in the binary system lead oxide-niobium pentoxide. U.S. National Bureau of Standards Journal of Research 62: 27-38. 1959.

51. Forster, F. Ein neues Messverfahren zur Bestimmung des Elastizitatsmoduls und der Dampfung. Zeitschrift fur Metallkunde 29: 109-115. 1937.

52. Spinner, S. and Tefft, W. E. A method for determining mechanical resonance frequencies and for calculating elastic moduli from these frequencies. American Society for Testing Materials Proceedings 61: 1221-1238. 1961.

53. Marlowe, M. O. Elasticity and kilocycle internal friction of Y_2O_3. Unpublished M.S. thesis. Ames, Iowa, Library, Iowa State University of Science and Technology. 1963.

54. Hasselman, D. P. H. Tables for the computation of shear modulus and Young's modulus of elasticity from resonant frequencies of rectangular prisms. Niagara Falls, New York, Carborundum Company. 1962.

55. Pickett, G. Equations for computing elastic constants from flexural and torsional resonant frequencies of vibration of prisms and cylinders. American Society for Testing Materials Proceedings 45: 846-865. 1945.

56. Zener, C. Elasticity and anelasticity of metals. Chicago, Illinois, University of Chicago Press. 1948.

57. Wachtman, J. B., Jr. and Tefft, W. E. Effect of suspension position on apparent values of internal friction determined by Forster's method. Review of Scientific Instruments 29: 517-520. 1958.

58. Astbury, N. F. and Davis, W. R. Internal friction in ceramics. British Ceramic Society Transactions 63: 1-18. 1964.

59. Souder, W. and Hidnert, P. Measurements on the thermal expansion of fused silica. U.S. National Bureau of Standards Scientific Paper No. 524. 1926.

60. Johnstone, J. K. The erbia-hafnia system. Unpublished Ph.D. thesis. Ames, Iowa, Library, Iowa State University of Science and Technology. 1970.

61. Stacy, D. W. An X-ray diffraction study of the yttria-hafnia system. Unpublished Ph.D. thesis. Ames, Iowa, Library, Iowa State University of Science and Technology. 1971.

62. Vogel, R. E. and Kempter, C. P. A mathematical technique for the precision determination of lattice parameters. Acta Crystallographica 14: 1130-1134. 1961.

63. Hess, J. B. A modification of the Cohen procedure for computing precision lattice constants from powder data. Acta Crystallographica 4: 209-215. 1950.

64. Hoch, M. and Momin, A. C. High temperature thermal expansion of UO_2 and ThO_2. High temperatures-High pressures. International Journal of Research 1: 401-407. 1969.

65. Baldock, P. J., Spindler, W. E., and Baker, T. W. An X-ray study of the variation of the lattice parameters of alumina, magnesia, and thoria up to 2000°C. United Kingdom Atomic Energy Authority AERE-R-5674 [Atomic Energy Research Establishment, Harwell, Berks, England]. 1968.

66. Grain, C. F. and Campbell, W. J. Thermal expansion and phase inversion of six refractory oxides. U.S. Bureau of Mines Report of Investigations 5982. 1962.

67. Brown, A. and Chitty, A. Thoria as a fertile component for a liquid metal breeder blanket. Journal of Nuclear Energy, Part B, 1: 145-152. 1960.

68. Kempter, C. P. and Elliot, R. O. Thermal expansion of <UN>, <UO_2>, <$UO_2 \cdot ThO_2$>, and <ThO_2>. The Journal of Chemical Physics 30: 1524-1526. 1959.

69. Skinner, B. J. The thermal expansions of thoria, periclase, and diamond. The American Mineralogist 42: 39-55. 1957.

70. Mauer, F. A. and Boltz, L. H. Measurement of thermal expansion of cermet components of high temperature X-ray diffraction. U.S. Atomic Energy Commission Report WADS-TR-55-473 [Wright Air Development Center, Wright-Patterson AFB, Ohio]. 1955.

71. Thiruvengadam, A., Gunasekaran, M., and Preiser, H. S. Use of internal damping measurements in the study of environmental cracking. Corrosion 25: 243-250. 1969.

72. Wachtman, J. B., Jr. and Lam, D. G., Jr. Young's modulus of various refractory materials as a function of temperature. American Ceramic Society Journal 42: 254-260. 1959.

73. Chang, R. High-temperature creep and anelastic phenomena in polycrystalline refractory oxides. Journal of Nuclear Materials 2: 174-181. 1959.

74. Marlowe, M. O. and Wilder, D. R. Elasticity and internal friction of polycrystalline yttrium oxide. American Ceramic Society Journal 48: 227-233. 1965.

75. Manning, W. R., Hunter, O., Jr., and Powell, B. R., Jr. Elastic properties of polycrystalline yttrium oxide, dysprosium oxide, holmium oxide, and erbium oxide: room temperature measurements. American Ceramic Society Journal 52: 436-442. 1969.

76. Forlano, R. J., Allen, A. W., and Beals, R. J. Elasticity and anelasticity of uranium oxides at room temperature: I, stoichiometric oxide. American Ceramic Society Journal 50: 93-96. 1967.

77. Nutt, A. W., Jr., Allen, A. W., and Handwerk, J. H. Elastic and anelastic response of polycrystalline UO_2-PuO_2. American Ceramic Society Journal 53: 205-210. 1970.

78. Charvat, F. R. and Kingery, W. D. Thermal conductivity: XIII, effect of microstructure on conductivity of single-phase ceramics. American Ceramic Society Journal 40: 306-315. 1957.

79. Buessem, W. R., Thielke, N. R., and Sarakauskas, R. V. Thermal expansion hysteresis of aluminum titanate. Ceramic Age 60: 38-40. 1952.

80. Wachtman, J. B., Jr., Scuderi, T. G., and Cleek, G. W. Linear thermal expansion of aluminum oxide and thorium oxide from 100° to 1100°K. American Ceramic Society Journal 45: 319-323. 1962.

81. Kirby, R. K. Thermal expansion of ceramics. In Wachtman, J. B., Jr., ed. Mechanical and thermal properties of ceramics. Pp. 41-61. National Bureau of Standards Special Publication 303. 1961.

82. Cartz, L. Anisotropic thermal expansion characteristics of some crystal structures. In Vahldiek, F. W. and Mersol, S. A., eds. Anisotropy in single-crystal refractory compounds. Volume I. Pp. 383-389. New York, N.Y., Plenum Press. 1968.

83. Yaggee, F. L. and Foote, F. G. A method for reconstructing a thermal expansion graph from two values of the mean expansion coefficient. U.S. Atomic Energy Commission Report ANL-7644 [Argonne National Laboratory, Argonne, Illinois]. 1969.

84. Laszlo, F. Tessellated stresses, I. Iron and Steel Institute (London) Journal 127: 173-199. 1943.

85. Kirchner, H. P. and Gruver, R. M. Strength-anisotropy-grain size relations in ceramic oxides. American Ceramic Society Journal 53: 232-236. 1970.

86. Kingery, W. D. Introduction to Ceramics. New York, N.Y., John Wiley and Sons, Inc. 1960.

87. Walsh, J. B. Effect of cracks on compressibility of rock. Journal of Geophysical Research 70: 381-389. 1965.

88. Hasselman, D. P. H. Analysis of the strain at fracture of brittle solids with high densities of microcracks. American Ceramic Society Journal 52: 458. 1969.

APPENDIX A. ELASTICITY AND INTERNAL FRICTION DATA

Table A1. Room-temperature resonant frequencies, elastic moduli, and internal friction for sintered samples

Sample No.	Flexural resonant frequency (cycles/second)	Torsional resonant frequency (cycles/second)	Young's modulus (kilobars)	Shear modulus (kilobars)	Internal friction (10^{-4})
D-3	3996	15,280	310	131	54
D-4	3736	11,357	342	144	150
D-5	4966	14,425	400	168	52
D-6	4565	14,107	423	178	61
D-7	4540	13,360	353	154	75
D-8	4466	13,808	320	137	91
S-1	3405	7826	420	179	46
S-2	2365	6477	381	162	32
D-9	2720	8510	282	131	146
S-3	2012	5932	289	127	89
S-4	2505	6852	328	148	42
D-10	3570	10,924	231	106	52
S-5	1874	4210	391	165	250

Table A2. Room-temperature resonant frequencies, elastic moduli, and internal friction for hot-pressed samples

Sample No.	Flexural resonant frequencies[a] (cycles/second)	Torsional resonant frequency (cycles/second)	Young's modulus (kilobars)	Shear modulus (kilobars)	Internal friction (10^{-4})
1	2019	5533	565	243	60
	9746		655		
2	2272	8036	851	335	66
	7906		794		
3	1758	6673	870	343	62
	7830		848		
4	2525	8953	818	320	78
	7790		822		
5	2443	8539	861	341	54
	8024		816		
6	2736	7718	1066	427	59
	10,700		1126		
7	3679	12,505	1174	446	58
	9060		1209		
8	2440	9173	1147	441	45
	7876		1108		
9	3138	11,384	1158	441	44
	7980		1215		
10	3003	11,110	1151	440	44
	7942		1216		

[a]For each sample the first value listed in the column is the flatwise flexural frequency and the second value is the edgewise flexural frequency.

Table A2. (Continued)

Sample No.	Flexural resonant frequencies[a] (cycles/second)	Torsional resonant frequency (cycles/second)	Young's modulus (kilobars)	Shear modulus (kilobars)	Internal friction (10^{-4})
11	2473	9169	1223	470	58
	8338		1205		
12	2891	11,116	1198	464	46
	7622		1194		
13	2946	10,222	1317	497	51
	9950		1341		
14	2731	10,127	1289	511	52
15	3027	10,163	1302	497	46
	11,886		1329		
16	2672	9788	1361	516	32
17	5561	14,580	1413	531	--
	13,641		1470		
18	3074	8832	1415	537	51
	13,135		1454		
19	3789	9899	1447	557	40
	15,928		1473		
20	4993	16,252	1397	539	33
21	3680	9244	1466	562	31
22	4356	12,315	1463	564	45
23	3924	10,906	1498	575	44

Table A3. Elevated temperature resonant frequencies and Young's moduli for sintered niobium pentoxide: Sample S-1, Run 1

Temp. (°C)	Elapsed time (min.)	Flexural resonant frequency (cycles/second)	Young's modulus (kilobars)
23	0	3268	387
70	50	3179	366
114	90	3125	353
184	200	3072	342
232	240	3040	334
307	290	3018	330
366	330	2956	316
422	400	2950	315
490	435	3018	330
534	480	3089	345
578	520	3200	371
655	550	3502	444
705	570	3922	557
758	665	5032	916
801	685	5124	950
834	705	5207	981
880	720	5248	996
915	740	5269	1005
956	760	5265	1003
982	785	5262	1002
1007	810	5253	999
726	850	5368	1043
428	900	5422	1064
23	933	3932	560
	938	3879	545
	945	3867	541
	950	3840	534
	960	3778	516
	1110	3429	425

Table A4. Elevated temperature resonant frequencies and Young's moduli for sintered niobium pentoxide: Sample S-1, Run 2

Temp. (°C)	Elapsed time (min.)	Flexural resonant frequency (cycles/second)	Young's modulus (kilobars)
26	0	3075	342
133	45	3010	328
217	85	2967	318
317	120	3072	341
392	170	3171	364
511	225	3408	420
616	265	3875	543
712	300	4866	857
793	335	5273	1006
884	365	5297	1015
1018	380	5251	997
930	415	5293	1014
844	455	5325	1026
750	480	5362	1040
654	505	5390	1051
450	615	5421	1063
403	650	5419	1062
329	740	5386	1049
248	820	5140	956
104	900	4095	607
23	1800	2985	322

Table A5. Elevated temperature resonant frequencies, elastic moduli, and internal friction for sintered niobium pentoxide: Sample S1, Run 3

Temp. (°C)	Elapsed time (min.)	Flexural resonant frequency (cycles/sec)	Torsional resonant frequency (cycles/sec)	Young's modulus (kilobars)	Shear modulus (kilobars)	Internal friction (10^{-4})
25	0	3485	7945	439	187	93
112	45	3422	7813	424	181	69
203	105	3403	7751	419	178	63
315	150	3383	7710	414	176	92
402	185	3315	7589	398	171	49
499	220	3303	7566	395	170	54
537	241	3343		404		88
	246	3344		404		81
	251	3343	7654	404	174	71
578	271	3370		411		66
	276	3390		416		
	281	3394		417		53
	286	3399		418		
	291	3402		419		
	296	3406		420		
	301	3406		420		
	306	3396		417		
	316	3400	7823	418	181	31
678	365	3626		475		40
	370	3655		483		
	375	3654		483		
	380	3660		485		46
	385	3680		490		
	390	3673		488		
	395	3692		493		52

Table A5. (Continued)

Temp. (°C)	Elapsed time (min.)	Flexural resonant frequency (cycles/sec)	Torsional resonant frequency (cycles/sec)	Young's modulus (kilobars)	Shear modulus (kilobars)	Internal friction (10^{-4})
	405	3704		497		
	415	3703		496		
	425	3725		502		
	435	3736		505		
	445	3742		507		
	455	3747	8560	508	217	40
720	480	3852		537		41
	490	3897		549		
	500	3934		560		
	510	3962		568		
	520	3989		576		28
	530	4013		583		
	540	4034		589		23
	550	4054		595		
	560	4072		600		
	570	4088	9325	605	257	23
755	590	4226		646		23
	600	4296		668		20
	610	4364		689		
	620	4421		707		
	630	4470		723		
	640	4509		736		
	650	4546		747		
	660	4578		758		
	670	4608		768		
	680	4633	10,420	776	322	21

Table A5. (Continued)

Temp. (°C)	Elapsed time (min.)	Flexural resonant frequency (cycles/sec)	Torsional resonant frequency (cycles/sec)	Young's modulus (kilobars)	Shear modulus (kilobars)	Internal friction (10^{-4})
800	705	4874		859		
	715	4952		887		32
	725	5008		907		
	735	5057		925		
	745	5093		939		
	755	5120		948		20
	765	5145		957		
	775	5163		964		
	785	5180		971		
	795	5198	11,530	978	394	26
900	810	5331		1028		
	815	5371		1044		
	820	5392		1052		21
	825	5407	11,815	1058	413	
987	840	5413		1060		22
836	865	5486		1089		26
	870	5486		1089		27
663	930	5545		1113		
438	970	5528		1106		
24	1055	3522		449		36
	1060	3511		446		35
	1165	3205		372		40
	1170	3193		369		42

Table A6. Resonant frequency and Young's modulus of a sintered sample as a function of time at 745°C: Sample S-1, Run 4

Elapsed time (min.)	Flexural resonant frequency (cycles/second)	Young's modulus (kilobars)
0	4433	711
5	4571	756
10	4656	784
15	4723	807
20	4772	824
25	4815	839
30	4848	850
35	4879	861
40	4906	871
50	4950	886
60	4986	899
70	5014	910
85	5045	921
100	5072	931
115	5094	939
130	5116	947
160	5153	961
310	5252	998
370	5275	1007
430	5290	1012

Table A7. Elevated temperature resonant frequencies, Young's moduli, and internal friction for nonstoichiometric hot-pressed niobium pentoxide, Sample 21

Temp. (°C)	Flexural resonant frequency (cycles/second)	Young's modulus (kilobars)	Internal friction (10^{-4})
25	3692	1466	38
112	3637	1422	16
166	3623	1412	14
260	3607	1399	10
313	3598	1393	11
360	3590	1387	11
445	3573	1374	16
515	3559	1362	21
592	3539	1347	25
671	3521	1334	15
739	3505	1321	13
808	3489	1309	15
868	3472	1296	17
913	3459	1287	17
954	3445	1277	24
994	3431	1267	37
1029	3416	1255	47
1101	3374	1224	77
1071	3392	1237	70
823	3486	1308	13
606	3539	1347	15
392	3586	1382	10
116	3639	1423	11
62	3658	1440	14
21	3683	1459	35

APPENDIX B. DILATOMETER DATA

Table B1. Percent linear thermal expansion of sintered niobium pentoxide, Sample D-1

Percent porosity: 36.9

Length at room temperature: 2.005 in.

Temp (°C)	Run 1		Run 2		Run 3	
	Heating	Cooling	Heating	Cooling	Heating	Cooling
R.T.	0.0000	-0.0488	0.0000	-0.0438	0.0000	-0.0448
50	.0059	- .0423	.0009	- .0413	-.0014	- .0473
100	.0029	- .0473	.0009	- .0413	-.0004	- .0453
150	.0024	- .0453	.0029	- .0413	.0039	- .0389
200	.0089	- .0443	.0089	- .0359	.0039	- .0354
250	.0104	- .0399	.0169	- .0289	.0119	- .0304
300	.0149	- .0299	.0279	- .0184	.0179	- .0209
350	.0224	- .0194	.0364	- .0059	.0249	- .0059
400	.0299	- .0064	.0438	.0094	.0349	.0069
450	.0389	.0059	.0543	.0219	.0438	.0209
500	.0493	.0194	.0693	.0369	.0583	.0344
550	.0633	.0334	.0842	.0498	.0733	.0493
600	.0812	.0483	.0987	.0618	.0862	.0618
650	.0987	.0603	.1152	.0812	.1017	.0802
700	.1132	.0763	.1306	.1012	.1167	.0977
750	.1291	.0942	.1476	.1192	.1341	.1167
800	.1441	.1097	.1615	.1381	.1511	.1346
850	.1576	.1286	.1775	.1561	.1680	.1536
900	.1725	.1491	.1910	.1775	.1810	.1750
950	.1845	.1695	.2054	--	.1985	.1945
960	--	--	--	--	.1995	--
1000	.1975	.1915	--	--	--	--
1050	.2059	--	--	--	--	--

Table B2. Percent linear thermal expansion of sintered niobium pentoxide, Sample D-2

Percent porosity: 36.3

Length at room temperature: 2.003 in.

Temp (°C)	Run 1		Run 2	
	Heating	Cooling	Heating	Cooling
R.T.	0.0000	-0.0139	0.0000	-0.0574
50	-.0029	- .0274	.0034	- .0624
100	.0029	--	-.0004	- .0798
150	.0149	--	-.0009	- .0863
200	.0139	--	-.0009	- .0893
250	.0184	- .0389	.0009	- .0873
300	.0279	- .0304	.0044	- .0823
350	.0289	- .0159	.0089	- .0743
400	.0374	- .0039	.0149	- .0644
450	.0454	.0079	.0239	- .0504
500	.0619	.0224	.0344	- .0349
550	.0748	.0384	.0459	- .0189
600	.0913	.0519	.0574	- .0054
650	.1068	.0678	.0718	.0114
700	.1243	.0873	.0889	.0299
750	.1427	.1053	.1053	.0469
800	.1577	.1258	.1213	.0673
850	.1752	.1462	.1387	.0888
900	.1887	.1677	.1562	.1118
950	.1987	.1872	.1757	.1347
970	.2006	--	--	--
1000	--	--	.1942	.1607
1050	--	--	.2096	.1812
1100	--	--	.2226	.2017
1150	--	--	.2371	.2222
1185	--	--	.2391	--

Table B3. Percent linear thermal expansion of sintered niobium pentoxide, Sample D-3

Percent porosity: 36.3

Length at room temperature: 1.998 in.

Temp (°C)	Heating	Cooling
R.T.	0.0000	-0.0120
50	.0045	- .0165
100	.0030	- .0340
150	.0030	--
200	.0065	--
250	.0130	- .0355
300	.0180	- .0260
350	.0175	- .0100
400	.0240	.0055
450	.0330	.0205
500	.0495	.0355
550	.0650	.0510
600	.0815	.0660
650	.0970	.0825
700	.1176	.1011
750	.1371	.1196
800	.1556	.1401
850	.1726	.1616
900	.1901	.1831
950	.2077	.2047
1000	.2232	.2257
1015	.2252	--

Table B4. Percent linear thermal expansion of sintered niobium pentoxide, Sample D-4

Percent porosity: 28.4

Length at room temperature: 2.001 in.

Temp (°C)	Heating	Cooling
R.T.	0.0000	-0.0289
50	.0069	- .0324
100	.0019	- .0474
150	.0014	- .0574
200	-.0009	- .0619
250	.0019	- .0589
300	.0044	- .0514
350	.0009	- .0404
400	.0024	- .0284
450	.0104	- .0164
500	.0269	- .0039
550	.0409	.0124
600	.0564	.0254
650	.0694	.0414
700	.0874	.0564
750	.1064	.0744
800	.1229	.0924
850	.1389	.1139
900	.1539	.1419
950	.1709	.1644
1000	.1854	.1849
1035	.1944	--

Table B5. Percent linear thermal expansion of sintered niobium pentoxide, Sample D-5

Percent porosity: 21.8

Length at room temperature: 1.996 in.

Temp (°C)	Run 1		Run 2	
	Heating	Cooling	Heating	Cooling
R.T.	0.0000	-0.0255	0.0000	-0.0390
50	.0020	- .0325	.0010	- .0490
100	-.0015	- .0526	-.0030	- .0771
150	-.0035	- .0676	-.0060	- .0966
200	-.0035	- .0711	-.0100	- .1112
250	-.0030	- .0541	-.0080	- .1142
300	-.0045	- .0821	-.0070	- .1077
350	-.0075	- .0706	-.0050	- .0976
400	-.0065	- .0576	.0000	- .0866
450	-.0010	- .0445	.0055	- .0721
500	.0080	- .0305	.0135	- .0551
550	.0165	- .0170	.0260	- .0365
600	.0270	- .0040	.0355	- .0220
650	.0390	.0115	.0470	- .0045
700	.0501	.0275	.0621	.0165
750	.0686	.0455	.0781	.0345
800	.0846	.0646	.0931	.0551
850	.0991	.0821	.1132	.0766
900	.1157	.1047	.1307	.0996
950	.1312	.1247	.1492	.1252
1000	.1457	--	.1683	.1513
1050	--	--	.1868	.1743
1100	--	--	.2034	.1959
1150	--	--	.2194	.2154
1190	--	--	--	.2315
1195	--	--	.2314	--

Table B6. Percent linear thermal expansion of sintered niobium pentoxide, Sample D-6

Percent porosity: 20.1

Length at room temperature: 1.997 in.

Temp (°C)	Heating	Cooling
R.T.	0.0000	-0.0390
50	.0010	- .0525
100	-.0030	- .0726
150	-.0010	- .0881
200	-.0020	- .0956
250	-.0005	- .0966
300	.0020	- .0866
350	.0000	- .0721
400	.0015	- .0580
450	.0055	- .0430
500	.0170	- .0290
550	.0285	- .0140
600	.0415	.0020
650	.0555	.0190
700	.0711	.0365
750	.0881	.0555
800	.1056	.0766
850	.1216	.0991
900	.1407	.1221
950	.1562	.1452
1000	.1707	.1692
1015	.1732	--

Table B7. Percent linear thermal expansion of sintered niobium pentoxide, Sample D-7

Percent porosity: 16.1

Length at room temperature: 2.001 in.

Temp. (°C)	Heating	Cooling
R.T.	0.0000	-0.0184
50	-.0014	- .0309
100	-.0014	- .0539
150	.0000	- .0719
200	-.0029	- .0884
250	-.0029	- .0949
300	.0014	- .0869
350	-.0009	- .0734
400	.0009	- .0579
450	.0039	- .0429
500	.0144	- .0289
550	.0244	- .0119
600	.0324	.0039
650	.0419	.0189
700	.0574	.0389
750	.0734	.0569
800	.0904	.0774
850	.1089	.0994
900	.1279	.1224
950	.1459	.1434
1000	.1624	--

Table B8. Percent linear thermal expansion of sintered niobium pentoxide, Sample D-8

Percent porosity: 12.5

Length at room temperature: 1.997 in.

Temp (°C)	Heating	Cooling
R.T.	0.0000	-0.0340
50	.0010	- .0375
100	-.0080	- .0650
150	-.0100	- .0856
200	-.0110	- .1096
250	-.0130	- .1266
300	-.0145	- .1251
350	-.0175	- .1121
400	-.0175	- .0971
450	-.0170	- .0831
500	-.0130	- .0681
550	-.0050	- .0505
600	.0025	- .0355
650	.0145	- .0185
700	.0260	.0010
750	.0395	.0220
800	.0540	.0415
850	.0706	.0650
900	.0916	.0871
950	.1101	.1101
990	.1256	--

Table B9. Percent linear thermal expansion of sintered niobium pentoxide, Sample D-9

Percent porosity: 9.9

Length at room temperature: 2.003 in.

Temp (°C)	Run 1		Run 2		Run 3	
	Heating	Cooling	Heating	Cooling	Heating	Cooling
R.T.	0.0000	-0.0199	0.0000	0.0009	0.0000	-0.0444
50	-.0064	- .0324	.0019	-.0114	-.0004	- .0519
100	-.0124	- .0559	-.0069	-.0399	-.0069	- .0698
150	-.0169	- .0738	-.0134	-.0678	-.0124	- .0878
200	-.0209	- .0968	-.0234	-.0968	-.0169	- .1153
250	-.0304	- .1253	-.0279	-.1238	-.0264	- .1362
300	-.0369	- .1472	-.0319	-.1487	-.0294	- .1587
350	-.0474	- .1607	-.0364	-.1627	-.0374	- .1717
400	-.0549	- .1577	-.0384	-.1577	-.0399	- .1717
450	-.0604	- .1462	-.0394	-.1467	-.0444	- .1617
500	-.0579	- .1352	-.0379	-.1337	-.0419	- .1487
550	-.0559	- .1213	-.0324	-.1198	-.0379	- .1347
600	-.0484	- .1063	-.0284	-.1053	-.0319	- .1213
650	-.0439	- .0918	-.0254	-.0918	-.0289	- .1043
700	-.0364	- .0738	-.0199	-.0723	-.0264	- .0863
750	-.0269	- .0569	-.0119	-.0544	-.0154	- .0639
800	-.0134	- .0349	-.0004	-.0339	-.0044	- .0434
850	-.0014	- .0134	.0114	-.0134	.0079	- .0219
900	.0129	.0054	.0239	.0054	.0219	.0009
950	.0274	.0259	.0359	.0259	.0374	.0234
978	--	--	.0329	--	--	--
983	.0369	--	--	--	--	--
1000	--	--	--	--	.0529	.0509
1035	--	--	--	--	.0609	--

Table B10. Percent linear thermal expansion of sintered niobium pentoxide, Sample D-10

Percent porosity: 9.4

Length at room temperature: 2.003 in.

Temp (°C)	Run 1		Run 2	
	Heating	Cooling	Heating	Cooling
R.T.	0.0000	-.0074	0.0000	-0.0004
50	.0000	-.0174	.0044	- .0074
100	-.0064	-.0349	-.0044	- .0264
150	-.0109	-.0639	-.0084	- .0464
200	-.0184	-.0808	-.0174	- .0693
250	-.0229	-.1023	-.0204	- .0928
300	-.0294	-.1323	-.0244	- .1188
350	-.0399	-.1467	-.0289	- .1342
400	-.0424	-.1452	-.0324	- .1362
450	-.0444	-.1337	-.0309	- .1253
500	-.0404	-.1213	-.0289	- .1103
550	-.0339	-.1038	-.0239	- .0963
600	-.0284	-.0903	-.0199	- .0803
650	-.0229	-.0759	-.0154	- .0659
700	-.0164	-.0559	-.0114	- .0474
750	-.0044	-.0354	-.0019	- .0249
800	.0044	-.0149	.0104	- .0059
850	.0199	.0064	.0239	.0139
900	.0319	.0289	.0394	.0369
950	.0489	.0509	.0559	.0559
1000	.0668	.0698	.0738	.0773
1015	.0698	--	--	--
1025	--	--	.0813	--

Table B10. (Continued)

Temp (°C)	Run 3		Run 4	
	Heating	Cooling	Heating	Cooling
R.T.	0.0000	0.0010	0.0000	-0.0189
50	.0049	-.0064	-.0014	- .0224
100	-.0069	-.0294	-.0114	- .0439
150	-.0109	-.0514	-.0159	- .0659
200	-.0209	-.0743	-.0184	- .0893
250	-.0229	-.0988	-.0204	- .1113
300	-.0294	-.1238	-.0194	- .1357
350	-.0339	-.1382	-.0224	- .1497
400	-.0349	-.1387	-.0214	- .1462
450	-.0369	-.1268	-.0204	- .1328
500	-.0319	-.1138	-.0154	- .1163
550	-.0279	-.0978	-.0089	- .0998
600	-.0224	-.0828	-.0044	- .0863
650	-.0204	-.0668	.0019	- .0708
700	-.0139	-.0474	.0069	- .0549
750	-.0044	-.0289	.0139	- .0379
800	.0079	-.0099	.0214	- .0184
850	.0214	.0129	.0349	.0014
900	.0369	.0329	.0504	.0194
950	.0539	.0569	.0599	.0434
1000	.0743	.0798	.0753	.0659
1043	.0878	--	--	--
1050	--	--	.0913	.0838
1100	--	--	.1078	.1043
1150	--	--	.1223	.1213
1200			.1352	.1352
1210			.1333	--

Table B11. Percent linear thermal expansion of hot-pressed niobium pentoxide, Sample D-11

Percent porosity: 15.6

Length at room temperature: 2.001 in.

Temp (°C)	Run 1		Run 2	
	Heating	Cooling	Heating	Cooling
R.T.	0.0000	-0.0039	0.0000	-0.0064
50	-.0004	- .0049	0.0000	- .0139
100	.0014	- .0114	-.0014	- .0164
150	.0004	- .0099	-.0019	- .0124
200	.0059	- .0034	.0014	- .0069
250	.0094	.0024	.0044	- .0014
300	.0204	.0114	.0054	.0064
350	.0234	.0219	.0174	.0169
400	.0314	.0329	.0239	.0284
450	.0419	.0444	.0329	.0419
500	.0569	.0554	.0469	.0534
550	.0684	.0674	.0634	.0644
600	.0854	.0779	.0779	.0769
650	.1004	.0909	.0934	.0889
700	.1169	.1079	.1109	.1049
750	.1344	.1244	.1269	.1229
800	.1454	.1419	.1454	.1399
850	.1619	.1614	.1619	.1584
900	.1794	.1779	.1779	.1794
950	.1974	.1969	.1959	.1959
1000	.2128	.2133	.2138	.2158
1015	.2153	--	--	--
1040	--	--	.2258	--

Table B11. (Continued)

Temp (°C)	Run 3 Heating	Cooling
R.T.	0.0000	-0.0629
50	.0019	- .0834
100	-.0019	- .0989
150	-.0059	- .1064
200	-.0059	- .1094
250	-.0014	- .1054
300	.0054	- .0999
350	.0144	- .0894
400	.0224	- .0769
450	.0319	- .0644
500	.0419	- .0494
550	.0549	- .0334
600	.0689	- .0204
650	.0834	- .0054
700	.0969	.0099
750	.1104	.0229
800	.1214	.0414
850	.1324	.0614
900	.1459	.0804
950	.1609	.1029
1000	.1729	.1259
1050	.1854	.1449
1100	.1979	.1639
1150	.2073	.1809
1200	.2128	.2038
1210	.2108	--

APPENDIX C. X-RAY DATA

Table C1. X-ray powder diffraction data for Nb_2O_5 at various temperatures: Run 1

Reflection (hkℓ)	2θ values (deg)						
	25°C	182°C	417°C	619°C	794°C	1002°C	1190°C
40$\bar{1}$	17.33	17.33	17.30	17.30	17.30	17.29	17.28
10$\bar{4}$	19.20	19.20	19.17	19.16	19.17	19.16	19.16
110	23.80	23.81	23.84	23.88	23.85	23.85	23.85
10$\bar{5}$	24.44	24.45	24.45	24.42	24.41	24.40	24.36
012	25.57	25.52	25.53	25.50	25.48	25.46	25.42
005	26.60	26.61	26.61	26.63	26.60	26.62	26.63
51$\bar{2}$	31.60	31.57	31.60	31.60	31.58	31.58	31.53
014	31.67	31.65	31.65	31.64	31.64	31.67	31.62
51$\bar{1}$	32.27	32.28	32.29	32.27	32.28	32.28	32.28
21$\bar{5}$	33.18	33.19	33.17	33.15	33.12	33.12	33.10
80$\bar{2}$	35.27	35.26	35.25	35.19	35.20	35.15	35.13
70$\bar{7}$	36.05	36.01	35.97	35.95	35.90	35.83	35.84
413	38.93	38.93	38.91	38.90	38.88	38.88	38.87
207	43.58	43.57	43.55	43.45	43.43	43.37	43.30
711	44.45	44.43	44.41	44.36	44.30	44.27	44.25
11$\bar{8}$	47.60	47.60	47.65	47.67	47.65	47.68	47.67
10,1,$\bar{3}$	50.09	50.08	50.03	50.01	49.95	49.88	49.80
11,0,$\bar{1}$	52.47	52.47	52.46	52.44	52.42	52.30	52.25
4,0,$\bar{1}\bar{1}$	52.96	52.92	52.84	52.78	52.78	52.72	52.62
606	54.51	54.48	54.40	54.37	54.28	54.25	54.23
1,1,$\bar{1}$0	57.88	57.82	57.79	57.75	57.70	57.65	57.62

Table C2. X-ray powder diffraction data for Nb_2O_5 at various temperatures: Run 2

Reflection (hkℓ)	2θ values (deg.) 25°C	282°C	514°C	695°C	876°C	1010°C	1102°C	1338°C
$40\bar{1}$	17.28	17.28	17.30	17.26	17.25	17.25	17.27	17.18
$10\bar{4}$	19.17	19.17	19.17	19.15	19.13	19.12	19.10	19.12
110	23.76	23.80	23.85	23.85	23.83	23.88	23.85	23.88
$10\bar{5}$	24.43	24.42	24.42	24.41	24.37	24.38	24.37	24.35
012	25.52	25.49	25.46	25.45	25.43	25.40	25.42	25.38
$51\bar{1}$	32.27	32.25	32.25	32.24	32.24	32.22	32.24	32.18
$80\bar{2}$	35.27	35.22	35.18	35.18	35.12	35.12	35.11	35.05
413	38.89	38.89	38.88	38.86	38.80	38.82	38.80	38.78
207	43.57	43.50	43.48	43.40	43.37	43.32	43.30	43.25
711	44.44	44.40	44.38	44.36	44.30	44.28	44.26	44.20
$10,1,\bar{3}$	50.10	50.00	50.00	49.98	49.93	49.85	49.85	49.75
$11,0,\bar{1}$	52.46	52.45	52.45	52.38	52.37	52.32	52.30	52.27
606	54.45	54.40	54.36	54.32	54.28	54.24	54.20	54.18
$1,1,\bar{1}\bar{0}$	57.85	57.78	57.75	57.73	57.65	57.58	57.57	57.55
$11,0,\bar{1}\bar{1}$	58.29	58.25	58.20	58.15	58.13	58.07	58.00	58.00
$13,0,\bar{9}$	59.33	59.24	59.21	59.14	59.07	59.02	58.97	58.90

Table C-3. X-ray powder diffraction data for Nb_2O_5 at various temperatures: Run 3

Reflection ($hk\ell$)	2θ values (deg.) 922°C	1194°C	1274°C	1336°C
$40\bar{1}$	17.25	17.23	17.22	17.18
$10\bar{4}$	19.15	19.09	19.08	19.09
110	23.87	23.86	23.86	23.87
$10\bar{5}$	24.37	24.36	24.34	24.32
012	25.44	25.37	25.36	25.37
$51\bar{2}$	31.56	31.56	31.51	31.52
014	31.66	31.61	31.62	31.63
$51\bar{1}$	32.26	---	32.26	32.27
$21\bar{5}$	33.05	33.02	33.02	32.97
$80\bar{2}$	35.12	35.08	35.07	35.03
$70\bar{7}$	35.85	35.78	35.77	35.75
413	38.82	38.80	---	38.83
207	43.35	43.29	43.23	43.17
711	44.27	44.20	44.21	44.16
$10,1,\bar{3}$	49.90	49.78	49.80	49.79
$11,0,\bar{1}$	52.26	---	---	---
606	54.25	54.20	54.15	54.16
$1,1,\bar{10}$	57.57	57.60	57.52	57.50
$11,0,\bar{11}$	58.09	58.05	58.03	58.00
$13,0,\bar{9}$	59.04	58.98	58.90	58.88

Table C-4. Lattice parameters of Nb_2O_5 at various temperatures

Temp. (°C)	a (Å)	b (Å)	c (Å)	β (deg)	Unit-cell volume V (Å^3)
25	21.08 ± 0.02	3.83 ± 0.01	19.33 ± 0.02	119.90 ± 0.05	1353
182	21.11	3.83	19.35	119.93	1356
282	21.10	3.83	19.36	119.86	1356
417	21.13	3.82	19.38	119.95	1360
514	21.12	3.83	19.38	119.87	1359
619	21.14	3.82	19.39	119.91	1361
695	21.13	3.83	19.39	119.86	1360
794	21.16	3.83	19.41	119.91	1364
876	21.15	3.84	19.40	119.86	1362
922	21.18	3.83	19.43	119.86	1366
1002	21.23	3.83	19.46	119.99	1372
1010	21.18	3.84	19.46	120.01	1368
1102	21.20	3.84	19.46	119.91	1370
1190	21.24	3.82	19.47	119.98	1373
1194	21.24	3.81	19.43	119.76	1370
1274	21.27	3.82	19.50	120.03	1377
1336	21.28	3.81	19.50	119.94	1378
1338	21.21	3.82	19.49	120.01	1373

ACKNOWLEDGEMENTS

The author wishes to express his sincere gratitude to Dr. O. Hunter for his guidance, advice, and encouragement, to Messrs. F. W. Calderwood and D. W. Stacy for their assistance in the thermal expansion measurements, to Dr. M. O. Marlowe for building the original resonance apparatus and for introducing the author to elastic properties of ceramic materials, to Dr. L. Weirick for introducing the author to niobium pentoxide, to Dr. D. R. Wilder for his support, to Miss Verna Thompson for typing this dissertation, and to his wife, Judith, for her patience, understanding, support and encouragement.